Master's thesis

NTNU
Norwegian University of Science and Technology
Faculty of Engineering
Department of Structural Engineering

Gianclaudio Pinto

Structural analysis of long-span suspension bridge top tower: Application of Non-linear finite element analysis

Master's thesis in Design of structures
Supervisor: Terje Kanstad
June 2019

NTNU
Norwegian University of
Science and Technology

Gianclaudio Pinto

Structural analysis of long-span suspension bridge top tower: Application of Non-linear finite element analysis

Master's thesis in Design of structures
Supervisor: Terje Kanstad
June 2019

Norwegian University of Science and Technology
Faculty of Engineering
Department of Structural Engineering

NTNU
Norwegian University of
Science and Technology

Abstract

The Norwegian Ministry of Transport and Communications has commissioned the Norwegian Public Roads Administration (NPRA) to explore a project on the Coastal Highway E39 along the Norwegian west coast.
This master thesis project analyse the case of the Hardanger Bridge which is a suspension bridge built in 2013: this case study is part of this vast and ambitious project which is not only a chance to turn Norway into a more developed nation, but it is also a technological challenge, in particular for what concern the fjords crossings.
In this thesis the top tower part of the Hardanger Bridge was analysed: starting from the design drawings provided by the "Staten Vegvesen", the geometry of the top tower was built in CAD environment (Autocad and Rhino software) and, then, implemented within a finite element software Abaqus/CAE. The first part of the project consists of the definition of the material properties and the loads acting on the top tower, in particular on the steel saddle. The properties of each material were evaluated according to the actual Eurocode 2 – EN 1992 -1-1(2004) (1). The loads, given by Staten Vegvesen's engineer, are calculated according to the standard's guideline: ultimate and serviceability limit state loads were provided in the form of force in the two main cables.
The second part of the thesis is based on the finite element modelling of the top tower: each choice of modelling is explained and shown, according to the software's manual.
The behaviour of the structure was examined, performing a linear or non-linear static analysis. A considerable research investigation was carried out in order to find the most suitable non-linear model capable of describing the non-linear behaviour of the structure in relations to the presence of cracking.
The non-linear analysis was performed using the "concrete damaged plasticity model": this model showed the presence and the distribution of the cracked regions.
Finally, a serviceability limit state verification was performed: in particular, considering the results from the non-linear analysis, the verification of the crack width limit was carried out using different standards (Eurocode 2 2004/ draft 2018 and Model Code draft – 2010).
The concrete damaged plasticity model revealed the presence of a crack pattern made of two main cracks: the verification of cracks width (SLS) proved that the width of both cracks is lower than the nominal limit value suggested by the standards.

Preface

This master thesis in Design of structures is written at the Department of Structural Engineering at the Norwegian University of Science and Technology (NTNU), Trondheim, Norway. The work was carried out during the spring semester of 2019.

I would like to express my sincere appreciation and gratitude to my supervisor Professor Terje Kanstad, for his guidance and support. His constant mentorship and suggestions have not only enriched my technical knowledge but have also provided me with the confidence and determination needed to complete this project.

Also, I would like to thank Arianna Minoretti and Håvard Johansen from the National Public Road Administration (NPRA) for having provided the technical documentation necessary to start and realise this project.

Finally, my deepest gratitude and appreciation go to my friend Alberto, for his constant presence in this journey of ups and downs called life, and to my fellow student Daniele, for teaching me what it means to be an engineer. Also, I would like to thank Vito D., Vito P., Riccardo, Francesco and Federica for their priceless friendship.
I would like to thank Rossella for being a constant source of light and for all the time she has dedicated to me.

I would like to dedicate this achievement to my parents and my sister. I am grateful for their unconditional love and encouragement throughout these years despite my unconventional attitude towards the loved ones.
For you: "If you look for a meaning, you will miss everything that happens".
My love and admiration forever.

Last but not least, I dedicate this to the man who would have appreciated it most, N.

Table of Contents

List of Figures

List of Tables

List of Abbreviations (or Symbols)

A_c	Cross-sectional area of concrete
$A_{c,eff}$	Effective tensile area
A_s	Cross-sectional area of reinforcement
CDP	Concrete Damaged Plasticity
E_{cm}	Secant modulus of elasticity of concrete
E_s	Design value of modulus of elasticity of reinforcing steel
G_k	Characteristic permanent action
G_f	Fracture energy
m	Meter (Length)
NTNU	The Norwegian University of Science and Technology
Q_k	Characteristic variable action
RP	Reference Point
SLS	Serviceability limit state
ULS	Ultimate limit state
c	Concrete cover
d	Effective depth of a cross-section
f_{ck}	Characteristic compressive cylinder strength of concrete
f_{cm}	Mean value of concrete cylinder compressive strength
f_{ctk}	Characteristic axial tensile strength of concrete
f_{ctm}	Mean value of axial tensile strength of concrete
f_{tk}	Characteristic tensile strength of reinforcement
f_{yk}	Yield strength of reinforcement
H	Height
h	Overall depth of a cross-section
$h_{c,eff}$	Height of effective area in the tensile zone
l	(or L) Length
r	(or R) Radius
$1/r$	Curvature at a particular section
t	Thickness
w	Width of a crack
w_{ck}	Cracking displacement
x	Neutral axis depth

ε_c	Compressive strain in the concrete
ε_{c1}	Compressive strain in the concrete at the peak f_c
ε_{cu}	Ultimate compressive strain in the concrete
ε_t	Tensile strain in the concrete
ε_o	Plastic strain
ν	Poisson's ratio
ρ	Density of concrete in kg/m^3
ρ_{eff}	Geometrical percentage of reinforcement
σ_c	Compressive stress in the concrete
σ_s	Stress in the reinforcement
σ_t	Tensile stress in the concrete
ϕ	Diameter of a reinforcing bar
e	Base of Naperian logarithms
exp	Power of the number e
$<$	Smaller than
$>$	Greater than

1 Introduction

The project developed for this master thesis is linked to the "Ferry-free E39 – Coastal Highway Route": E39 is a coastal road which is going to connect the cities along the west coast of Norway. In particular, the route runs from Kristiansand in the south to Trondheim in the north, through six counties, and the cities of Bergen, Stavanger Ålesund and Molde. The route is approximately 1100 km long.

This national project aims to create an improved highway without ferries, which will reduce travel time by half and increase the possibilities for the local economy through value creation. In order to achieve a continuous highway route without ferries, it is necessary to build several significant fiord crossings with different innovative technologies (sub-merged tunnels, offshore technologies-TLP, multi-span suspension bridge with floating towers). With this background, many teams of engineers are working on the advanced knowledge of the existing suspension bridge in order to improve the design of the new ones (for example, Bjørnafjorden and Sulafjord bridges). Thus, this master thesis's project is part of an extensive analysis campaign which the Norwegian National Public Road Administration is performing. Also, this project aims to become a useful groundwork for the future topics that both the Department of structural engineering at NTNU and external work teams are going to be involved.

The primary purpose of this thesis is to analyse the top pylon part of the Hardanger Bridge which is part of the E39 project: in particular, the attention was focused on the behaviour of the system made of the steel saddle which supports the suspension cables and the reinforced concrete part below the saddle.

In particular, this project aimed to provide information about the non-linear behaviour of this particular structure: this topic involved the adoption of a non-linear material model in order to identify the most likely crack pattern and how it influences the response of the structure.

Furthermore, during recent years, interest in nonlinear analysis of concrete structures has increased steadily, because of the extensive use of reinforced and prestressed concrete as a structural material, and because of the development of finite element procedures.

First, an important consideration is that the constitutive properties of concrete have not as yet been identified completely, and there is still no generally accepted material law available to model concrete behaviour in the non-linear stage. A second important factor is that non-linear finite element analysis of concrete structures can be very time consuming and may require considerable user expertise. The considerable cost of nonlinear analysis of concrete structures is primarily due to the difficulties experienced in the accuracy and stability of the solutions.

In the following chapters, in order to fulfil the task of this project, a non-linear analysis was performed taking into account all the problematics that comes both from the finite element modelling and the presence of cracking.

All these aspects were carefully analysed, in order to be able to provide, at the end of the project, a complete overview of all the factors that improve or worsen the response of the structure.

1.1 The Hardanger Bridge

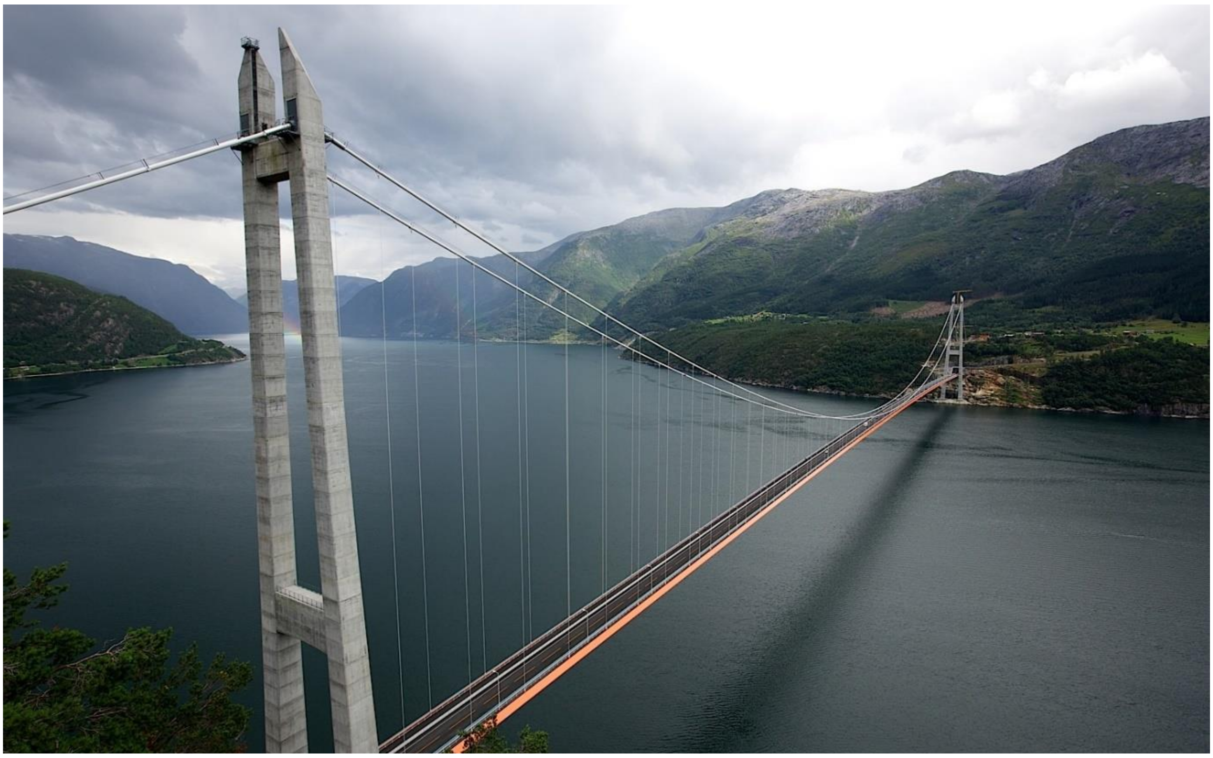

Figure 1.1 - *Hardanger bridge top view* (2)

The Hardanger Bridge is a 1380 m long suspension bridge connecting Vallavik and Bu and crossing the Hardanger Fjord in Hordaland. The construction started in autumn 2009 with the erection of the towers, and it was completed in 2013.
The bridge consists of one girder span between two pylons and hangers connected in between. The pylons are made of reinforced concrete, rising over 200 m above the sea level, standing on solid ground on each side of the Eidfjord.

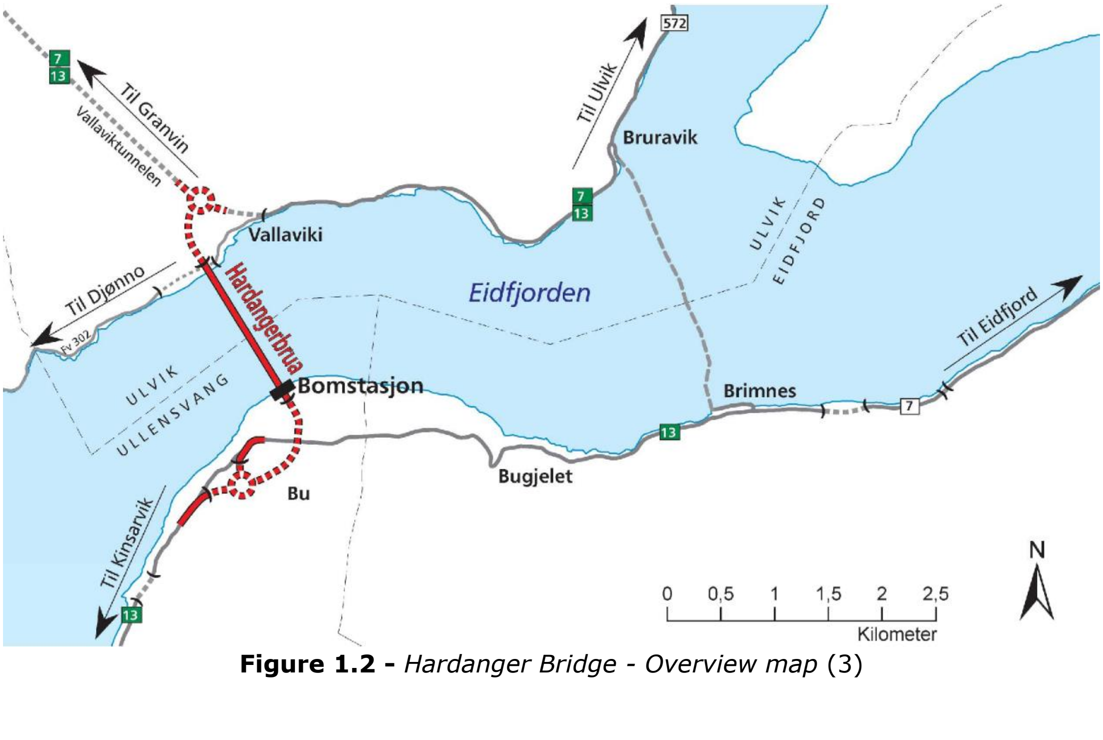

Figure 1.2 - *Hardanger Bridge - Overview map* (3)

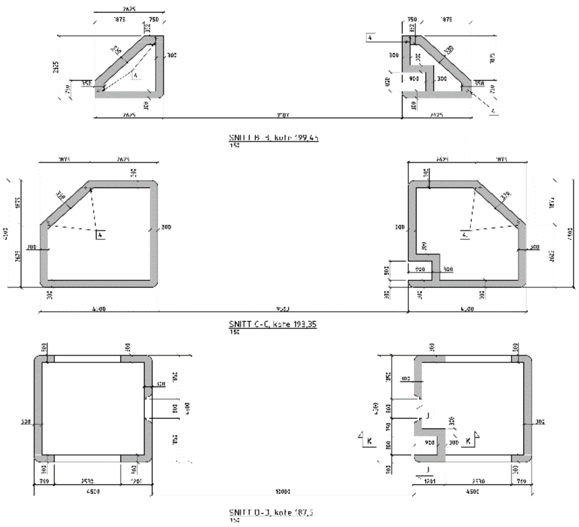

Figure 1.3 - *Geometry - Horizontal section cut*

The pylon construction was carried out adopting climbing formwork for a total of 44 sections, each of them representing 4 m of pouring. This particular type of vertical formwork was also used for the pouring of 6 shorter sections at the top of the pylons. The bridge pylon consists of two reinforced concrete columns connected by three cross beams: each pylon stands on two concrete foundations (10 x 12 m basal area and 6 m height). The pylons columns have a rectangular shape, which is hollowed inside, and the corner are rounded. On the top of the column, in the saddle housing, there are two steel saddles which support the suspension cables. Furthermore, inside one of the pylon columns, there is a lift, and inside the other one, there are stairs(3).
The two main cables consist of 19 strands, each containing 528 steel wires, each wire with a diameter of 5.3mm. Each main cable weigh 6.400 tonnes and has a diameter of 60 cm. Hangers are placed at a distance of 20 m along the girder: they have different lengths, varying from 3 m up to 127 m, with spiral-laid wires except for the five shortest hangers, which were made of one cast steel.
The girder is made of 23 steel sections each weighing 400 tonnes: the assembly of the sections was made lifting them from the deck of the ship using two cranes fastened on top of the cables. Then the girders were bolted and welded in site after connected to the hanger(4).

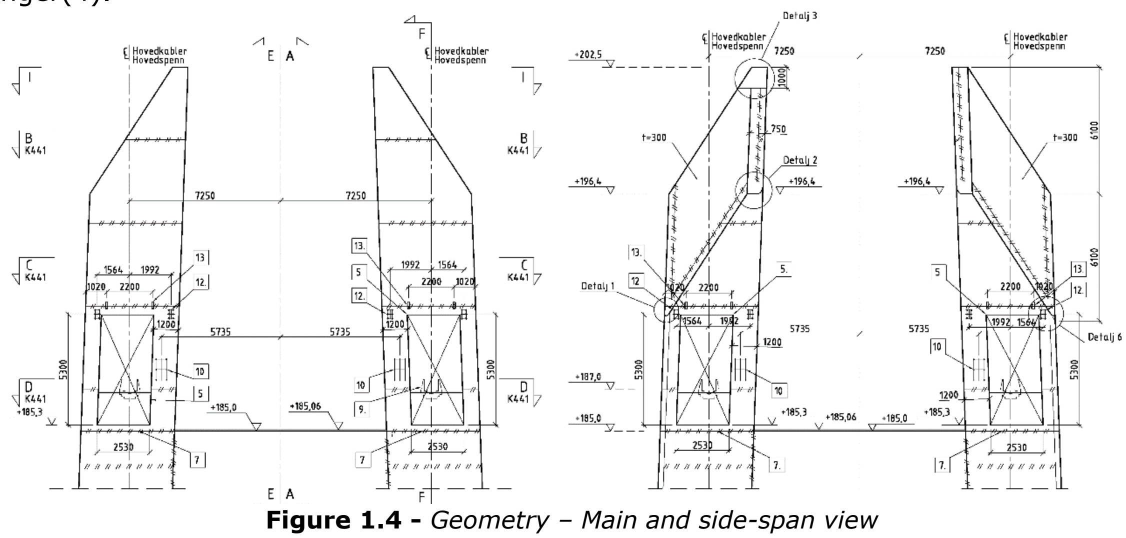

Figure 1.4 - *Geometry – Main and side-span view*

This project focused the attention on the top part of the towers and, in particular, the part between 183,1 m and 202,5 m of height was examined.
The examined part is characterised by two rectangular shaped towers linked together by a prestressed beam which was not considered.
The geometry of the structure in this range of height is not symmetric. The dimensions can be approximately estimated as 4,5 m x 4,5 at 183,1 m and 2,625 m x 2,625 m at 202,5 m (figure 1.2-1.3): in particular, the cross-section changes from a rectangular to a triangular shape on the top. Further details about are given in Appendices K440-K441.

2 Material Properties

The project involves the use of the following existing materials:

- concrete class - C45/55;
- concrete class - C55/67;
- Steel saddle "GX3CrNi13-4";
- reinforcement "B500NC";
- friction plate made of steel "S355";

These materials adopted in the top tower part are described in the following chapters.

2.1 Concrete

The top tower bridge part is realized with two different concrete strength classes, B45-SV40 and B55-SV 40: in particular, the B45-SV40 is used for the entire top tower, from the height of 179 m to the top (202,5m). Instead, the B55 is used only for the concrete regions below the steel saddle, between 185 m and 186,5 m, as mentioned in the Appendices K440.

Fasthetsklasse NS	*B10*	*B20*	*B25*	*B30*	*B35*	*B45*	*B55*	*B65*	*B75*
CEN betegnelse	-	*C20/25*	*C25/30*	*C30/37*	*C35/45*	*C45/55*	*C55/67*	-	-
Karakteristik sylinder fashet fcck	*10*	*20*	*25*	*30*	*35*	*45*	*55*	*65*	*75*
Karakteristik terning-fasthet fck	*12*	*25*	*30*	*37*	*45*	*55*	*67*	*80*	*90*
Tidligere betegnelse	*C12*	*C25*	*C30*	-	*C45*	*C55*	-	*C80*	*C90*

Table 2.1 - *Comparison of Norwegian and European standards (5)*

Since the adopted concrete follows the Norwegian national codes, literature research was made to understand better the classification of the concrete classes. The old "*C*" designations for firmness classes has been replaced in the European standard with double notations with "*C*" and following numbers for both cylinder and cubic strength. For example, concrete with previous designation C45 (compressive strength measured on cube 45 N/mm^2) has been replaced by the designation C35/45.
In Norway, it has been chosen to use single notation with the designation B and a number. The number after the "B" designation indicates the cylinder strength value for that particular concrete class. For example, concrete with a previous designation C45 (compressive strength 45 N/mm^2) replaced by designation B35 (5).

f_{ck}	*45 MPa*
$f_{ck,c}$	*55 MPa*
f_{cm}	*53 MPa*
E_{cm}	*33643 MPa*
f_{ctm}	*3.8 MPa*
v	*0,2*
ρ	*2500 kg/m3*

Table 2.2 *– Mechanical properties concrete C45/55*

f_{ck}	*55 MPa*
$f_{ck,c}$	*67 MPa*
f_{cm}	*63 MPa*
E_{cm}	*39708 MPa*
f_{ctm}	*4.2 MPa*
v	*0,2*
ρ	*2500 kg/m3*

Table 2.3 *- Mechanical properties for concrete C55/67*

The SV40 classification describes the Norwegian Public Roads Administration's requirements for concrete properties, and that was introduced to make it easier for customers and contractors to decide concrete quality in the Norwegian Public Roads Administration's projects. Concrete class with SV40 classification are supposed to have a mass ratio $\rho \leq 0{,}4$.
The mechanical properties of concrete are calculated according to Eurocode 2: EN 1992-1-1 (1).

2.2 Steel Saddle

The pylon saddles are made of cast steel grade “GX3CrNi13-4”. The mechanical properties are identified according to the European standards (“Steel castings for pressure purposes”(6);” Steel castings for general engineering uses”(7)), as shown in Table 2.3.

f_{yk}	*570 MPa*
f_{tk}	*900 MPa*
E_s	*190000 MPa*
v	*0,28*
ρ	*7700 kg/m3*

Table 2.4 - *Mechanical properties of steel saddle*

2.3 Steel Saddle Plates

The saddle plates, whether vertical and horizontal, are made of structural steel S355N and have a nominal thickness of 20mm. The mechanical properties are according to the standards (7), as shown in the following table:

Minimum yield strength	*Nominal thickness*
fy [MPa]	*thk [mm]*
355	*≤16*
345	*16 <thk ≤40*
335	*40 <thk ≤ 63*

Table 2.5 - *Extract from Table 7 of EN 10025-2/ structural steel*

The elastic modulus E_s and the density ρ correspond to *190000 MPa* and *7580* kg/m^3 respectively.

2.4 Reinforcement

The reinforcement steel adopted in the top tower bridge is B500-NC type. In this case of study, prestressed reinforcements, relatives to the prestressed cross-beam, were not taken into account. Products used as reinforcing steel may be bars, wires or welded fabric. The reinforcing steel is characterised by:

- geometrical properties;
- mechanical properties;
- technological properties.

The most common properties are geometrical and mechanical, as depicted in the following tables.

f_{yk}	*500 MPa*
f_{tk}	*550 MPa*
E_s	*200000 MPa*
ε_{uk}	*2,50e-03*
ρ	*7850 kg/m3*

Table 2.6 *- Mechanical properties for steel reinforcement B500NC*

Rebar size	*Nominal diameter (mm)*	*Cross sectional area*	
-	*[mm]*	*[mm2]*	*[m2]*
Φ12	*12*	*113,04*	*1,13e-04*
Φ16	*16*	*200,96*	*2,01e-04*
Φ20	*20*	*314*	*3,14e-04*
Φ32	*32*	*803,84*	*8,04e-04*

Table 2.7 *- Geometrical properties for steel reinforcement B500NC*

3 Loads

According to the European standards, actions are classified by their variation in time as it follows:

- permanent actions (*G*), self-weight of structures, fixed equipment and road surfacing;
- variable actions (*Q*), imposed loads on building floors, beams and roofs, wind actions or snow loads;
- accidental actions (*A*), explosion or impact from vehicles.

The structure shall then be checked in the following limit states, using the right load combinations for each limit state:

- Ultimate limit state (ULS)
- Serviceability limit state (SLS)
- Accident limit state (ALS)
- Fatigue limit state (FLS)

In this project, all the bridge loads are given by the Norwegian Public Roads Administration and, in particular, since the attention was focused on the top tower bridge, only the loads on the saddle were relevant due to reach the thesis goal. For this reason, the Norwegian public roads administration provided only the loads (forces) acting on the main cable (MN, per cable) towards side span (T_1) and towards main span (T_2).
The loads acting in the cable are defined, as follows:

	T1	***T2***	***T1***	***T2***
	[MN]	***[MN]***	***[N]***	***[N]***
Permanent Load	*119*	*125*	*1,19E+08*	*1,25E+08*
Traffic Load	*21*	*22*	*2,10E+07*	*2,20E+07*
Wind Load	*9*	*9*	*9,00E+06*	*9,00E+06*
Temperature Load	*1*	*1*	*1,00E+06*	*1,00E+06*

Table 3.1 - *Cable loads*

Then, the ultimate and serviceability limit state were defined as follows:

	T1	***T2***	***T1***	***T2***
	[MN]	***[MN]***	***[N]***	***[N]***
Ultimate Limit State	*170*	*179*	*1,7E+08*	*1,79E+08*
Serviceability Limit State	*133*	*140*	*1,33E+08*	*1,4E+08*

Table 3.2 – *Limit state combination*

These calculations of the loads are necessary for reaching the next step: the total load, expressed as a force in the suspended cables, was then converted into distributed pressure on saddle through bottom and sides. The suspended cable force whether at ultimate and serviceability limit state correspond to a tensile force in each of the 19 strands of:

- P_s (ULS) = $\frac{179}{(19*1000000)} = 9{,}4E+06\ N$

- P_s (SLS) = $\frac{140}{(19*1000000)} = 7{,}34E+06\ N$

Then, the forces per linear metre and the radial pressure on each curved bottom plate are calculated using the following equations:

$$P\ [MN/m] = \frac{n_S * P_S}{R}$$

$$p_v\ [MPa] = \frac{P_S}{w}$$

where:

- n_s is the number of the stacks of the strands, as previously described in 1.1;
- P_s is the force calculated in previous equations;
- $R = 4500mm$ is the saddle radius;
- $w = 121mm$ is the width of the friction plate.

These calculations carried out values of the radial pressure for each plate, as described in the next table:

	Load ULS	**Load ULS**	**Load SLS**	**Load SLS**
	[MPa]	***[Pa]***	***[MPa]***	***[Pa]***
L1_5	*51,8*	*5,18E+08*	*40,5*	*4,05E+07*
L2_4	*69,1*	*6,91E+07*	*53,9*	*5,39E+07*
L3	*86,3*	*8,63E+07*	*67,4*	*6,74E+07*

Table 3.3 - *Loads on plates*

In the following image, it is possible to understand the load distribution: the red part represent the vertical pressure (radial) on the saddle characterised by a linear distribution. However, uniform distribution for each plate is assumed.
In regards to the green part, which is the horizontal pressure p_h to the trough sides, the average stack height of 3 strands were used. The lateral pressure is taken as 1/3 as the corresponding vertical pressure at the same level: starting from a maximum pressure of *13,4 MPa* value and linearly varying to 0 at the top of the 3 strands.

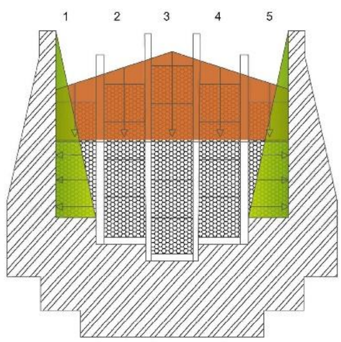

Figure 3.1 - *Saddle load detail*

The last type of load used is related to the solid local model, as described in 5.2.3. The local model is realised to minimise computational issues when adopting a non-linear model for the behaviour of the concrete. These loads represent the top tower part ad depicted in the following image.
The top tower part above the saddle was cut by a horizontal plane made at the height of 4.5m from the bottom. Then, the removed part was divided by two vertical planes into four parts (two parts for each tower).

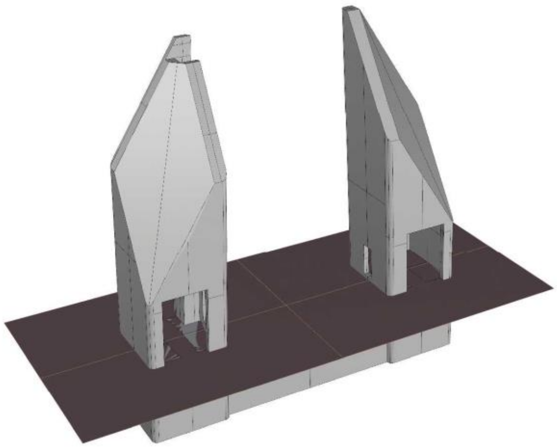

Figure 3.2 - *First cut plane*

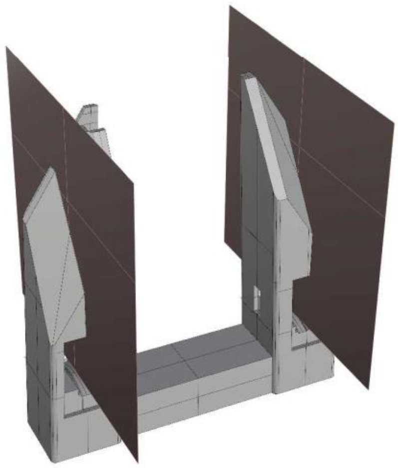

Figure 3.3 - *Second cut plane*

In figure 3.4 is shown the final version after the cut. In particular, the yellow parts represent the area on which the loads are calculated. Starting from the left side, the highlighted areas are classified as follows:

- *L_Sx1;*
- *L_Dx2;*
- *L_Sx2;*
- *L_Dx2.*

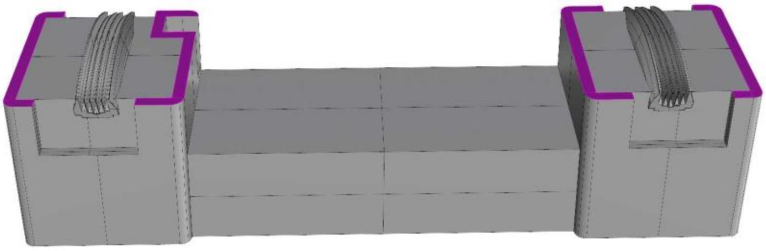

Figure 3.4 - *Loaded area local model*

The values of the loads acting on each area are:

Area	***Volume***	***Density***	***Force***		***Area***	***Pressure***
	[m3]	***[kN/m3]***	***[kN]***	***[N]***	***[mm2]***	***[MPa]***
L_Sx1	*19,25*	*25*	*481,25*	*481250*	*1,59E+06*	*0,3*
L_Dx1	*36,4*	*25*	*910*	*910000*	*1,85E+06*	*0,49*
L_Sx2	*40,38*	*25*	*1009,25*	*1009500*	*2,12E+06*	*0,47*
L_Dx2	*18,57*	*25*	*464,25*	*464250*	*1,59E+06*	*0,29*

Table 3.4 - *Loads local model*

Finally, the reactions on the saddle, as depicted in figure 3.5, were calculated: however, they were not considered in this thesis project since the suspended cables were not modelled in the FEM software and the friction was not taken into account. (8).

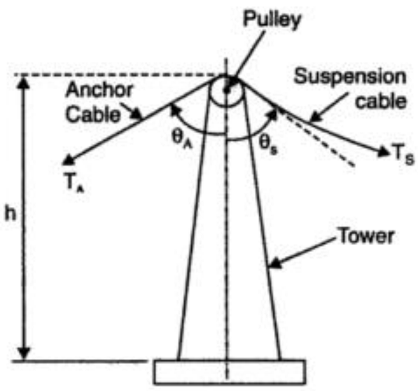

Figure 3.5 - *Guide pulley support*

4 Finite Element Modelling

4.1 Software

Structural modelling consists of a synthesis procedure through which the structure and the static actions acting on it are reduced to a simplified scheme, in order to realistically simulate the behaviour in terms of stress and strain parameters.
It is advisable to identify the key variables that influence the physical system to be analysed and to reconcile the correctness of the result with operational practicality and, therefore, with the economy of the procedure. The definition of a structural scheme that is at the same time quite simple and sufficiently complex to take into account the effect of the most important variables is fundamental since the reliability of the results depends on this definition.
The model of the structure was created in a CAD environment through *Rhinoceros 3D* (version 5.12), commercial software for technical drawing developed by the company Robert McNeel & Associates. The geometries of the software are based on the mathematical model NURBS (*Non-Uniform Rational Basis Spline*) which allows an accurate definition of curves and surfaces. The software is also compatible with other applications, supporting different formats for the interchange of design files.
A ".*dxf"* file, containing the drawings of the structure under examination, was imported into *Rhinoceros*: in particular, the top tower section cut, the drawings of the steel saddle and all the reinforcement details concerning the top tower (Appendices K440-441-445-652-680-681).
In particular, various models were obtained in this CAD environment:

- a solid element model;
- a shell element model

These were exported as IGES format, for 2D elements, and ASCI format, for 3D elements, to preserve their properties and then imported into *Abaqus CAE*, software suite for finite element analysis.
The different ABAQUS commands and techniques, which were utilized in creating a finite element model of reinforced concrete, are discussed in this chapter. This chapter includes both the mechanics behind each command and the variables which are input into ABAQUS to quantify the behaviour; also, the different modelling techniques available within ABAQUS which were used within this research for the purposes of modelling the non-linear behaviour of reinforced concrete are discussed.

4.2 Models

The entire geometry of the structure was rebuilt mainly starting from the three horizontal and vertical section cut. Since the geometry is quite complex, two different approaches were performed: a 3D model, as in figure 4.1-4.2, and a 2D model.

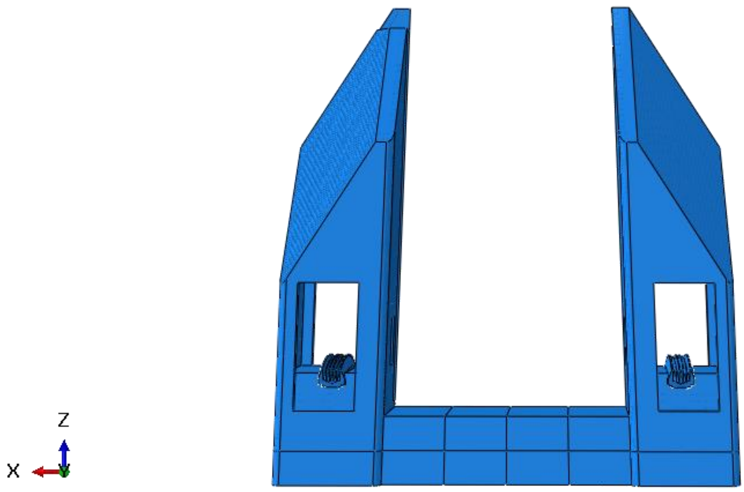

Figure 4.1 - *Solid Model - Front view*

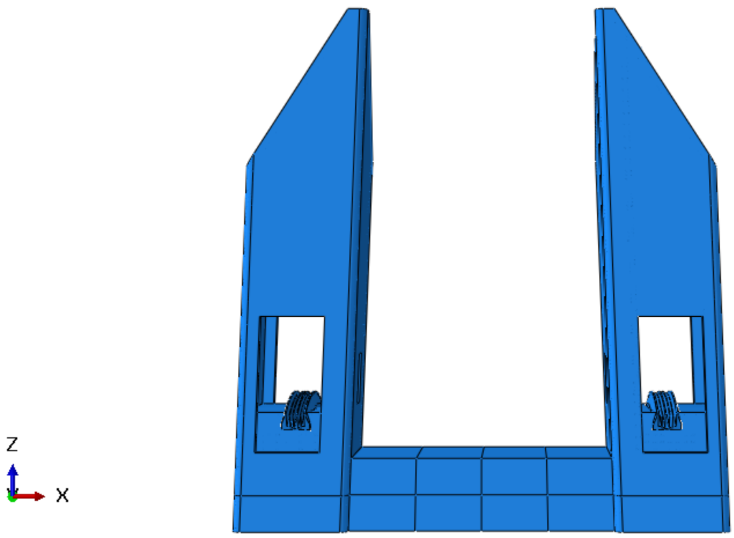

Figure 4.2 - *Solid Model - Back view*

The 3D model was created using the exact geometry provided by the design drawings and keeping the thickness of the real structure unchanged. The 2D model, on the other hand, was created by referring to the middle plane of the structure, which is a common and useful strategy when modelling shell element.
However, the top tower has many corners and relatively close to each other, so this way of modelling requires to pay proper attention when connecting the different shell element each other. Furthermore, this kind of model showed many problematic aspects in modelling the concrete support part for the steel saddle: although the corners and the walls might

also be discretized as shell elements, these cannot be used to describe the behaviour of a part mostly solid.

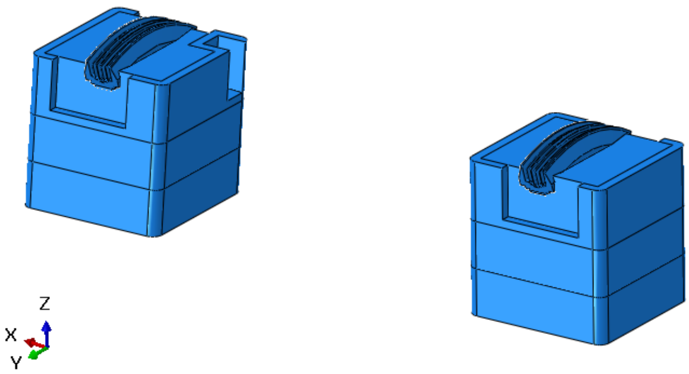

Figure 4.3 - *Local model #2.1-#2.2*

Therefore, for this particular study, it is more convenient to use solid elements in order to get a more accurate representation of the stress and strains concentrations whether at the corner and mostly through the concrete support part.
This solid model denominated "global model", was meant to be used for the linear static analysis, but it was mostly used whether to perform a mesh sensitivity analysis and to validate the smaller models. In fact, for the application of the linear and non-linear analysis, the two simpler models, called "*local model #1 and #2*" were adopted (fig.4.3a-4.3b).
This adoption was done to decrease the computational time and to focus the attention on more details and variables of the structure.
In particular, performing a non-linear analysis on a complex model such as the "global model" would not allow to entirely understand all the variables that affect the problem since the computational time estimated would be about more than a day.

4.3 Modelling Approach

In structural mechanic, advanced static and dynamic problems can be solved using the finite element method. The general procedure of modelling any structure within *ABAQUS* consists of assembling meshed parts of finite elements into one global assembly, and then evaluate its overall response under loading.
ABAQUS provides an extensive library of elements that can be effectively used to model a variety of materials. The geometry and the type of element are characterized by several parameters, including family, degree of freedom, number of nodes, formulation, and integration. Each element integrated into ABAQUS has a unique name such as "*T2D2*", "*S4R*", "*C3D8I*", or "*C3D8R*", which are derived from the five aspects mentioned previously. Letters of an element's name or the first letter state to which family the element belongs. For example, "*S4R*" is a shell element and "*C3D8*I" is a continuum element.
The following figure 4.4 illustrates briefly some of the most commonly used elements.
The degrees of freedom are the primary variables calculated during the analysis. For a stress-displacement simulation, the degrees of freedom are whether the translations and the rotations in correspondence of each node.

Displacements or other degrees of freedom are calculated at the nodes of the element. At any other point in the element, the displacements are obtained by interpolating from the nodal displacements. Usually, the number of nodes used in the element determines the interpolation order.
In theory, second-order elements provide more accurate results than first-order elements. However, the use of higher-order elements has some of the drawbacks associated with convergence issues, mainly when used in highly nonlinear analyses.

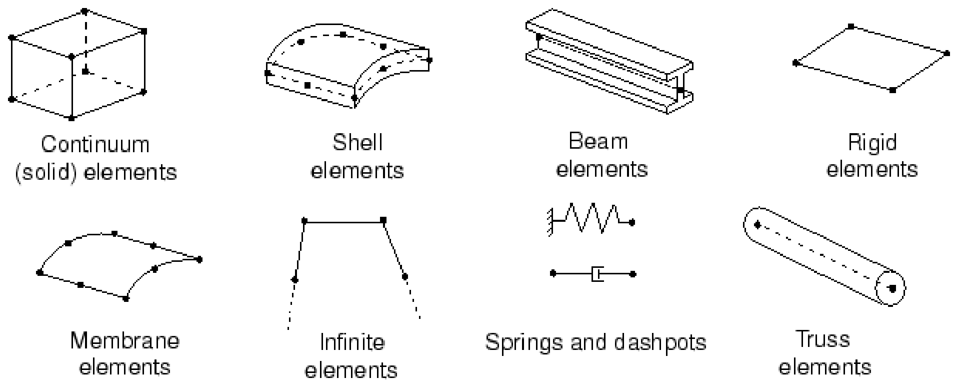

Figure 4.4 - *Commonly used element families*

Before starting to define a model in Abaqus/CAE, a system of units must be chosen. Abaqus/CAE has no built-in system of units, and hence, all input data must be specified in consistent units. SI unit system was chosen, and the units used are the following:

Quantity	***SI (mm)***
Length	*mm*
Mass	*tonne (10^3 kg)*
Force	*N*
Density	*tonne/mm^3*
Stress	*MPa (N/mm^2)*

Table 4.1 – *Units*

4.3.1 Concrete

A material definition in Abaqus (9):

- specifies the behaviour of a material and supplies all the relevant property data;
- can contain multiple material behaviours;
- is assigned a name, which is used to refer to those parts of the model that are made of that material;
- can have temperature and field variable dependence;
- can have solution variable dependence in Abaqus/Standard;

For this project, variable dependence and material coordinate system were not specified.
As stated previously in Section 2.1, both of the concrete type, C45/55 and C55/67, utilise the same linear-elastic behaviour. For this behaviour, the modulus of elasticity for concrete E_C, as well as Poisson's ratio v.
These material properties are defined using the "elastic" command within Abaqus. For the purpose of these analyses, it was assumed that the material was isotropic, and this parameter was included in the "elastic" command. In addition to the "elastic" command, the density was also defined for the concrete. The exact values, which were used for these commands, can be found in Section 2.1. These commands do not directly take into consideration f_{cd} or $f_{ct.}$ For what concerns the non-linear behaviour of the concrete, the modelling techniques are widely described in Section 5.2.
The concrete is modelled using "Continuum" elements (Figure 4.4) as they are more suitable for three-dimensional materials. Also, this type of elements is typically used when plasticity and large deformations are expected, such as in the case of the concrete structure.
The linear reduced-integration option was not used throughout the analysis of concrete parts: this option is capable of withstanding severe distortions, but at the same time, it might affect the analysis results.
Lastly, "*C3D4*" elements were employed to model all concrete region. These elements are continuum elements (C) three dimensional (3D), 4-noded linear brick (8)

4.3.2 Rebar

As for the concrete modelling, also for the modelling of the rebar, the "elastic "command was performed using the same elastic parameters; furthermore, plastic properties were defined in the appropriate command.
In particular, metal behaviour is defined as a stress/plastic-strain relationship idealized using bi-linear segments, as shown in Figure 4.5.
The slope of the first linear segment represents the elastic modulus, E_S, associated with a yield strength of 500MPa, as previously described in Section 2.4. Beyond the yield strain, the slope of the stress-strain curve was assumed to be equal to zero (straight line).

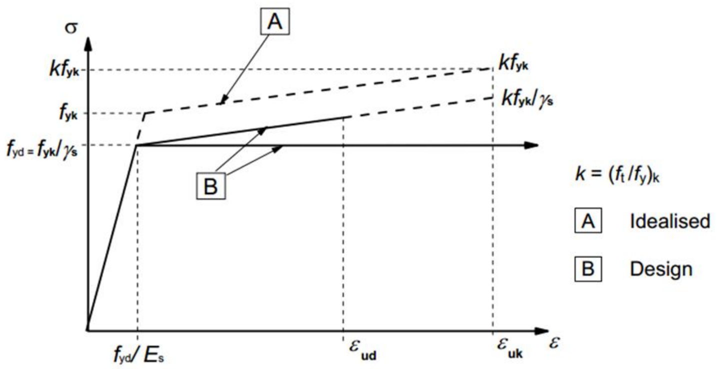

Figure 4.5 - *Idealized stress-strain relationship for steel (Eurocode 2-part 1.1)*

The steel reinforcements were modelled using "Truss" elements. Truss elements are slender structural elements that can only transmit axial force and do not transmit moments or transverse loads. These elements are available in either 2-noded form or 3-noded form in ABAQUS. The former implements linear interpolation of the nodal displacement values and carry constant strains. The T3D2 elements were chosen to model the truss sections,

as (T) refers to truss elements, (3D) refers to three-dimensional, and (2) corresponds to 2-nodes per linear element.
Each reinforcing steel bar is then embedded into the concrete body through the "embedded region" constraint that is available in ABAQUS tools. This type of constraint defines the truss elements as the "embedded region" and the solid continuum concrete as the "host region". The nodes of the embedded region become tied to the nodes of the host region, and thus the translational degrees of freedom of the rebars are constrained to that of the concrete.
The advantage of this model is that it allows an independent choice of the concrete mesh. The embedded approach is used to create a bond between the two instances of steel reinforcement and the concrete instance and overcome the mesh dependency. The embedded constraint available in Abaqus couples the nodal degree of freedom automatically assuming a full bond action between the reinforcement and concrete elements with no relative slip. The transverse steel reinforcement (stirrups) were modelled using truss elements as in the main rebars of the proposed model. They were embedded individually into the concrete region through the embedded region tool, as mentioned earlier. Therefore, in the proposed models, the influence of the interaction between the concrete and steel bars was not considered. The model of the reinforcement was first developed in the CAD environment, following the design drawing, and, then, completed with all the mechanical and geometrical properties within Abaqus (figure 4.6).

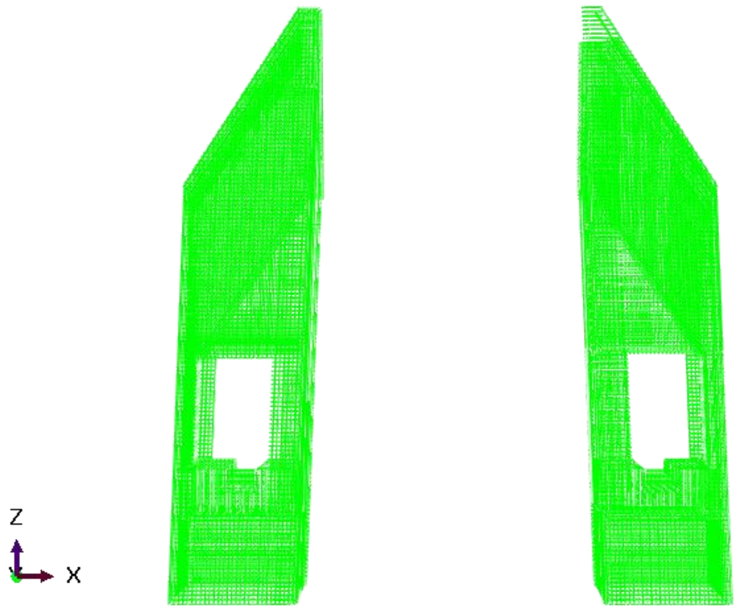

Figure 4.6 - *Reinforcement model*

4.3.3 Steel saddle and friction plate

The steel saddle and the friction plate are modelled using the "plasticity" tool in the Abaqus command, and their elastic and plastic parameters are described in Section 2.2 and 2.3.

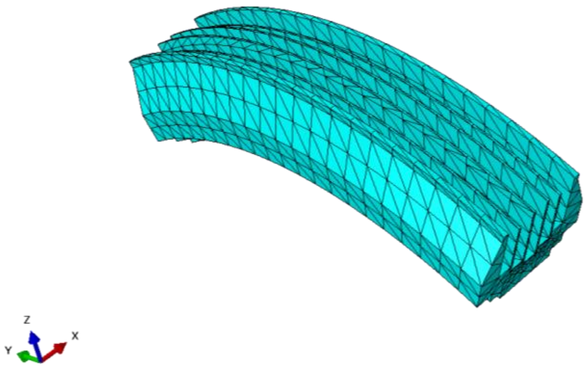

Figure 4.7 - *Steel saddle-Friction Plate FEM model*

Finally, they are modelled the same way as the concrete parts (Figure4.6): continuum elements, in particular, C3D4 elements were employed to model this region.

4.3.4 Boundary conditions

Boundary conditions are constraints necessary for the reach of the solution of a problem. These have a significant impact on the result of analysis and a simple mistake in the definition of the boundary conditions might bring a high error percentage of the results.
In Abaqus when creating a boundary condition, it is necessary to specify the name of the boundary condition, the step in which to activate them, the type of boundary condition, and the region of the assembly to constraint. As described in the previous section, the models adopted in the FEM environment are the solid top tower, which presents the entire geometry, and the local solid models defined using a horizontal and vertical cutting plane. The first model was constrained at the bottom, as displayed in figure 4.8: in particular, the displacements *U1, U2, U3* and the rotations *UR1, UR2, UR3* of the bottom surfaces of the tower were fixed. Thus, this boundary condition was used to fully constrain the movement of the points and set their degrees of freedom to zero.

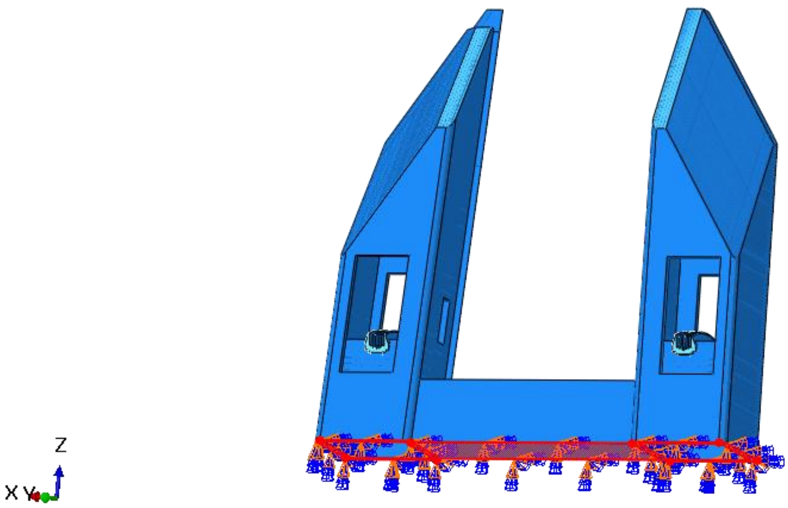

Figure 4.8 - *Boundary conditions global model*

This boundary condition, called "*BC1*" persists in each of the model used in the analysis. In particular, the local models are realized with the following boundary conditions:

- "*BC1*" (*U1, U2, U3, UR1, UR2, UR3 = 0*);
- "BC2" (*UR1, UR2, UR3 = 0*);
- "BC3" (*U1, U2, U3, UR1, UR2, UR3 = 0*).

The boundary condition number two ("BC2") is applied to the specific surfaces created using the horizontal cutting plane (figure 4.6). Instead, the boundary condition number three ("*BC3*") is applied only for the local model (figure 4.7-4.8) to constrain the parts where the cross concrete beam is suppressed.

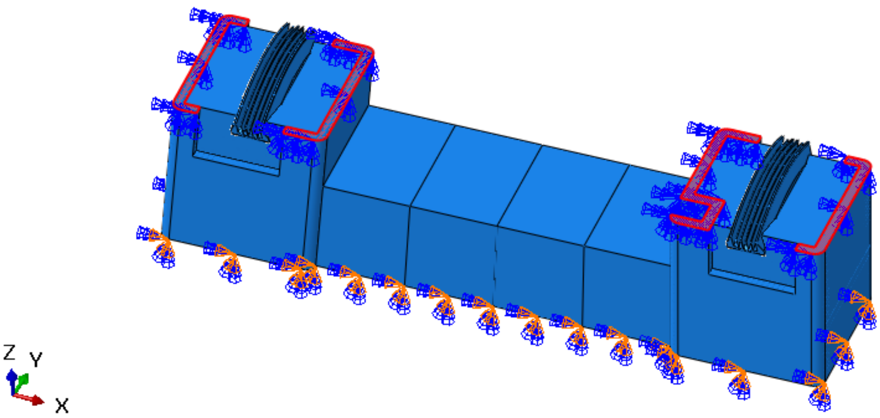

Figure 4.9 - *BC1-BC2 local model #1*

These two boundary conditions were created to simulate the real behaviour of the entire structure when some of his parts are removed. In particular, "*BC2*" was firstly created to fix all the displacements and rotations, in the same way as "*BC1*", but this situation produced a high-stress concentration along the edge of the surfaces where they were applied on and above all the results were not accurate due to excessive distortion of the elements.

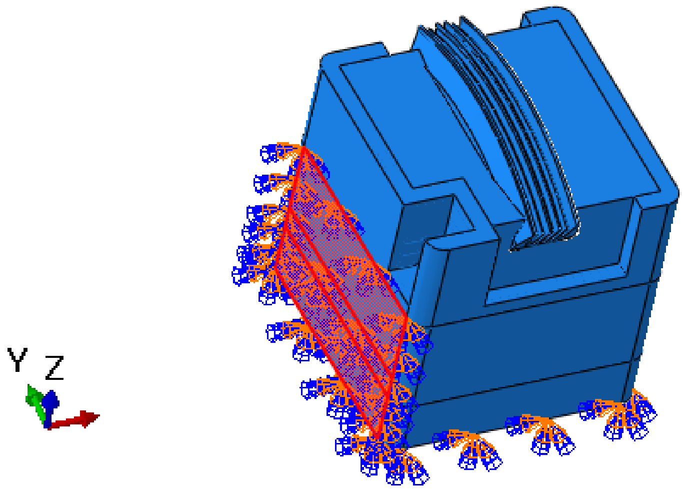

Figure 4.10 - *BC3 local model #2.1*

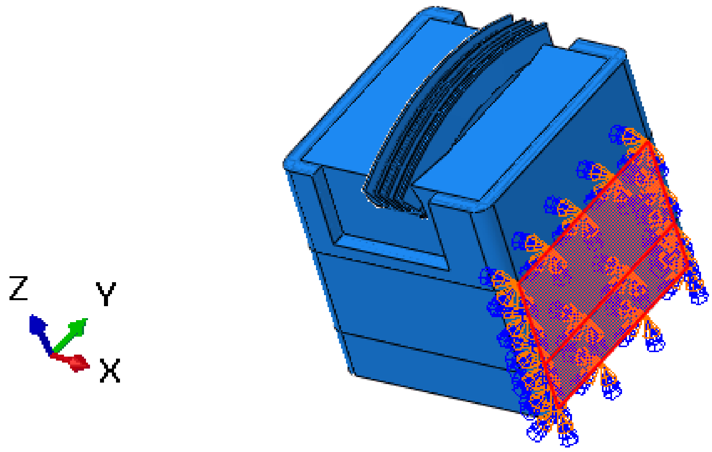

Figure 4.11 - *BC3 local model #2.2*

The last boundary condition was defined for the steel saddle: U1 displacement and UR3 rotation were fixed. Without these boundary conditions, there were many stability and convergence problem during the analysis because the saddle was not whether constraint too much or not at all.

4.3.5 Interaction

Abaqus contains an extensive set of tools for modelling contact and interface problems for stress analysis, heat transfer analysis, coupled stress-heat transfer cases, coupled pore fluid-stress analysis, and coupled acoustic pressure-structural response analysis.
Contact is typically modelled by identifying surfaces, which may interact, and pairing them by name. Interactions between deforming bodies or between a deforming body and a rigid body are allowed. Both small and finite sliding may be modelled in either two or three dimensions. A Coulomb friction model may be used for shear interaction or, for a more sophisticated response, a user subroutine may be used to define the frictional behaviour (10).
In this project a surface-to-surface contact definition is used as an alternative to general contact to model contact interactions between specific surfaces in a model: in particular, it was chosen to assign this property to the surfaces of the steel saddle and the concrete part, which are in contact each other.

4.3.6 Mesh sensitivity analysis

A mesh is a network which is formed of cells and points. It can have different shapes in any size and is used to solve *Partial Differential Equations*. Each cell of the mesh represents a solution of the equation which, when combined for the whole network, results in a solution for the entire mesh(11).
The exact size of these elements was varied in order to determine the most computationally efficient and accurate size. A mesh sensitivity analysis for the part of the tower below the saddle was performed, and the mesh size which were tested are 250 mm, 200 mm, 150 mm, 100 mm, 75 mm and 50 mm. For the reinforcement and steel saddle meshes, values of 200 mm and 150 mm were used. Furthermore, the remaining parts of the top tower were meshed with size elements of 150 mm and 75 mm, only for the rounded corner.

Mesh Size [mm]	*Number of elements*
250	*424.809*
200	*499.631*
150	*751.865*
100	*1.357.932*
75	*2.337.014*
50	*5.527.248*

Table 4.2 - *Number of elements for each mesh size*

Table 4.2 shows the number of elements created for each model: in particular, the model with 250 mm^{2}mesh size did not converge, due to the excessive distortion of the elements mainly located in the corner and below the steel saddle. For a complex geometry like this, it was reasonable thinking not to solve the analysis with such a significant value of mesh elements.

For this mesh sensitivity analysis, some particular points were considered, and for each of them, the variable taken into account is the Von Mises stress, defined as the equivalent or effective stress at which yielding is predicted to occur in ductile materials.

Thus, defined as:

$$\sigma = \frac{1}{\sqrt{2}}\left[\left(\sigma_x - \sigma_y\right)^2 + \left(\sigma_y - \sigma_z\right)^2 + \left(\sigma_z - \sigma_x\right)^2 + 6\left(\tau_{xy}^2 + \tau_{yz}^2 + \tau_{zx}^2\right)\right]^{1/2}$$

The controlling points, defined in Abaqus as "Reference Point", are shown in the following figure:

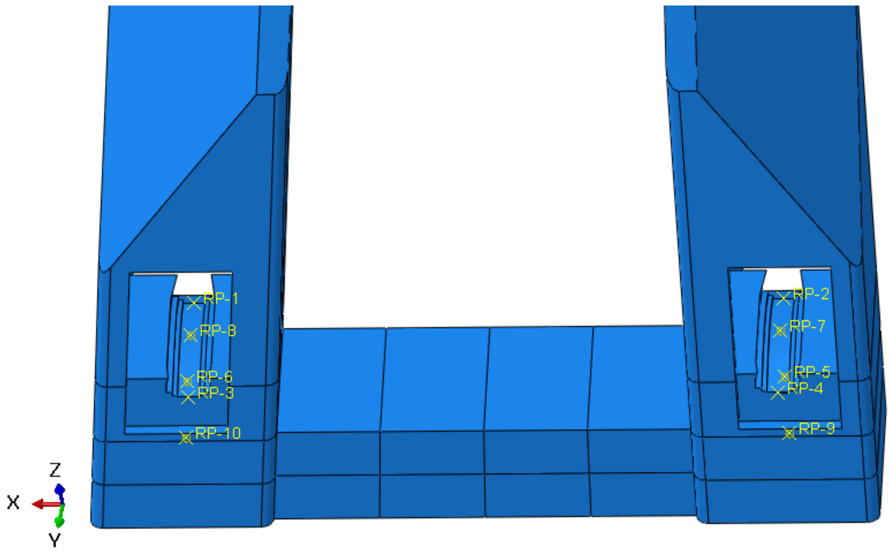

Figure 4.12 - *Reference Point -1st view*

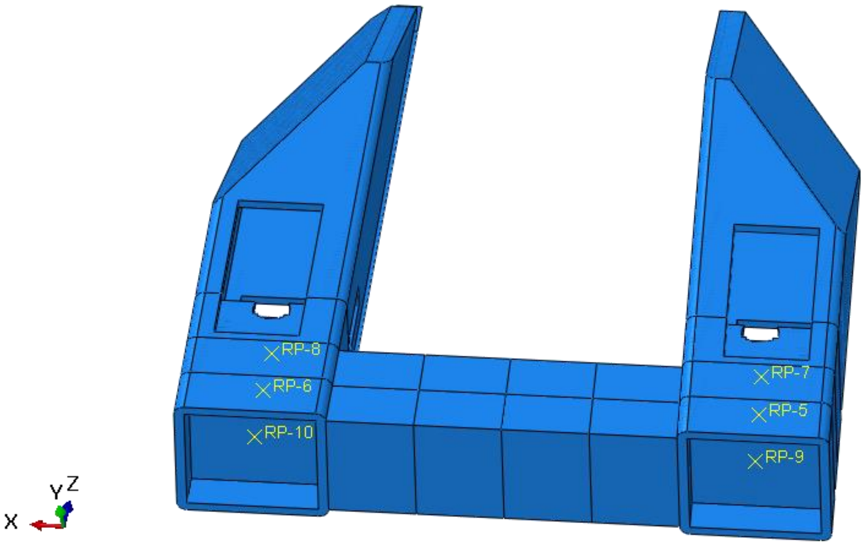

Figure 4.13 - *Reference Point -2nd view*

In particular:

- reference points 1-2-3-4 are located on the contact surface between the saddle and the concrete, in particular, in positions where the saddle ends;
- reference points 5-6-7 and 8-9-10 both belong to two vertical axes passing through the middle point of the concrete support part of the steel saddle but at different heights (z).

About the reference points and their results, it is necessary to understand how Abaqus works in the post-processing phase. Abaqus allows the user to select one or more field output variables to include in the tabular report(12).
The available variables consist of those saved to the output database for the current step and frame.
The programme can calculate and report values for a given variable at a variety of positions. In particular, the possible report positions are:

- integration point;
- centroid;
- element nodal;
- unique nodal.

Element nodal and unique nodal positions both involve reporting results at the nodes of the model; however, reporting of unique nodal values produces only a single value at each node, whereas reporting of element nodal values produces one value for each mesh element that has a contribution at that node. In particular, nodal stress solutions are given to the user in the averaged form at each global node. The stress value at a global node is the average of all the local node stress values of all the elements sharing that global node. It means that there is a unique nodal value associated with a particular node of each element.

In this case, it was illogical considering element nodal or integration point for the following reasons:

- there are too many elements, so it was almost impossible to choose and identify the right elements with which describe the reference point behaviour;
- the elements are tetrahedral: for this reason, their distribution along the reference points was always unsymmetrical and chaotic.

So "unique nodal" option was chosen to get stress results of the reference point: this found out to be the easiest and fastest way to extrapolate data since only the position or the name of the control point required to be established. In this way, instead of picking up every single tetrahedral element surrounding the reference point, Abaqus calculate the stress values for each node of the element that share our reference point. For example, if two elements share the node of the reference point, selecting the "unique nodal" option, two values are given: the average of this two value is the final value of the reference point in terms of output variable chosen (stress, strain, displacement, ecc..).
So, ideally, using these reference points as control points and the Von Mises stress, as output variable, as the mesh size decrease, the results from the analysis should converge to a constant value.
A linear static analysis, with loads, material and geometrical properties described in the previous chapters, was performed on same models with different mesh sizes, in order to get the results for the reference points, as described in the following tables.
In the following pages are shown the stress results for each reference point corresponding to different mesh size; the results are also plotted for a better understanding.

Reference point 1				
Mesh 200mm	***Mesh 150mm***	***Mesh 100mm***	***Mesh 75mm***	***Mesh 50mm***
2,45E+01	*2,18E+01*	*2,66E+01*	*3,34E+01*	*3,34E+01*
2,04E+01	*2,15E+01*	*4,88E+01*	*1,59E+01*	*1,59E+01*
2,25E+01	*2,11E+01*	*3,87E+01*	*3,36E+01*	*3,36E+01*
2,22E+01	*2,73E+01*	*5,38E+01*	*4,34E+01*	*4,34E+01*
2,37E+01	*2,67E+01*	*6,22E+01*	*3,50E+01*	*3,51E+01*
1,51E+01	*1,55E+01*	*1,73E+01*	*3,45E+01*	*3,46E+01*
1,43E+01	*2,05E+01*	*1,88E+01*	*3,76E+01*	*3,77E+01*
1,45E+01	*2,04E+01*	*6,05E+01*	*3,93E+01*	*3,93E+01*
2,35E+01	*2,10E+01*	*1,59E+01*	*3,57E+01*	*3,58E+01*
2,17E+01	*2,12E+01*	*1,35E+01*	*2,55E+01*	*2,56E+01*
2,36E+01	*1,65E+01*	*2,88E+01*	*6,58E+01*	*6,58E+01*
2,59E+01	*2,37E+01*	*5,54E+01*	*5,40E+01*	*5,40E+01*
2,29E+01	*1,98E+01*	*5,77E+01*	*1,84E+01*	*1,85E+01*
2,42E+01	*2,26E+01*	*2,08E+01*	*1,39E+01*	*1,40E+01*
2,34E+01	*1,52E+01*	*2,72E+01*	*1,97E+01*	*1,98E+01*
2,19E+01	*1,93E+01*	*1,43E+01*	*5,19E+01*	*5,20E+01*
-	*2,44E+01*	*1,17E+01*	*3,41E+01*	*3,41E+01*
-	*2,36E+01*	*3,75E+01*	*4,38E+01*	*2,48E+01*

	-	2,40E+01	2,01E+01	1,57E+01	-
	-	2,64E+01	1,44E+01	3,56E+01	-
	-	2,46E+01	-	1,28E+01	-
	-	1,90E+01	-	2,50E+01	-
	-	2,54E+01	-	4,84E+01	-
	-	-	-	2,81E+01	-
Average	*2,14E+01*	*2,18E+01*	*3,22E+01*	*3,34E+01*	*3,43E+01*
Δ [%]	*-38%*	*-36%*	*-6%*	*-3%*	*-*

Table 4.3 - *Von Mises stress RP1*

	Reference point 2				
	Mesh 200mm	***Mesh 150mm***	***Mesh 100mm***	***Mesh 75mm***	***Mesh 50mm***
	6,67E+01	2,27E+01	3,85E+01	5,33E+01	5,33E+01
	9,28E+01	2,13E+01	5,20E+01	5,59E+01	5,59E+01
	7,03E+01	2,45E+01	1,95E+01	2,66E+01	2,67E+01
	7,24E+01	1,25E+01	2,78E+01	2,46E+01	2,46E+01
	1,92E+02	1,35E+01	3,23E+01	2,49E+01	2,50E+01
	7,05E+01	1,25E+01	2,94E+01	3,15E+01	3,15E+01
	1,28E+02	2,16E+01	4,43E+01	2,86E+01	2,86E+01
	1,21E+02	1,99E+01	1,65E+01	2,71E+01	2,72E+01
	1,44E+02	1,93E+01	3,53E+01	2,81E+01	3,11E+01
	1,05E+02	1,77E+01	3,38E+01	3,16E+01	3,24E+01
	9,62E+01	1,55E+01	3,67E+01	5,88E+01	5,89E+01
	1,17E+02	2,46E+01	2,89E+01	3,10E+01	3,10E+01
	1,16E+02	2,48E+01	2,43E+01	2,82E+01	2,82E+01
	1,04E+02	2,34E+01	3,92E+01	3,24E+01	3,24E+01
	1,18E+02	2,16E+01	2,82E+01	-	2,89E+01
	8,91E+01	2,55E+01	7,38E+01	-	2,92E+01
	7,86E+01	2,69E+01	3,92E+01	-	3,92E+01
	6,74E+01	2,41E+01	3,36E+01	-	4,58E+01
	1,09E+02	2,33E+01	3,79E+01	-	-
	7,20E+01	2,49E+01	3,75E+01	-	-
	-	2,28E+01	4,16E+01	-	-
	-	-	3,25E+01	-	-
	-	-	4,36E+01	-	-
	-	-	2,58E+01	-	-
	-	-	4,49E+01	-	-
	-	-	3,26E+01	-	-
	-	-	3,96E+01	-	-
	-	-	3,10E+01	-	-
Average	*6,71E+01*	*2,11E+01*	*3,57E+01*	*3,45E+01*	*3,35E+01*
Δ [%]	*100%*	*-37%*	*7%*	*3%*	*-*

Table 4.4 - *Von Mises stress RP2*

	Reference point 3				
	Mesh 200mm	***Mesh 150mm***	***Mesh 100mm***	***Mesh 75mm***	***Mesh 50mm***
	2,20E+01	*2,84E+01*	*4,16E+01*	*4,91E+01*	*4,88E+01*
	2,10E+01	*2,10E+01*	*5,44E+01*	*5,38E+01*	*5,30E+01*
	2,02E+01	*2,18E+01*	*4,38E+01*	*6,02E+01*	*5,94E+01*
	2,08E+01	*2,24E+01*	*4,26E+01*	*6,63E+01*	*6,58E+01*
	2,62E+01	*2,48E+01*	*4,34E+01*	*4,29E+01*	*4,24E+01*
	2,39E+01	*2,47E+01*	*4,42E+01*	*4,70E+01*	*4,65E+01*
	2,48E+01	*2,61E+01*	*6,77E+01*	*6,63E+01*	*6,58E+01*
	2,44E+01	*2,39E+01*	*2,84E+01*	*1,50E+01*	*1,45E+01*
	2,84E+01	*2,66E+01*	*4,35E+01*	*4,82E+01*	*4,82E+01*
	2,39E+01	*2,53E+01*	*2,36E+01*	*4,79E+01*	*4,59E+01*
	2,20E+01	*2,63E+01*	*4,61E+01*	*2,07E+01*	*2,07E+01*
	2,42E+01	*2,41E+01*	*2,40E+01*	*1,77E+01*	-
	2,29E+01	-	*3,00E+01*	-	-
	2,42E+01	-	*2,03E+01*	-	-
	2,34E+01	-	*4,21E+01*	-	-
	2,19E+01	-	*2,17E+01*	-	-
Average	*2,24E+01*	*2,46E+01*	*3,86E+01*	*4,46E+01*	*4,65E+01*
Δ [%]	*-52%*	*-47%*	*-17%*	*-4%*	-

Table 4.5 - *Von Mises stress RP3*

	Reference point 4				
	Mesh 200mm	***Mesh 150mm***	***Mesh 100mm***	***Mesh 75mm***	***Mesh 50mm***
	2,12E+01	*2,55E+01*	*3,31E+01*	*6,68E+01*	*6,65E+01*
	2,38E+01	*2,21E+01*	*6,77E+01*	*3,06E+01*	*2,98E+01*
	2,52E+01	*2,29E+01*	*5,79E+01*	*3,79E+01*	*3,71E+01*
	2,72E+01	*2,69E+01*	*5,67E+01*	*2,88E+01*	*2,93E+01*
	2,52E+01	*2,41E+01*	*5,08E+01*	*2,34E+01*	*2,39E+01*
	2,19E+01	*2,66E+01*	*4,98E+01*	*7,01E+01*	*6,96E+01*
	2,40E+01	*2,51E+01*	*3,26E+01*	*4,09E+01*	*4,59E+01*
	2,82E+01	*2,68E+01*	*5,04E+01*	*3,22E+01*	*3,19E+01*
	2,46E+01	*2,56E+01*	*3,76E+01*	*2,92E+01*	*2,84E+01*
	2,32E+01	*2,80E+01*	*4,30E+01*	*2,74E+01*	*3,34E+01*
	2,15E+01	*2,58E+01*	*3,52E+01*	*2,67E+01*	*2,62E+01*
	2,10E+01	*2,53E+01*	*6,09E+01*	*7,63E+01*	*7,58E+01*
	2,45E+01	*2,46E+01*	*4,32E+01*	-	*8,40E+01*
	2,43E+01	*2,22E+01*	*2,78E+01*	-	*2,78E+01*
	2,34E+01	-	*2,79E+01*	-	-
	2,19E+01	-	*3,29E+01*	-	-
Average	*2,26E+01*	*2,51E+01*	*4,42E+01*	*4,08E+01*	*4,16E+01*
Δ [%]	*-46%*	*-40%*	*6%*	*-2%*	-

Table 4.6 - *Von Mises stress RP4*

Reference point 5				
Mesh 200mm	**Mesh 150mm**	**Mesh 100mm**	**Mesh 75mm**	**Mesh 50mm**
8,44E+00	5,99E+00	6,24E+00	6,19E+00	5,89E+00
9,57E+00	6,12E+00	6,00E+00	6,26E+00	5,46E+00
8,62E+00	5,87E+00	6,06E+00	6,21E+00	5,41E+00
9,32E+00	5,72E+00	6,28E+00	6,36E+00	6,86E+00
9,44E+00	6,18E+00	6,00E+00	6,33E+00	4,33E+00
9,50E+00	6,21E+00	6,06E+00	6,25E+00	2,25E+00
8,15E+00	6,16E+00	6,16E+00	6,30E+00	1,13E+01
8,20E+00	5,71E+00	6,05E+00	6,25E+00	6,25E+00
8,17E+00	6,19E+00	6,28E+00	6,25E+00	5,45E+00
8,93E+00	5,85E+00	6,18E+00	6,28E+00	7,28E+00
8,82E+00	6,10E+00	6,13E+00	6,31E+00	5,81E+00
9,36E+00	6,11E+00	6,17E+00	6,18E+00	5,68E+00
8,68E+00	6,31E+00	6,27E+00	6,17E+00	7,17E+00
8,57E+00	6,04E+00	6,03E+00	6,15E+00	2,78E+01
8,98E+00	7,21E+00	5,89E+00	6,18E+00	5,18E+00
8,30E+00	7,01E+00	6,13E+00	6,27E+00	1,27E+00
1,07E+01	6,71E+00	6,06E+00	6,22E+00	5,42E+00
8,99E+00	7,00E+00	5,98E+00	6,11E+00	5,61E+00
9,75E+00	6,57E+00	5,99E+00	6,97E+00	7,47E+00
9,78E+00	6,70E+00	6,21E+00	6,91E+00	6,41E+00
1,02E+01	6,78E+00	6,14E+00	6,77E+00	6,77E+00
9,91E+00	6,98E+00	6,07E+00	6,76E+00	6,46E+00
1,08E+01	6,71E+00	5,99E+00	6,94E+00	6,14E+00
1,01E+01	6,75E+00	5,95E+00	6,98E+00	1,30E+01
-	-	7,06E+00	6,74E+00	6,24E+00
-	-	6,89E+00	6,92E+00	6,42E+00
-	-	7,01E+00	6,85E+00	6,98E+00
-	-	6,69E+00	6,98E+00	1,02E+01
-	-	6,68E+00	6,98E+00	6,68E+00
-	-	6,65E+00	6,90E+00	6,10E+00
-	-	6,99E+00	6,71E+00	-
-	-	6,81E+00	6,91E+00	-
-	-	6,79E+00	7,03E+00	-
-	-	7,15E+00	6,99E+00	-
-	-	6,91E+00	6,99E+00	-
-	-	7,13E+00	6,90E+00	-
-	-	6,80E+00	-	-
-	-	7,07E+00	-	-
-	-	6,80E+00	-	-
-	-	6,98E+00	-	-
-	-	6,99E+00	-	-
-	-	7,13E+00	-	-
-	-	6,77E+00	-	-

	-	-	*7,05E+00*	-	-
	-	-	*7,11E+00*	-	-
	-	-	*7,00E+00*	-	-
	-	-	*7,05E+00*	-	-
	-	-	*6,99E+00*	-	-
Average	*1,39E+01*	*6,37E+00*	*6,52E+00*	*6,57E+00*	*7,11E+00*
Δ [%]	*95%*	*-10%*	*-8%*	*-8%*	-

Table 4.7 - *Von Mises stress RP5*

Reference point 6				
Mesh 200mm	***Mesh 150mm***	***Mesh 100mm***	***Mesh 75mm***	***Mesh 50mm***
5,92E+00	*5,76E+00*	*6,13E+00*	*6,17E+00*	*5,87E+00*
5,80E+00	*5,89E+00*	*6,02E+00*	*6,17E+00*	*5,87E+00*
5,74E+00	*5,71E+00*	*5,95E+00*	*6,19E+00*	*5,89E+00*
5,50E+00	*5,66E+00*	*6,27E+00*	*6,37E+00*	*6,07E+00*
5,47E+00	*5,73E+00*	*6,26E+00*	*6,37E+00*	*6,07E+00*
5,89E+00	*5,69E+00*	*5,92E+00*	*6,23E+00*	*5,93E+00*
5,83E+00	*5,67E+00*	*6,21E+00*	*6,32E+00*	*6,02E+00*
6,22E+00	*5,77E+00*	*6,05E+00*	*6,05E+00*	*5,75E+00*
5,78E+00	*5,68E+00*	*5,91E+00*	*6,08E+00*	*5,78E+00*
5,53E+00	*5,81E+00*	*6,13E+00*	*6,14E+00*	*5,84E+00*
5,77E+00	*5,76E+00*	*5,91E+00*	*6,19E+00*	*5,89E+00*
5,75E+00	*5,88E+00*	*5,83E+00*	*6,23E+00*	*5,93E+00*
5,53E+00	*5,90E+00*	*6,03E+00*	*6,36E+00*	*1,04E+01*
6,93E+00	*5,75E+00*	*6,00E+00*	*6,18E+00*	*5,88E+00*
6,66E+00	*6,81E+00*	*5,90E+00*	*6,03E+00*	*6,33E+00*
6,61E+00	*6,80E+00*	*5,92E+00*	*6,12E+00*	*6,42E+00*
7,22E+00	*6,47E+00*	*5,87E+00*	*6,11E+00*	*6,41E+00*
6,75E+00	*6,80E+00*	*6,07E+00*	*6,07E+00*	*6,37E+00*
6,75E+00	*6,64E+00*	*6,03E+00*	*6,66E+00*	*6,96E+00*
6,99E+00	*6,88E+00*	*5,91E+00*	*6,78E+00*	*7,08E+00*
7,02E+00	*6,85E+00*	*6,25E+00*	*6,85E+00*	*6,55E+00*
7,17E+00	*6,63E+00*	*6,13E+00*	*6,76E+00*	*6,46E+00*
6,89E+00	*6,57E+00*	*6,00E+00*	*6,95E+00*	*6,65E+00*
6,62E+00	*6,76E+00*	*5,92E+00*	*6,93E+00*	*6,63E+00*
6,94E+00	*6,75E+00*	*6,72E+00*	*6,90E+00*	*6,60E+00*
6,99E+00	*6,70E+00*	*6,82E+00*	*6,92E+00*	*6,62E+00*
7,11E+00	-	*6,62E+00*	*6,84E+00*	*6,54E+00*
6,55E+00	-	*6,72E+00*	*6,98E+00*	*6,68E+00*
6,94E+00	-	*6,72E+00*	*6,85E+00*	*6,55E+00*
6,94E+00	-	*6,93E+00*	*6,85E+00*	*6,55E+00*
6,89E+00	-	*6,61E+00*	*6,85E+00*	*6,55E+00*
6,91E+00	-	*6,85E+00*	*6,83E+00*	*6,53E+00*
-	-	*6,94E+00*	*6,95E+00*	*1,19E+01*

	-	*-*	*6,84E+00*	*6,83E+00*	*-*
	-	*-*	*7,11E+00*	*6,66E+00*	*-*
	-	*-*	*6,77E+00*	*6,84E+00*	*-*
	-	*-*	*6,81E+00*	*-*	*-*
	-	*-*	*6,81E+00*	*-*	*-*
	-	*-*	*6,99E+00*	*-*	*-*
	-	*-*	*6,96E+00*	*-*	*-*
	-	*-*	*7,03E+00*	*-*	*-*
	-	*-*	*7,08E+00*	*-*	*-*
	-	*-*	*6,94E+00*	*-*	*-*
	-	*-*	*6,93E+00*	*-*	*-*
	-	*-*	*7,06E+00*	*-*	*-*
	-	*-*	*6,77E+00*	*-*	*-*
	-	*-*	*6,74E+00*	*-*	*-*
	-	*-*	*6,70E+00*	*-*	*-*
Average	*1,12E+01*	*6,20E+00*	*6,44E+00*	*6,52E+00*	*6,59E+00*
Δ [%]	*70%*	*-6%*	*-2%*	*-1%*	*-*

Table 4.8 - *Von Mises stress RP6*

	Reference point 7				
	Mesh 200mm	***Mesh 150mm***	***Mesh 100mm***	***Mesh 75mm***	***Mesh 50mm***
	1,85E+01	*1,62E+01*	*2,37E+01*	*1,96E+01*	*1,99E+01*
	1,96E+01	*1,64E+01*	*1,80E+01*	*2,11E+01*	*2,14E+01*
	1,95E+01	*1,67E+01*	*1,43E+01*	*2,08E+01*	*2,11E+01*
	1,86E+01	*1,71E+01*	*4,28E+01*	*2,19E+01*	*2,22E+01*
	1,86E+01	*1,87E+01*	*3,41E+01*	*2,11E+01*	*2,14E+01*
	2,04E+01	*1,70E+01*	*1,97E+01*	*2,67E+01*	*2,70E+01*
	2,22E+01	*1,45E+01*	*2,00E+00*	*2,05E+01*	*2,08E+01*
	1,99E+01	*1,44E+01*	*5,35E+01*	*2,37E+01*	*2,40E+01*
	2,00E+01	*1,87E+01*	*1,70E+01*	*2,43E+01*	*2,46E+01*
	1,92E+01	*1,81E+01*	*-*	*2,19E+01*	*2,22E+01*
	1,97E+01	*1,91E+01*	*-*	*2,44E+01*	*2,47E+01*
	2,08E+01	*1,79E+01*	*-*	*2,44E+01*	*2,47E+01*
	2,00E+01	*1,79E+01*	*-*	*1,79E+01*	*1,82E+01*
	2,08E+01	*1,77E+01*	*-*	*-*	*-*
	1,98E+01	*-*	*-*	*-*	*-*
	2,04E+01	*-*	*-*	*-*	*-*
Average	*2,06E+01*	*1,72E+01*	*2,50E+01*	*2,25E+01*	*2,28E+01*
Δ [%]	*-10%*	*-25%*	*9%*	*-1%*	*-*

Table 4.9 - *Von Mises stress RP7*

	Reference point 8				
	Mesh 200mm	**Mesh 150mm**	**Mesh 100mm**	**Mesh 75mm**	**Mesh 50mm**
	1,62E+01	*1,68E+01*	*2,36E+01*	*1,46E+01*	*1,49E+01*
	1,63E+01	*1,62E+01*	*1,34E+01*	*2,24E+01*	*2,27E+01*
	1,71E+01	*1,71E+01*	*1,13E+01*	*1,70E+01*	*1,73E+01*
	1,60E+01	*1,76E+01*	*1,79E+01*	*2,12E+01*	*2,15E+01*
	1,57E+01	*1,73E+01*	*1,76E+01*	*2,32E+01*	*2,35E+01*
	1,65E+01	*1,78E+01*	*1,81E+01*	*2,17E+01*	*2,20E+01*
	1,74E+01	*1,87E+01*	*1,90E+01*	*2,27E+01*	*2,22E+01*
	1,69E+01	*1,98E+01*	*2,01E+01*	*1,45E+01*	*1,40E+01*
	1,78E+01	*1,87E+01*	*1,90E+01*	*1,72E+01*	*1,67E+01*
	1,65E+01	*1,79E+01*	*1,82E+01*	*1,63E+01*	*1,66E+01*
	1,77E+01	*1,98E+01*	*1,16E+01*	*1,61E+01*	*2,11E+01*
	1,99E+01	*1,62E+01*	*1,62E+01*	*2,13E+01*	-
	1,69E+01	*1,79E+01*	*2,69E+01*	*1,61E+01*	-
	1,79E+01	*1,79E+01*	*1,99E+01*	*1,77E+01*	-
	1,82E+01	-	*1,74E+01*	-	-
	1,80E+01	-	-	-	-
	1,79E+01	-	-	-	-
	1,78E+01	-	-	-	-
Average	*1,91E+01*	*1,79E+01*	*1,85E+01*	*1,87E+01*	*1,93E+01*
Δ [%]	*-1%*	*-8%*	*-4%*	*-3%*	-

Table 4.10 - *Von Mises stress RP8*

Reference point 9				
Mesh 200mm	**Mesh 150mm**	**Mesh 100mm**	**Mesh 75mm**	**Mesh 50mm**
4,29E+00	*5,64E+00*	*6,63E+00*	*6,74E+00*	*7,04E+00*
4,75E+00	*5,65E+00*	*6,58E+00*	*6,74E+00*	*7,04E+00*
5,32E+00	*6,43E+00*	*6,67E+00*	*6,70E+00*	*7,00E+00*
4,95E+00	*6,54E+00*	*6,63E+00*	*6,82E+00*	*7,12E+00*
4,42E+00	*6,54E+00*	*6,71E+00*	*6,84E+00*	*7,14E+00*
5,69E+00	*6,28E+00*	*6,72E+00*	*6,78E+00*	*7,08E+00*
5,56E+00	*5,46E+00*	*6,16E+00*	*6,41E+00*	*6,71E+00*
5,24E+00	*5,89E+00*	*6,15E+00*	*6,67E+00*	*6,97E+00*
5,47E+00	*6,59E+00*	-	*6,35E+00*	*6,65E+00*
5,47E+00	*6,42E+00*	-	*6,47E+00*	*6,77E+00*
5,02E+00	*6,81E+00*	-	*6,61E+00*	*6,91E+00*
4,87E+00	*6,51E+00*	-	*6,24E+00*	*6,54E+00*
1,25E+01	-	-	*6,34E+00*	*6,64E+00*

	-	-	-	6,66E+00	6,96E+00
	-	-	-	6,17E+00	-
	-	-	-	6,36E+00	-
	-	-	-	6,63E+00	-
	-	-	-	6,20E+00	-
Average	*1,25E+01*	*6,23E+00*	*6,53E+00*	*6,54E+00*	*6,90E+00*
Δ [%]	*82%*	*-10%*	*-5%*	*-5%*	*-*

Table 4.11 - *Von Mises stress RP9*

	Reference point 10				
	Mesh 200mm	***Mesh 150mm***	***Mesh 100mm***	***Mesh 75mm***	***Mesh 50mm***
	6,29E+00	*6,02E+00*	*6,75E+00*	*6,55E+00*	*6,85E+00*
	5,40E+00	*6,38E+00*	*6,00E+00*	*6,75E+00*	*7,05E+00*
	6,73E+00	*5,86E+00*	*6,60E+00*	*6,28E+00*	*6,58E+00*
	5,66E+00	*5,69E+00*	*6,54E+00*	*6,89E+00*	*7,19E+00*
	5,21E+00	*5,44E+00*	*6,68E+00*	*6,83E+00*	*7,13E+00*
	5,96E+00	*5,43E+00*	*6,73E+00*	*6,89E+00*	*7,19E+00*
	6,36E+00	*6,48E+00*	*6,83E+00*	*6,84E+00*	*7,14E+00*
	6,51E+00	*6,61E+00*	*6,77E+00*	*6,93E+00*	*7,23E+00*
	5,18E+00	*6,84E+00*	*6,10E+00*	*6,86E+00*	*7,16E+00*
	6,23E+00	*5,63E+00*	*6,30E+00*	*6,72E+00*	*7,02E+00*
	6,70E+00	*5,40E+00*	*6,39E+00*	*6,45E+00*	*6,75E+00*
	5,78E+00	*5,75E+00*	*6,62E+00*	*6,44E+00*	*6,74E+00*
	6,61E+00	*6,64E+00*	*6,35E+00*	*6,71E+00*	*4,71E+00*
	6,59E+00	*6,65E+00*	*6,20E+00*	*6,25E+00*	*-*
	-	*6,67E+00*	*-*	*6,28E+00*	*-*
	-	*6,59E+00*	*-*	*6,73E+00*	*-*
Average	*1,33E+01*	*6,13E+00*	*6,49E+00*	*6,65E+00*	*6,83E+00*
Δ [%]	*95%*	*-10%*	*-5%*	*-3%*	*-*

Table 4.12 - *Von Mises stress RP10*

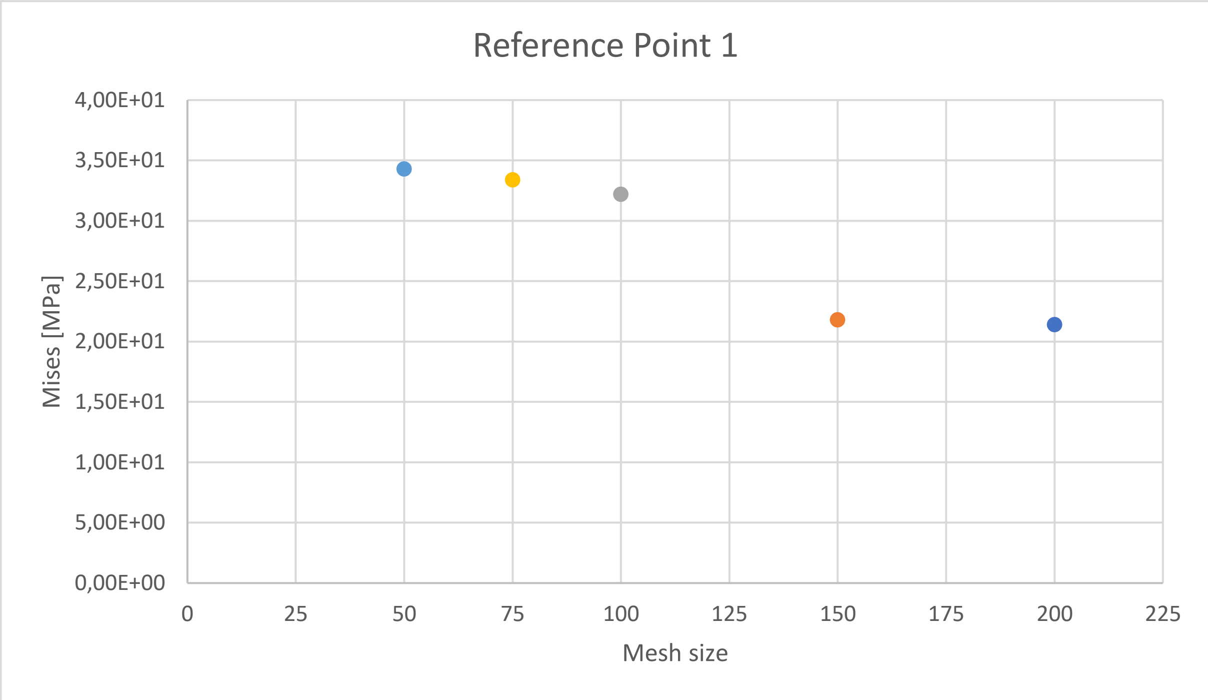

Table 4.13 - *Von Mises stress-Mesh size RP1*

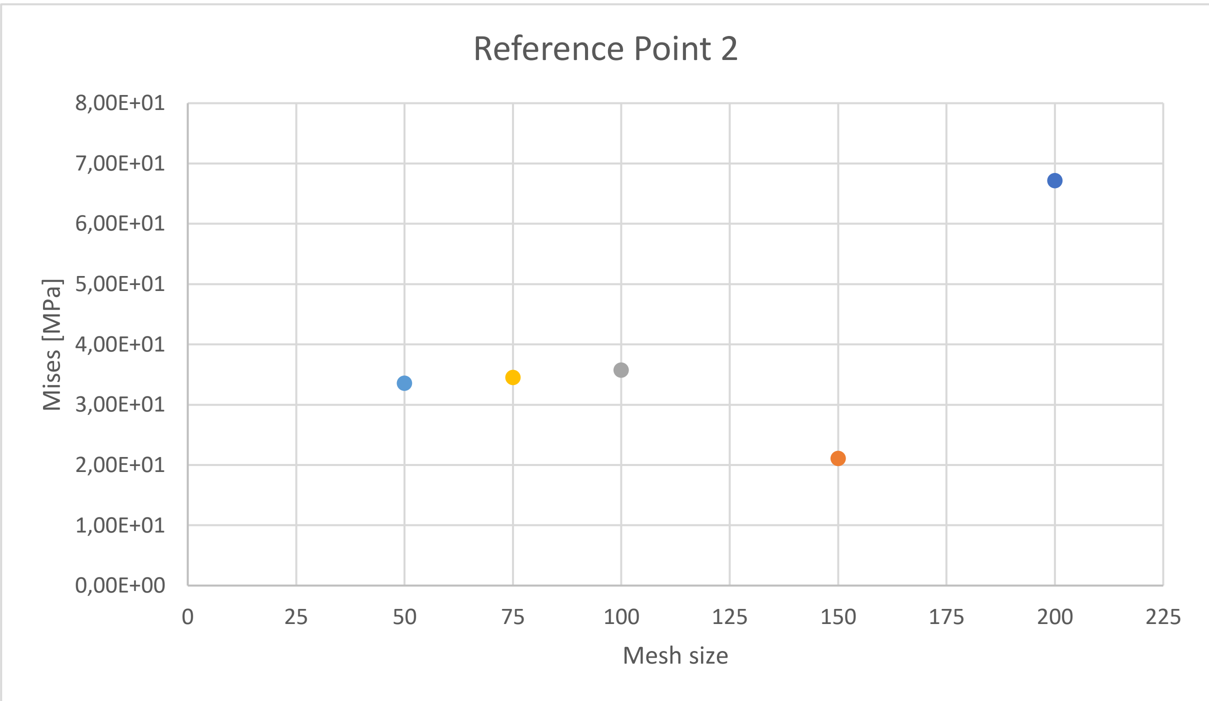

Table 4.14 - *Von Mises stress-Mesh size RP2*

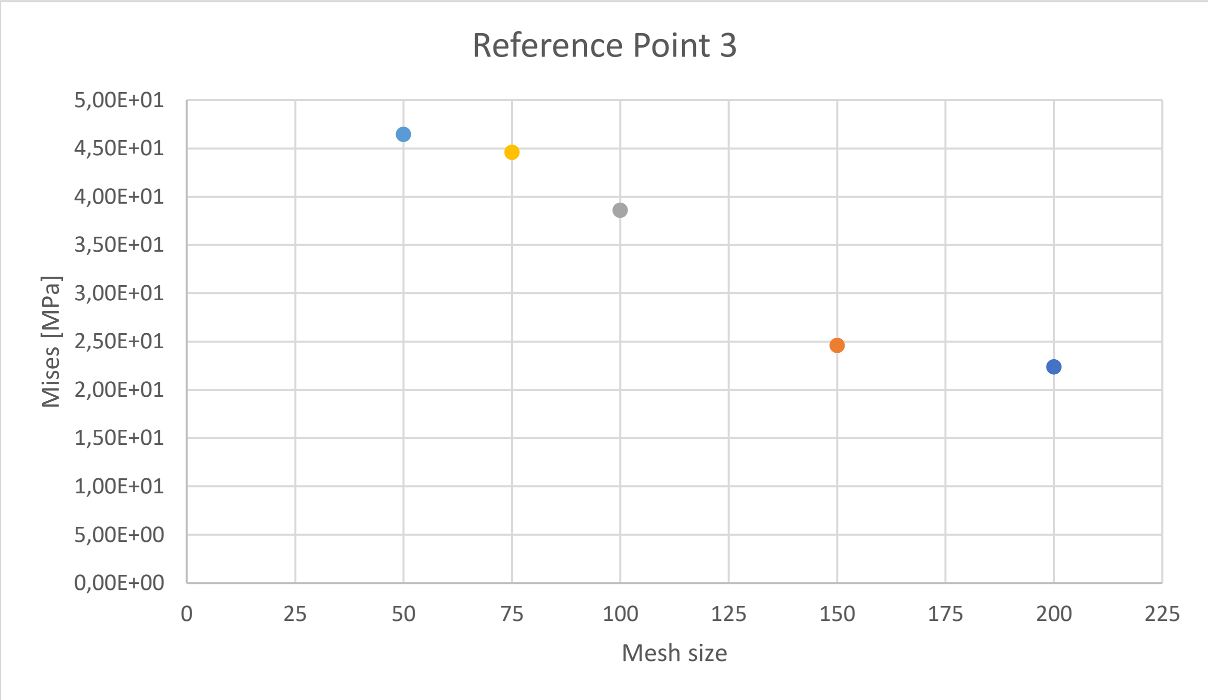

Table 4.15 - *Von Mises stress-Mesh size RP3*

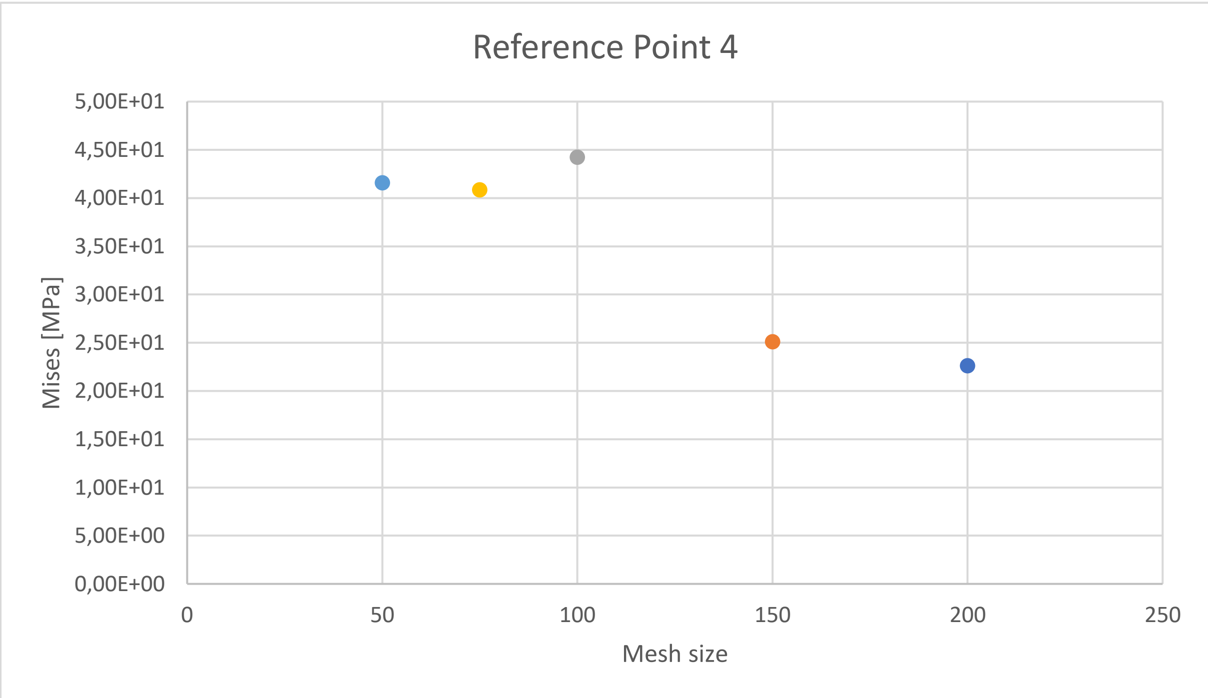

Table 4.16 - *Von Mises stress-Mesh size RP4*

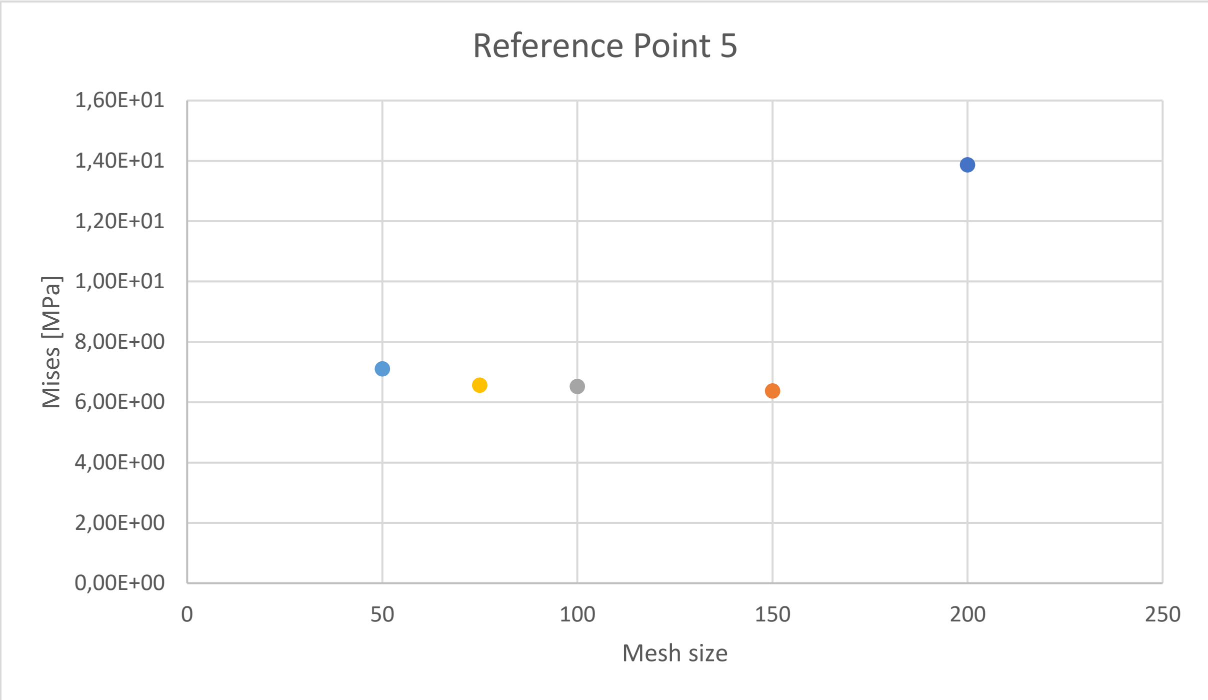

Table 4.17 - *Von Mises stress-Mesh size RP5*

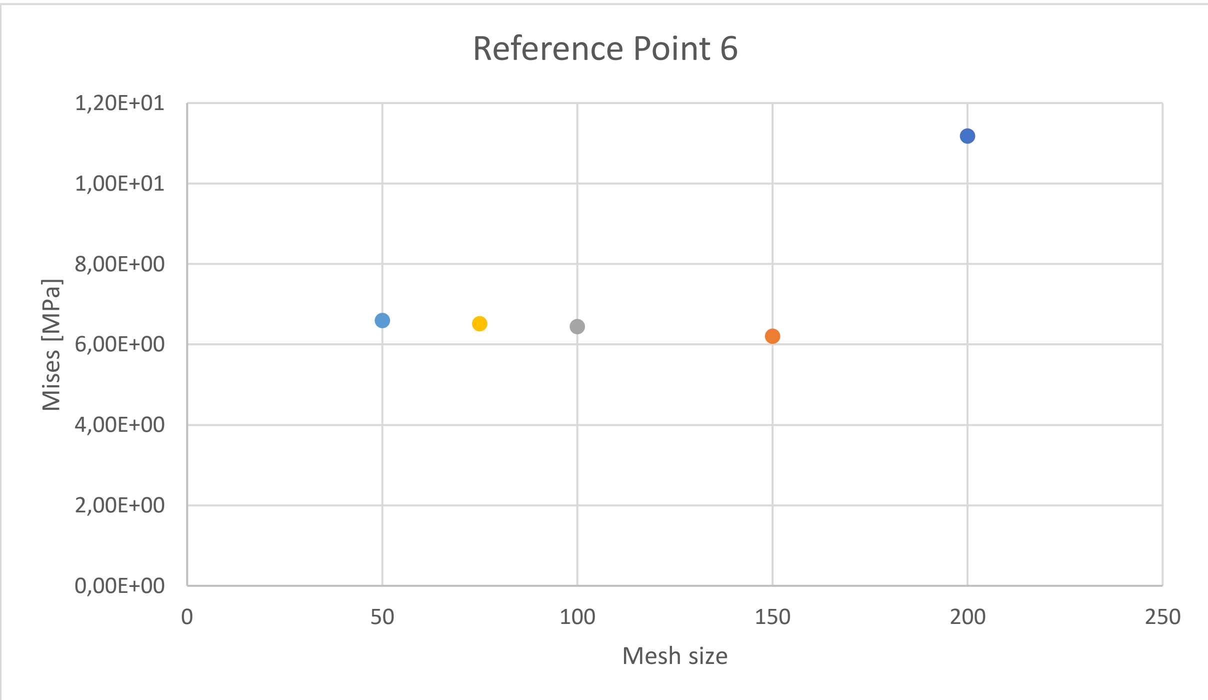

Table 4.18 - *Von Mises stress-Mesh size RP6*

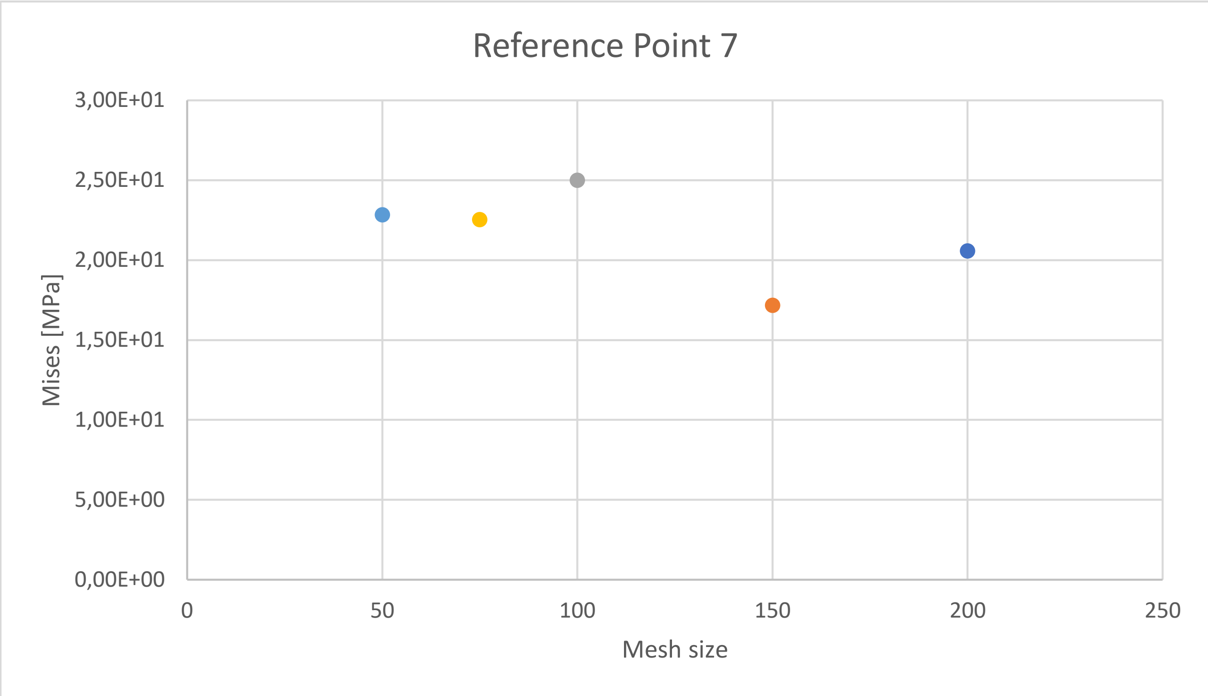

Table 4.19 - *Von Mises stress-Mesh size RP7*

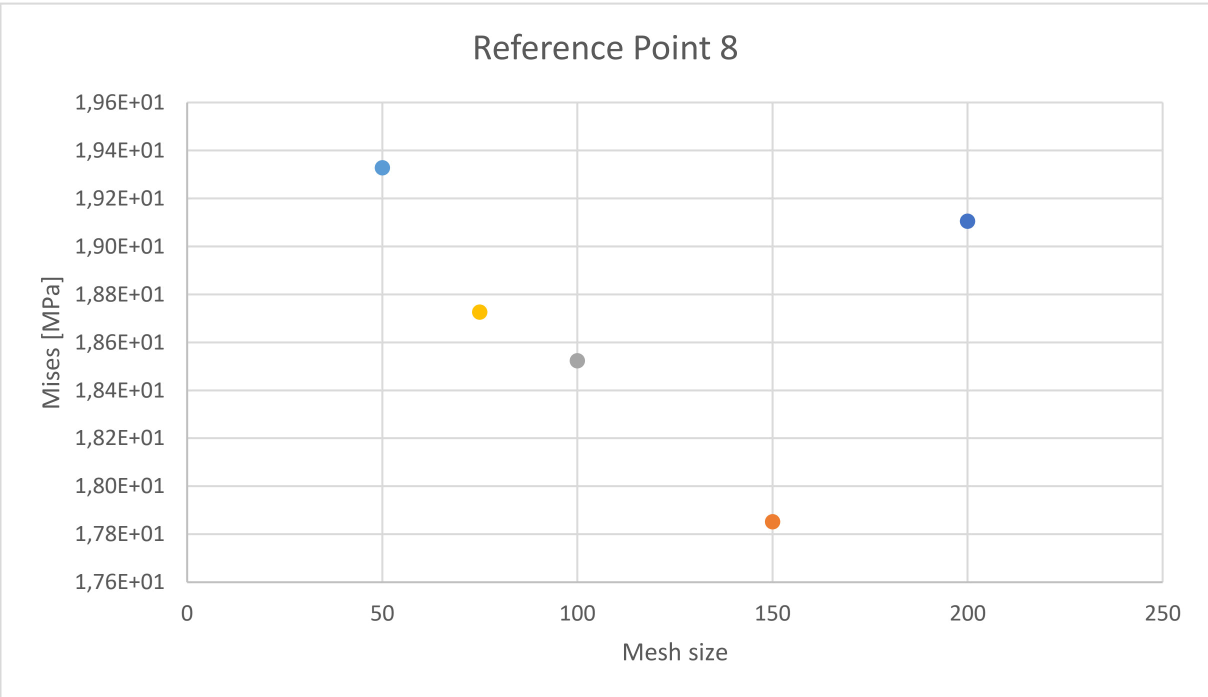

Table 4.20 - *Von Mises stress-Mesh size RP8*

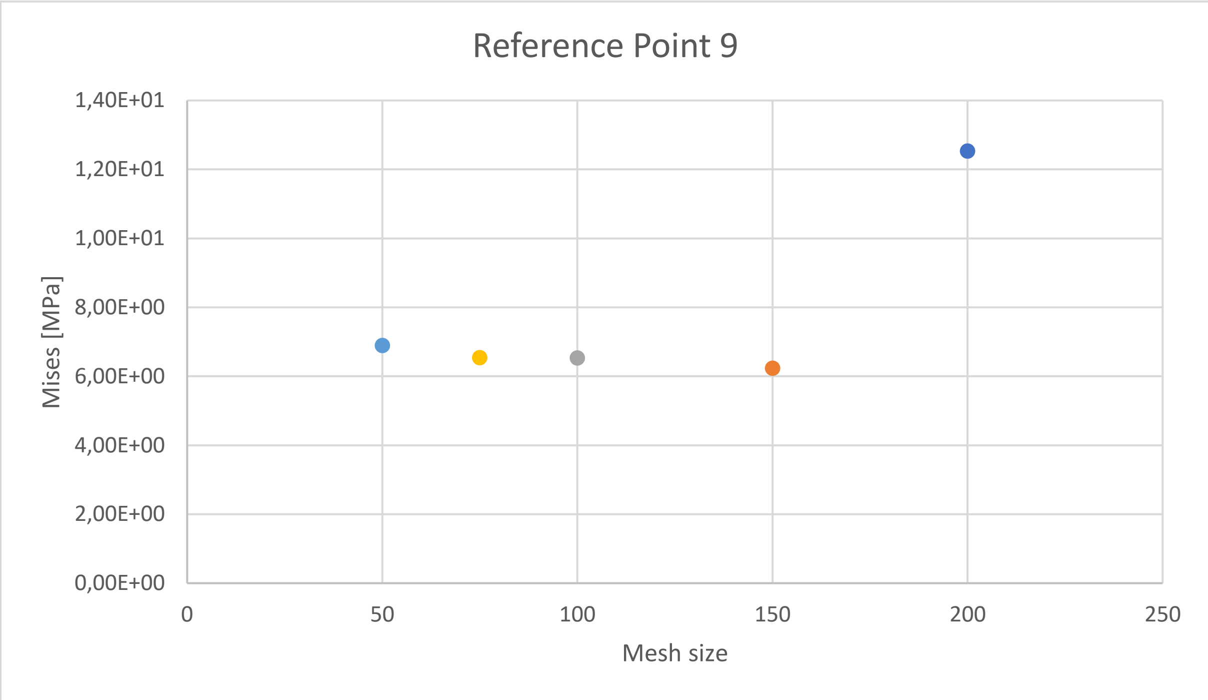

Table 4.21 - *Von Mises stress-Mesh size RP9*

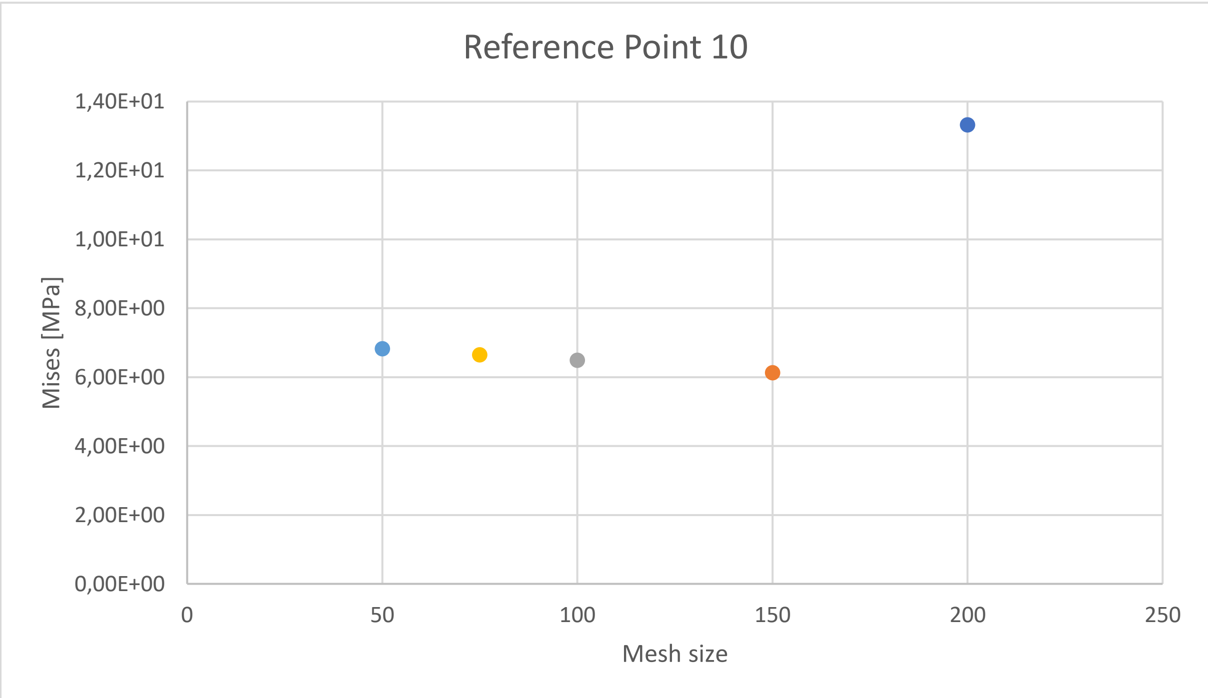

Table 4.22 - *Von Mises stress-Mesh size RP10*

These results indicate that, except the 250 mm mesh, which did not converged, the values begin to become relatively constant as the mesh size decrease: in particular, as can be seen from the tables and the figures, using a mesh size between 100 and 50 mm produces almost similar results.
In order to validate these two "local models", a check on the Von Mises stresses was performed, using the same mesh size (50 mm^2); as described in the following tables.
Definitely, as it can be seen in the following tables, it is evident that the two local models behave not too much different from the global model: in fact, the average difference percentage between them is of -9%, which is acceptable. This check about the Von Mises stresses was both necessary to justify their adoption in the linear and non-linear analysis.

	Reference Point 1		
	Tower 1 model	***Tower 2 model***	***Complete model***
	-	*2,42E+01*	*3,34E+01*
	-	*2,02E+01*	*1,59E+01*
	-	*2,36E+01*	*3,36E+01*
	-	*3,38E+01*	*4,34E+01*
	-	*2,84E+01*	*3,51E+01*
	-	*2,86E+01*	*3,46E+01*
	-	*5,21E+01*	*3,77E+01*
	-	*2,60E+01*	*3,93E+01*
	-	*2,70E+01*	*3,58E+01*
	-	*2,97E+01*	*2,56E+01*
	-	*2,28E+01*	*6,58E+01*
	-	*2,24E+01*	*5,40E+01*
	-	*2,90E+01*	*1,85E+01*
	-	*3,12E+01*	*1,40E+01*
	-	*2,88E+01*	*1,98E+01*
	-	*2,52E+01*	*5,20E+01*
	-	*3,03E+01*	*3,41E+01*
	-	*2,34E+01*	*2,48E+01*
	-	*2,82E+01*	-
	-	*6,55E+01*	-
	-	*2,95E+01*	-
	-	*2,75E+01*	-
Average	-	*2,99E+01*	*3,43E+01*
Δ [%]	-	*-13%*	-

Table 4.23 - *Check local - complete model (RP1)*

	Reference Point 2		
	Tower 1 model	***Tower 2 model***	***Complete model***
	2,42E+01	-	*5,33E+01*
	5,63E+01	-	*5,59E+01*
	3,40E+01	-	*2,67E+01*
	2,73E+01	-	*2,46E+01*
	2,72E+01	-	*2,50E+01*
	2,49E+01	-	*3,15E+01*
	2,22E+01	-	*2,86E+01*
	3,86E+01	-	*2,72E+01*
	4,53E+01	-	*3,11E+01*
	2,65E+01	-	*3,24E+01*
	2,64E+01	-	*5,89E+01*
	3,36E+01	-	*3,10E+01*
	2,43E+01	-	*2,82E+01*
	3,19E+01	-	*3,24E+01*
	-	-	*2,89E+01*
	-	-	*2,92E+01*
	-	-	*3,92E+01*
	-	-	*4,58E+01*
Average	*2,99E+01*	-	*3,35E+01*
Δ [%]	*-11%*	-	-

Table 4.24 - *Check local - complete model (RP2)*

Reference Point 3		
Tower 1 model	***Tower 2 model***	***Complete model***
-	*5,14E+01*	*4,88E+01*
-	*3,44E+01*	*5,30E+01*
-	*4,68E+01*	*5,94E+01*
-	*3,31E+01*	*6,58E+01*
-	*2,21E+01*	*4,24E+01*
-	*4,45E+01*	*4,65E+01*
-	*3,06E+01*	*6,58E+01*
-	*2,98E+01*	*1,45E+01*
-	*6,03E+01*	*4,82E+01*
-	*4,39E+01*	*4,59E+01*
-	*3,40E+01*	*2,07E+01*
-	*6,49E+01*	-
-	*4,93E+01*	-

	-	*3,60E+01*	-
	-	*5,38E+01*	-
	-	*4,35E+01*	-
Average	-	*4,24E+01*	*4,65E+01*
Δ [%]	-	*-9%*	-

Table 4.25 - *Check local - complete model (RP3)*

	Reference Point 4		
	Tower 1 model	***Tower 2 model***	***Complete model***
	4,35E+01	-	*6,65E+01*
	3,71E+01	-	*2,98E+01*
	3,13E+01	-	*3,71E+01*
	3,47E+01	-	*2,93E+01*
	2,86E+01	-	*2,39E+01*
	2,59E+01	-	*6,96E+01*
	6,80E+01	-	*4,59E+01*
	2,78E+01	-	*3,19E+01*
	4,50E+01	-	*2,84E+01*
	2,48E+01	-	*3,34E+01*
	7,47E+01	-	*2,62E+01*
	4,51E+01	-	*7,58E+01*
	2,33E+01	-	*2,78E+01*
	4,31E+01	-	*8,40E+01*
	3,14E+01	-	-
	8,34E+01	-	-
	-	-	-
Average	*3,52E+01*	-	*4,16E+01*
Δ [%]	*-15%*	-	-

Table 4.26 - *Check local - complete model (RP4)*

	Reference Point 5		
	Tower 1 model	***Tower 2 model***	***Complete model***
	7,11E+00	*-*	*5,89E+00*
	7,00E+00	*-*	*5,46E+00*
	7,25E+00	*-*	*5,41E+00*
	7,00E+00	*-*	*6,86E+00*
	7,22E+00	*-*	*4,33E+00*
	7,07E+00	*-*	*2,25E+00*
	7,03E+00	*-*	*1,13E+01*
	7,16E+00	*-*	*6,25E+00*
	7,10E+00	*-*	*5,45E+00*
	7,00E+00	*-*	*7,28E+00*
	6,99E+00	*-*	*5,81E+00*
	7,00E+00	*-*	*5,68E+00*
	7,08E+00	*-*	*7,17E+00*
	7,25E+00	*-*	*2,78E+01*
	6,81E+00	*-*	*5,18E+00*
	6,72E+00	*-*	*1,27E+00*
	6,68E+00	*-*	*5,42E+00*
	6,56E+00	*-*	*5,61E+00*
	6,80E+00	*-*	*7,47E+00*
	6,63E+00	*-*	*6,41E+00*
	6,81E+00	*-*	*6,77E+00*
	6,85E+00	*-*	*6,46E+00*
	6,70E+00	*-*	*6,14E+00*
	6,75E+00	*-*	*1,30E+01*
	6,75E+00	*-*	*6,24E+00*
	6,66E+00	*-*	*6,42E+00*
	6,56E+00	*-*	*6,98E+00*
	6,66E+00	*-*	*1,02E+01*
	-	*-*	*6,68E+00*
	-	*-*	*6,10E+00*
Average	*6,90E+00*	*-*	*7,11E+00*
Δ [%]	*-3%*	*-*	*-*

Table 4.27 - *Check local - complete model (RP5)*

	Reference Point 6		
	Tower 1 model	***Tower 2 model***	***Complete model***
	-	6,57E+00	5,87E+00
	-	6,66E+00	5,87E+00
	-	6,92E+00	5,89E+00
	-	6,88E+00	6,07E+00
	-	6,68E+00	6,07E+00
	-	6,60E+00	5,93E+00
	-	6,63E+00	6,02E+00
	-	6,89E+00	5,75E+00
	-	6,62E+00	5,78E+00
	-	6,63E+00	5,84E+00
	-	6,78E+00	5,89E+00
	-	6,59E+00	5,93E+00
	-	6,58E+00	1,04E+01
	-	6,82E+00	5,88E+00
	-	6,76E+00	6,33E+00
	-	6,78E+00	6,42E+00
	-	6,80E+00	6,41E+00
	-	6,93E+00	6,37E+00
	-	7,36E+00	6,96E+00
	-	7,31E+00	7,08E+00
	-	7,09E+00	6,55E+00
	-	7,08E+00	6,46E+00
	-	7,25E+00	6,65E+00
	-	7,02E+00	6,63E+00
	-	7,26E+00	6,60E+00
	-	7,03E+00	6,62E+00
	-	7,07E+00	6,54E+00
	-	7,28E+00	6,68E+00
	-	7,14E+00	6,55E+00
	-	7,16E+00	6,55E+00
	-	7,35E+00	6,55E+00
	-	7,36E+00	6,53E+00
	-	7,33E+00	1,19E+01
	-	6,29E+00	-
	-	7,14E+00	-
	-	7,14E+00	-
Average	-	6,94E+00	6,59E+00
Δ [%]	-	5%	-

Table 4.28 - *Check local - complete model (RP6)*

	Reference Point 7		
	Tower 1 model	***Tower 2 model***	***Complete model***
	2,59E+01	*-*	*1,99E+01*
	2,57E+01	*-*	*2,14E+01*
	2,68E+01	*-*	*2,11E+01*
	1,64E+01	*-*	*2,22E+01*
	1,63E+01	*-*	*2,14E+01*
	2,64E+01	*-*	*2,70E+01*
	1,62E+01	*-*	*2,08E+01*
	2,70E+01	*-*	*2,40E+01*
	1,64E+01	*-*	*2,46E+01*
	1,68E+01	*-*	*2,22E+01*
	2,64E+01	*-*	*2,47E+01*
	3,70E+01	*-*	*2,47E+01*
	-	*-*	*1,82E+01*
Average	*1,98E+01*	*-*	*2,25E+01*
Δ [%]	*-12%*	*-*	*-*

Table 4.29 - *Check local - complete model (RP7)*

	Reference Point 8		
	Tower 1 model	***Tower 2 model***	***Complete model***
	-	*1,58E+01*	*1,49E+01*
	-	*1,67E+01*	*2,27E+01*
	-	*1,71E+01*	*1,73E+01*
	-	*1,66E+01*	*2,15E+01*
	-	*1,56E+01*	*2,35E+01*
	-	*1,59E+01*	*2,20E+01*
	-	*1,61E+01*	*2,22E+01*
	-	*1,66E+01*	*1,40E+01*
	-	*1,67E+01*	*1,67E+01*
	-	*1,68E+01*	*1,66E+01*
	-	*1,67E+01*	*1,51E+01*
	-	*1,70E+01*	*-*
	-	*1,61E+01*	*-*
	-	*1,66E+01*	*-*
Average	*-*	*1,64E+01*	*1,88E+01*
Δ [%]	*-*	*-12%*	*-*

Table 4.30 - *Check local - complete model (RP8)*

	Reference Point 9		
	Tower 1 model	***Tower 2 model***	***Complete model***
	7,69E+00	*-*	*7,04E+00*
	6,72E+00	*-*	*7,04E+00*
	7,73E+00	*-*	*7,00E+00*
	5,70E+00	*-*	*7,12E+00*
	5,67E+00	*-*	*7,14E+00*
	7,67E+00	*-*	*7,08E+00*
	5,37E+00	*-*	*6,71E+00*
	7,36E+00	*-*	*6,97E+00*
	5,44E+00	*-*	*6,65E+00*
	6,41E+00	*-*	*6,77E+00*
	6,39E+00	*-*	*6,91E+00*
	5,63E+00	*-*	*6,54E+00*
	7,62E+00	*-*	*6,64E+00*
	6,41E+00	*-*	*6,96E+00*
Average	*6,06E+00*	*-*	*6,90E+00*
Δ [%]	*-12%*	*-*	*-*

Table 4.31 - *Check local - complete model (RP9)*

	Reference Point 10		
	Tower 1 model	***Tower 2 model***	***Complete model***
	-	*6,49E+00*	*6,85E+00*
	-	*5,85E+00*	*7,05E+00*
	-	*5,80E+00*	*6,58E+00*
	-	*7,84E+00*	*7,19E+00*
	-	*5,82E+00*	*7,13E+00*
	-	*5,82E+00*	*7,19E+00*
	-	*5,82E+00*	*7,14E+00*
	-	*5,50E+00*	*7,23E+00*
	-	*7,53E+00*	*7,16E+00*
	-	*5,50E+00*	*7,02E+00*
	-	*5,52E+00*	*6,75E+00*
	-	*5,52E+00*	*6,74E+00*
	-	*6,78E+00*	*4,71E+00*
	-	*5,76E+00*	*-*
Average	*-*	*6,11E+00*	*6,83E+00*
Δ [%]	*-*	*-11%*	*-*

Table 4.32 - *Check local - complete model (RP10)*

5 Analysis

5.1 Linear Static Analysis

In the last chapter, a linear static analysis was initially performed to get information about the mesh size to use and to validate the local models (figure 4.3), which were then employed to perform whether the linear and the non-linear analysis.
In particular, for what concerns the linear analysis, both models were analysed using:

- a mesh size of 50 mm;
- loads and boundary conditions (section 3 - 4.3.4);
- linear behaviour for concrete (section 2.1 – 4.3.1);
- elastic behaviour for reinforcement (section 2.4 – 4.3.2).

As a result of the linear static analysis, it was chosen to pay particular attention about how the stresses evolve with height. The distribution was evaluated referring to a vertical axis, passing through the two reference points, which are located exactly in the middle of the concrete support surface (the surface where the steel saddle lays on) and in the middle of the concrete bottom part. Furthermore, Abaqus allows the user to create a path on which the data are calculated and plotted with the distance from the starting point to the ending point: this path, depicted in figure 5.1a-5.1b, was created locating the exact position of the points for both the local models.

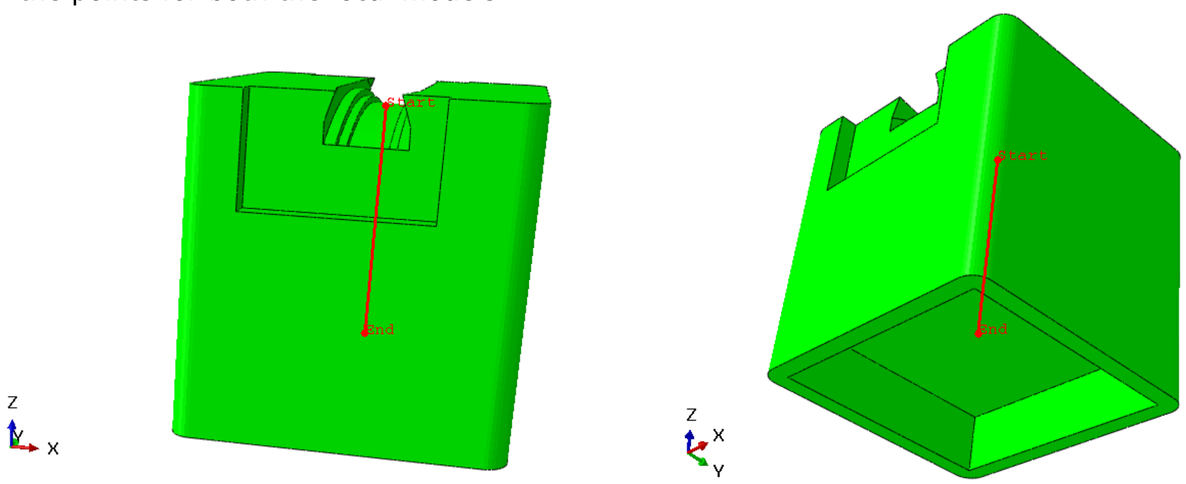

Figure 5.1 - *Path - local model #1*

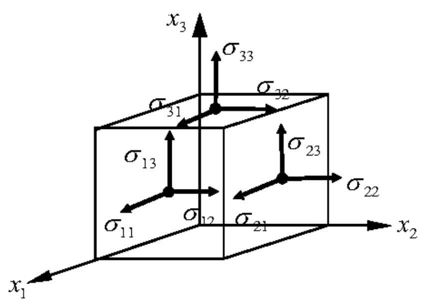

Figure 5.2 - *Tensor stress*

Finally, stress distribution in *X* (axis 1) and *Y* (axis 2) direction were plotted along the distance, in particular (figure 5.2-5.12):

- normal stresses (σ_{11} – σ_{22});
- shear stress (σ_{12} – σ_{13} – σ_{23});

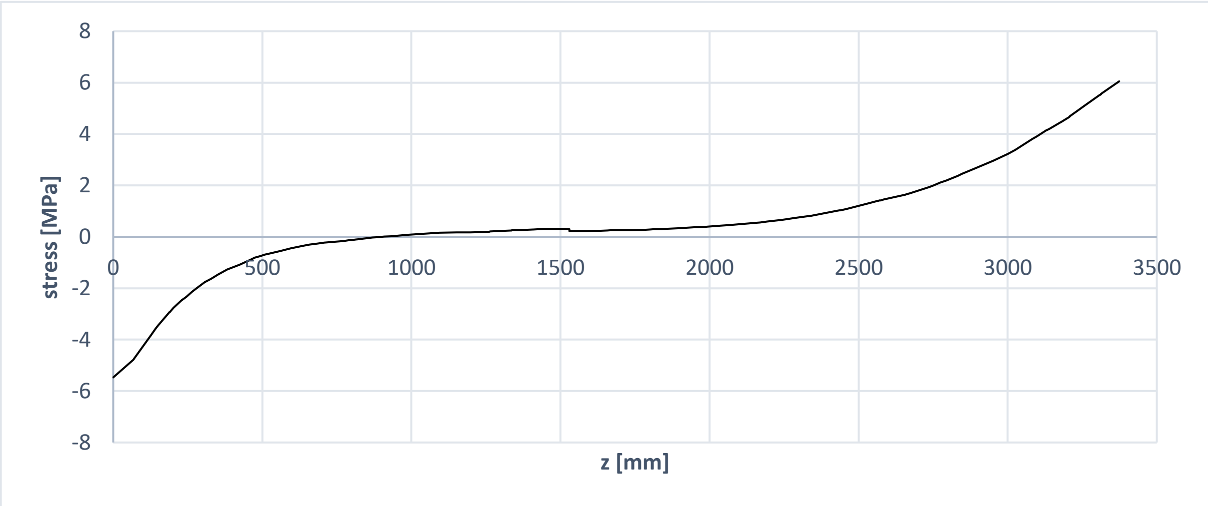

Figure 5.3 - *Normal stress σ_{11} – z (local model #1)*

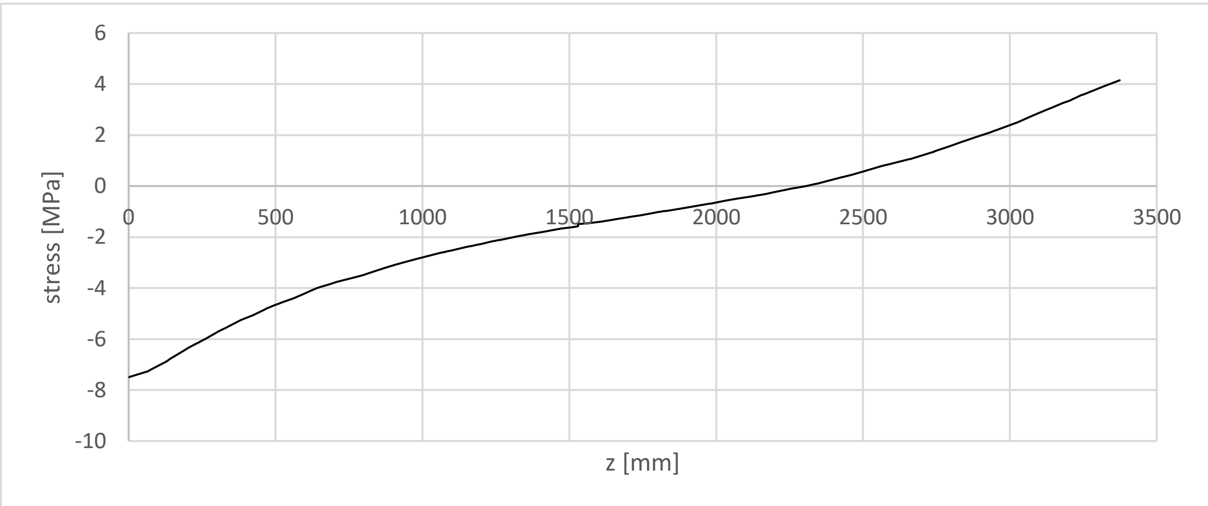

Figure 5.4 - *Normal stress σ_{22} – z (local model #1)*

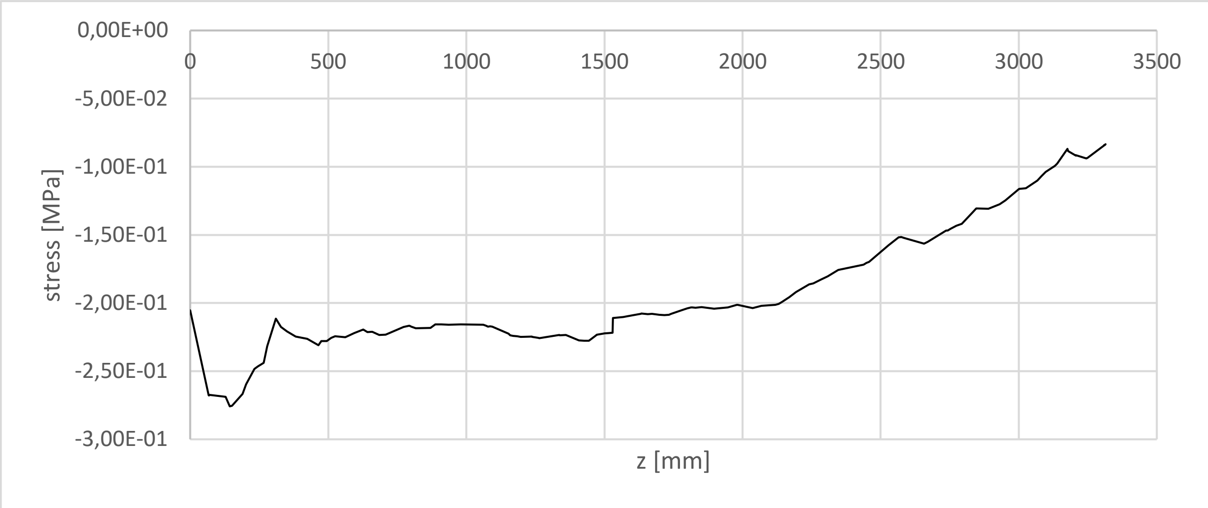

Figure 5.5 - *Shear stress σ₁₂ – z (local model #1)*

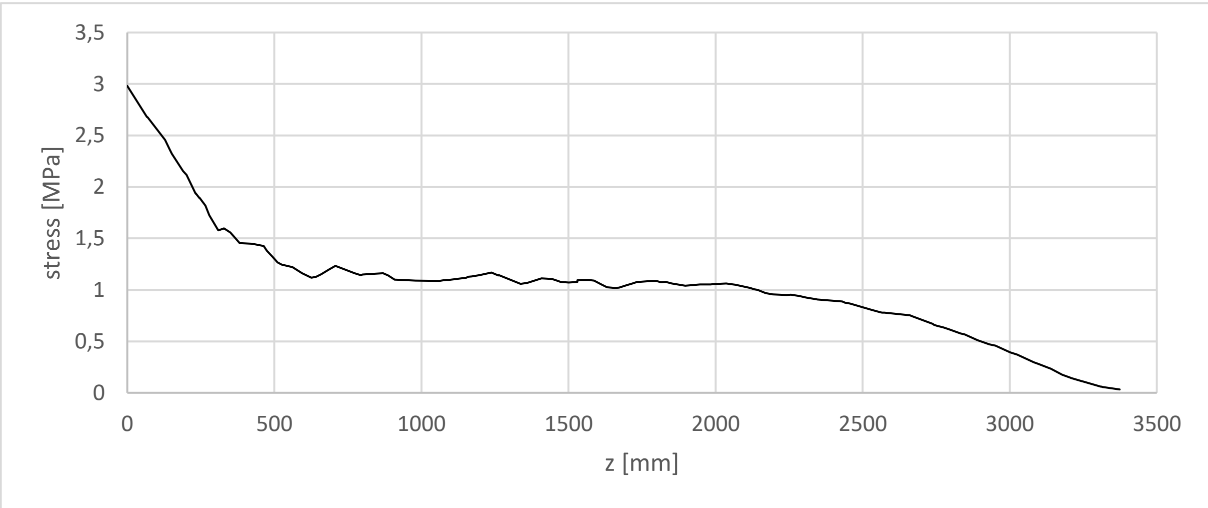

Figure 5.6 - *Shear stress σ₁₃ – z (local model #1)*

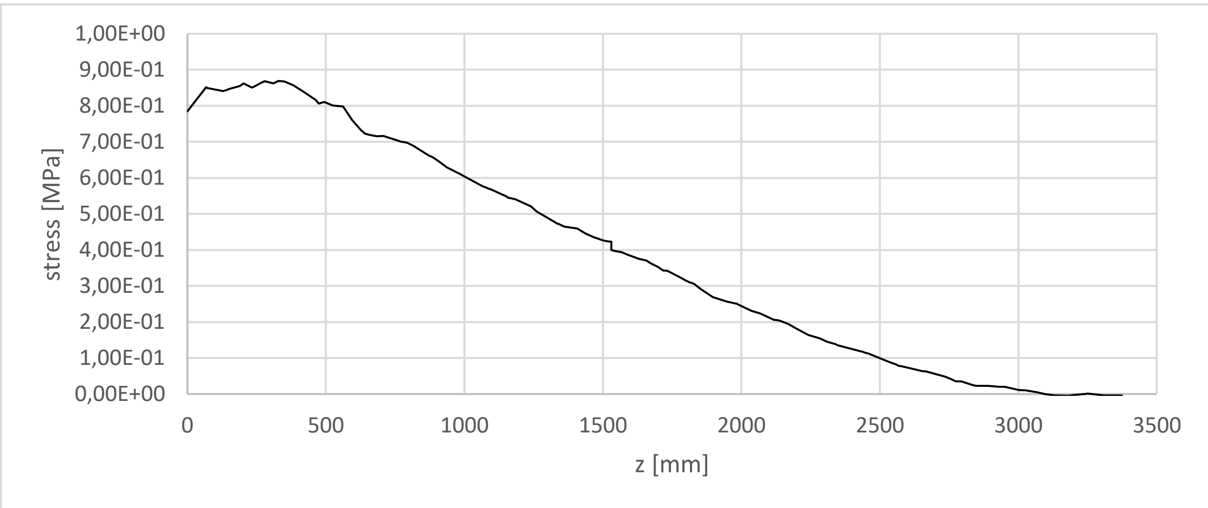

Figure 5.7 - *Shear stress σ₂₃ – z (local model #1)*

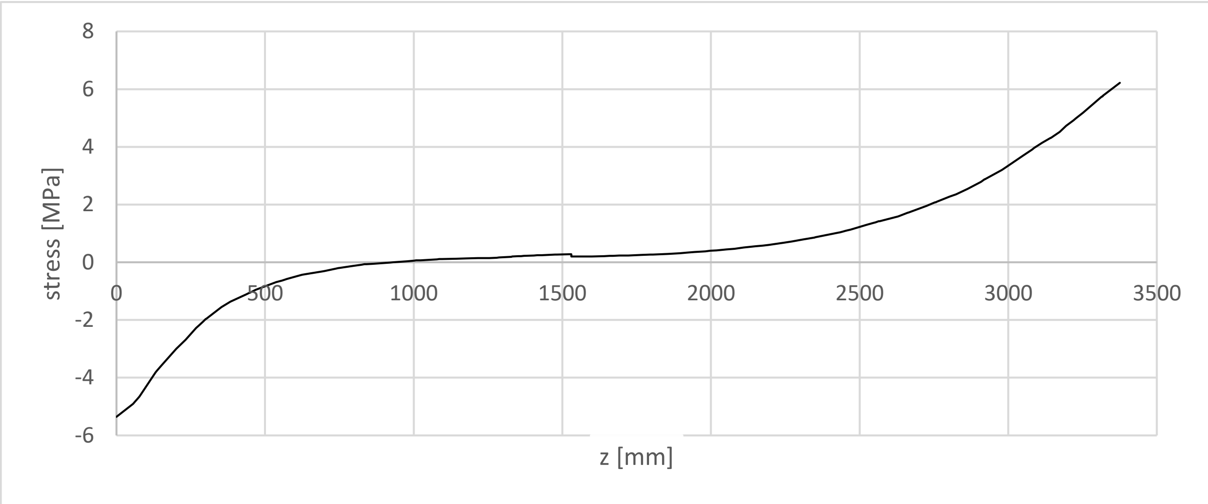

Figure 5.8 - *Normal stress σ_{11} – z (local model #2)*

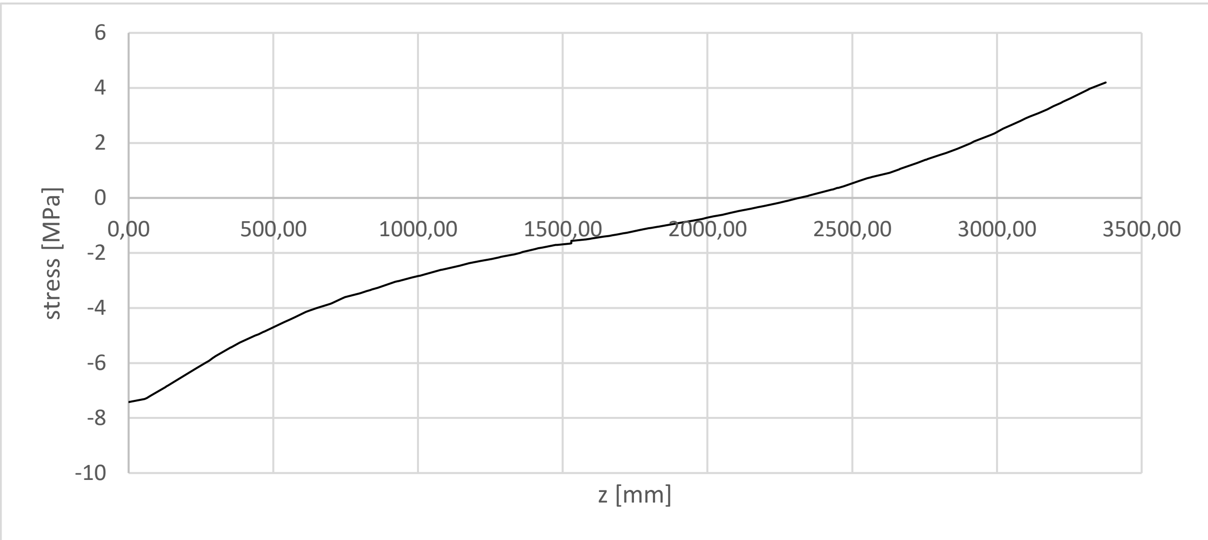

Figure 5.9 - *Normal stress σ_{22} – z (local model #2)*

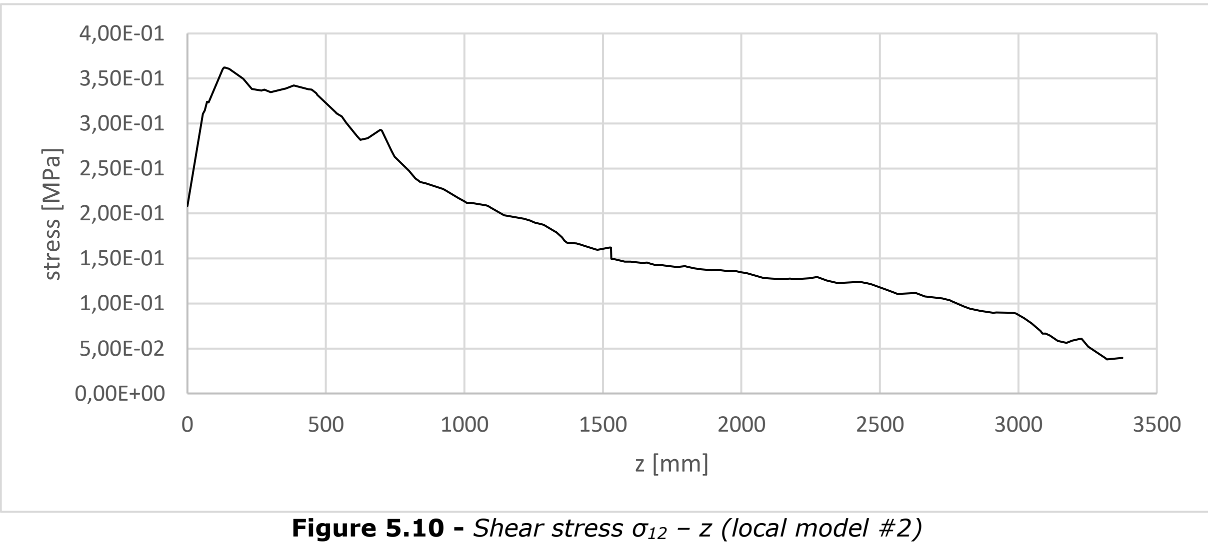

Figure 5.10 - *Shear stress σ_{12} – z (local model #2)*

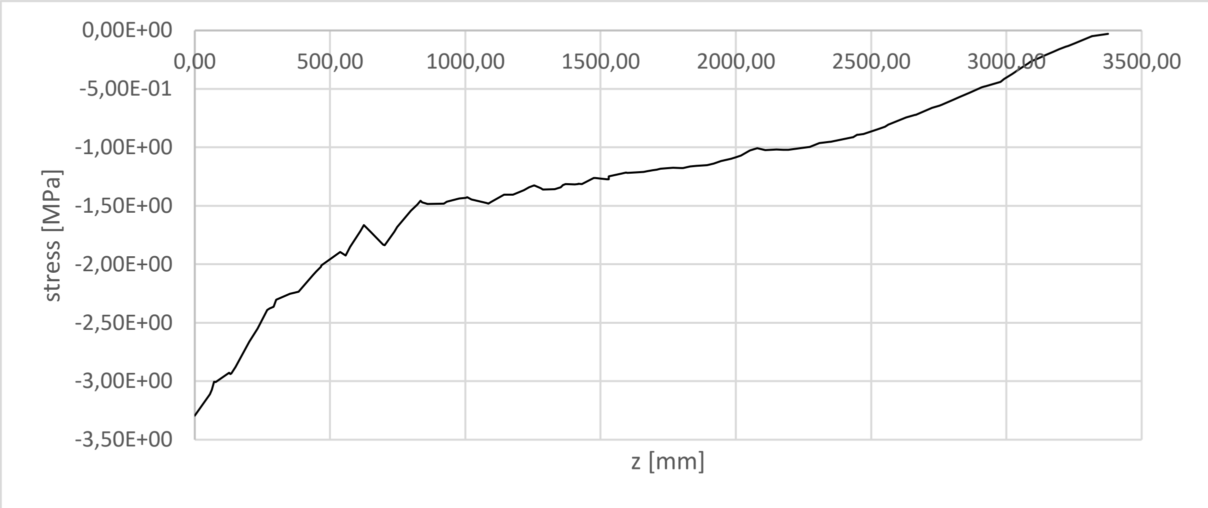

Figure 5.11 - *Shear stress σ_{13} - z (local model#2)*

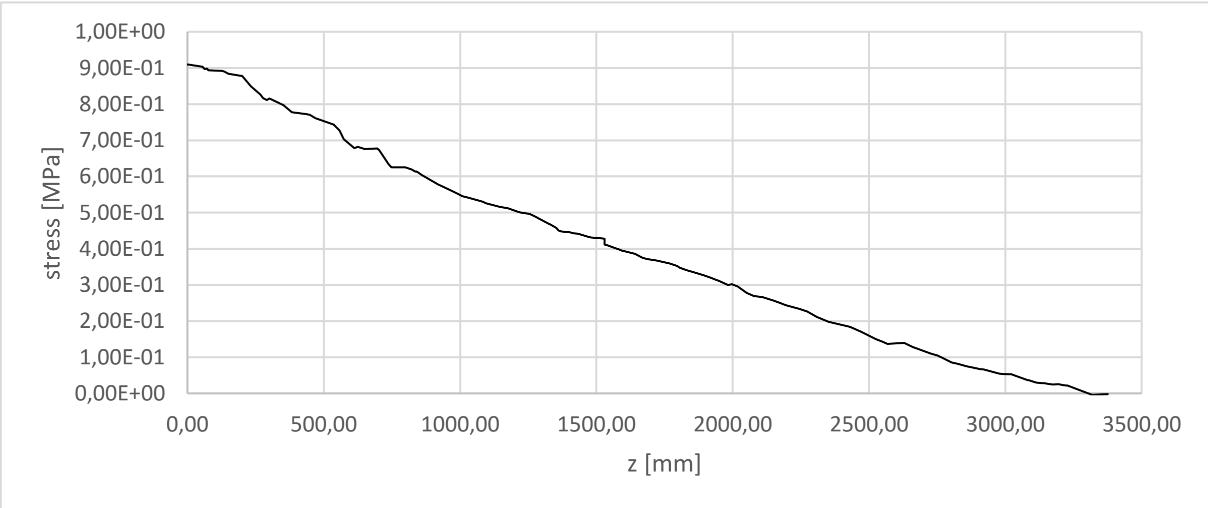

Figure 5.12 - *Shear stress σ_{23} - z (local model #2)*

This check was useful to have a general idea of the behaviour of this particular structure; in particular, as can be deduced from the following graphs:

- the normal stress σ_{11} and σ_{22} switch from compression value to tensile value respectively around 1 m and 2,3 m of height. Tensile stress value reach and exceed the maximum tensile strength: this is because the concrete was assumed to be linear, so the software does not recognise any yield point for the concrete;
- the shear stress σ_{12}, σ_{13} and σ_{23} for both models tend to decrease, up to zero, with the increase of tensile stress.
- both models show the same distribution and the same trend for the normal stress, while the shear stresses show an opposite trend although having almost the same stress in terms of absolute value. This difference may be addressed to not identical geometry.

5.2 Non-Linear Static Analysis

Concrete exhibits a complex structural response with various significant nonlinearities: in particular, a non-linear stress-strain behaviour, tensile cracking and compression crushing material failures and creep cracking(13). Also, since reinforced concrete shows a complex behaviour, both elastic and plastic behaviour of concrete in compression and tension need to be accurately simulated and improved within a finite element analysis.
Simulation of concrete under tension requires to pay particular attention to how the behaviour changes and evolves once the tensile characteristic stress is reached: in particular, tension stiffening should be included in the material model.
There are many different ways to model the behaviour of concrete in the post-elastic phase: some of the most adopted models are based on classic plasticity model, fracture mechanics and continuum damage mechanics" (CDM)"(14). The plasticity model is capable in representing hardening and softening characteristics: the main characteristic of these model is the yield surface, which includes a hardening-softening function. Regardless, these models do not explicitly incorporate damage process due to microcracks such as stiffness degradation and unilateral effects(15).
Conversely, continuum damage mechanics model are based on the concept of a decrease of the elastic stiffness: in particular, strain softening, stiffening decrease and unilateral effects due to microcracking and microvoids are taken into account(16). Thus, considering the positive and negative aspects of both models, it is desirable to combine these two approaches for concrete modelling since whether irreversible deformations and microcracking contribute to the non-linear behaviour of concrete.
There are several models implemented in Abaqus which are capable of describing the post-elastic behaviour such as Drucker Prager or Mohr-Coulomb model differently.
In particular, there are three models implemented in Abaqus capable of representing the cracked concrete behaviour:

- the smeared cracked model (SC);
- the brittle cracking model;
- the concrete damaged plasticity model(CDP).

These models require multiple parameters, which are usually calculated from experimental material tests. The brittle cracking and the smeared cracked model were not used because the first technique is only available for Abaqus/Explicit, and the second is not very explored in literature projects. Thus, the concrete damaged plasticity model was selected in the present project thesis for modelling non-linear behaviour of concrete both in compression and in tension, including damage characteristics.

5.2.1 Concrete Damaged Plasticity Model

Concrete damaged plasticity model is a useful and convenient technique to simulate concrete behaviour due to its capabilities to represent plastic strains but also stiffness degradations.
CDP model is a continuum, plasticity-based, damage model for concrete, assuming that the two main failure mechanisms are tensile cracking and compressive crushing(17). Furthermore, this model defines the inelastic behaviour of concrete using the theory of isotropic damaged elasticity in combination with isotropic tensile and compressive

plasticity: this theory is based on the plasticity model proposed by Lubliner (18) and Lee and Fenves (19).
The concrete damaged plasticity model is capable of predicting and representing the formation of cracks in the concrete, subjected to various loading conditions, including cyclic loading(20). Two hardening variables related to concrete failure mechanisms under tension and compression are used in the aim of controlling the evolution of the yield surface. The CDP model takes into account the degradation of the elastic stiffness caused by plastic straining (in compression and tension) by introducing two independents scalar damage variables for tension and compression, respectively. For what concerns the elastic range, the model assumes the elastic behaviour of concrete to be isotropic and linear.
In concrete modelling, a non-associated plastic flow potential is implemented using the Drucker-Pager hyperbolic function to represent flow potential.
Finally, a visco-plastic regularisation of the constitutive models is sometimes used to improve the convergence rate in the concrete softening and stiffness regimes, but it was not used in this project.

5.2.1.1 Concrete compression model

The stress-strain relation for a given concrete can be described based on uniaxial compression tests carried out on it if no data set from tests are available, the relation can be described using the relations in the literature or standards. It is observed that concrete behaves linearly within the elastic region until the initial yield, σ_{co}. After reaching the initial yield point, concrete starts behaving in a plastic fashion and exhibits some work-hardening up to the ultimate stress σ_{cu} followed by strain-softening (figure 5.12).

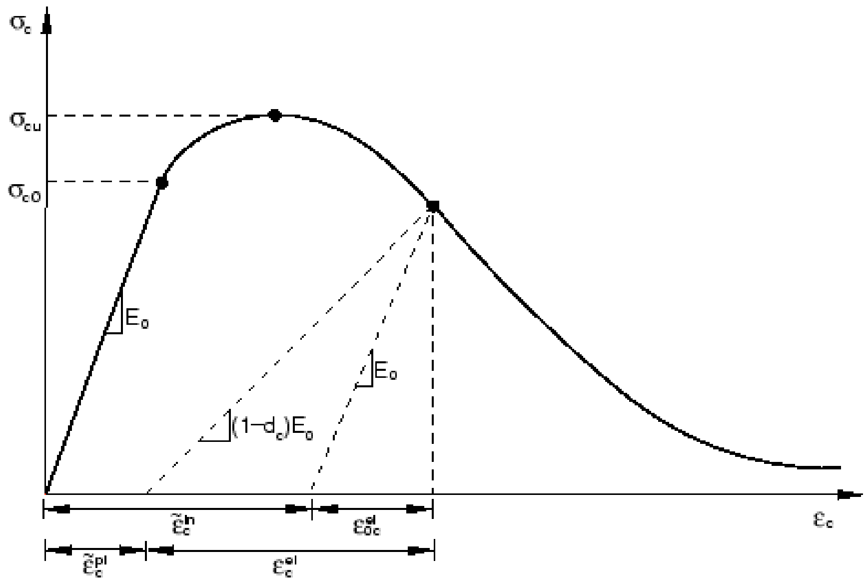

Figure 5.13 - *Compressive stress-strain response of concrete* **(17)**

For the inelastic response, compressive stresses are provided in a tabular form as a function of the inelastic strain, ε_c^{in}, used in the model to describe the hardening rule, and which can be calculated by the following equation:

$$\varepsilon_c^{in} = \varepsilon_c - \varepsilon_{0c}^{el} = \varepsilon_c - \frac{\sigma_c}{E_c}$$

where ε_c is the total compressive strain, ε_{0c}^{el} is the elastic compressive strain corresponding to the undamaged material, σ_c is the compressive stress, and E_c is the initial undamaged modulus of elasticity.

The constitutive equation under uniaxial compression for the CDP model is (17,18):

$$\sigma_c = (1 - d_c)E_c(\varepsilon_c - \varepsilon_c^{pl}) = E(\varepsilon_c - \varepsilon_c^{pl})$$

where $d_c$is the damage variable: if its value is 0 , it represents the undamaged material and, instead, if it is 1 it represents the material under the total loss of strength. Furthermore, $E = (1 - d_c)E_c$ is the degraded elastic stiffness in compression. The effective compressive stress is defined as:

$$\bar{\sigma}_c = \frac{\sigma_c}{(1 - d_c)} = E_c(\varepsilon_c - \varepsilon_c^{pl})$$

where ε_c^{pl} is the equivalent plastic strain in compression.

5.2.1.2 Concrete tension model

The stress-strain relation under uniaxial tension is similar to that in compression (figure 5.13):

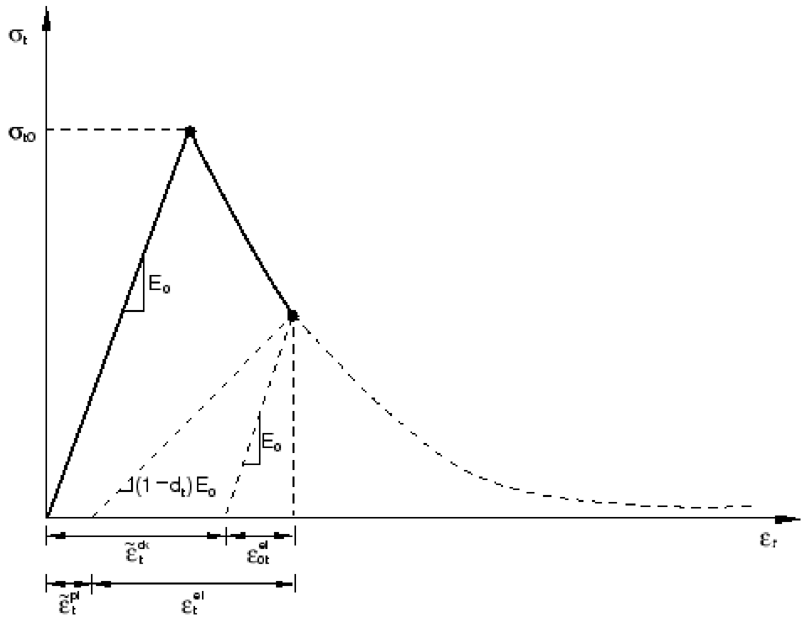

Figure 5.14 - *Tensile stress-strain response of concrete (17)*

moreover takes the following form (18,21):

$$\sigma_t = (1 - d_t)E_t(\varepsilon_t - \varepsilon_t^{pl}) = E(\varepsilon_t - \varepsilon_t^{pl})$$

where $d_t$is the damage variable in tension and $E = (1 - d_t)E_c$ is the degraded elastic stiffness in tension. The effective compressive stress is defined as:

$$\bar{\sigma}_t = \frac{\sigma_t}{(1 - d_t)} = E_t(\varepsilon_t - \varepsilon_t^{pl})$$

where ε_t^{pl} is the equivalent plastic strain in compression. Furthermore, it can be seen that the stress-strain response is linear elastic until the peak stress σ_{t0} and once this value is

reached, cracks start to appear. The strain-softening behaviour for cracked concrete is defined by the "*tension stiffening*": the tensile capacity of concrete is usually neglected when analysing a reinforced concrete structure, even though concrete continues to carry tensile stress between the cracks due to the transfer of stresses from the tensile reinforcement to the concrete through bond. This kind of contribution affects the stiffness after cracking, the deflection of the member and the width of the cracks under service loads(22).
In Abaqus, the effects of the tension stiffening can be specified in three different ways:

1. the tensile stress in concrete can be entered in a tabular form as a function of the corresponding cracking strain ε_t^{ck}, defined as:

$$\varepsilon_t^{ck} = \varepsilon_t - \varepsilon_{0t}^{el} = \varepsilon_t - \frac{\sigma_t}{E}$$

   where ε_t^{ck} is the cracking strain, ε_t is the total tensile strain, ε_{0t}^{el} is the elastic tensile strain corresponding to the undamaged material, σ_t is the tensile stress, and E is the initial undamaged modulus of elasticity.

2. the tensile stress can be entered in a tabular form as a function of the crack-opening-displacement, w.
3. using the fracture energy G_f.

In the second method, the post-peak tensile behaviour of concrete is defined in a way that the user has to input the tensile stress as a function of the crack-opening-displacement w. In particular, the cracking displacement at which complete loss of strength takes place is defined as(23):

$$w_c = \frac{5G_f}{f_{ctm}}$$

where f_{ctm} is the tensile strength in *MPa*. In particular, the descending branch can be represented using bilinear or non-linear tension softening curve, as described in section 5.2.2.2.
In the third method, the fracture energy of concrete G_f, proposed by (24), is defined as the energy required to propagate a tensile crack of unit area. The fracture energy should be determined by related tests but in the absence of experimental data G_f in *N/m* for normal weight concrete may be estimated from the following equation(23):

$$Gf = 73 * f_{cm}^{0.13}$$

where f_{cm} is the mean compressive strength in *MPa*. The descending branch is presented using a linear tension softening curve (17).
Further attention to these three methods and their characteristics are given in section 5.2.2.2.

5.2.1.3 Plastic flow and yield surface

The concrete damaged plasticity model assumes a non-associated potential plastic flow function and a yield surface which make use of two stress invariants of the effective stress tensor, namely the hydrostatic pressure stress and the Mises equivalent effective stress, defined as:

- $\bar{p} = -\frac{1}{3}tr(\sigma)$
- $\bar{q} = \sqrt{\frac{3}{2}}\|dev(\sigma)\|$

where $\|dev(\sigma)\|$ is the effective stress deviator (or deviatoric part of the effective stress tensor).
The concrete damaged plasticity assumes a non-associated plastic flow, defined as (25):

$$\dot{\varepsilon}_p = \dot{\lambda}\frac{\partial G}{\partial \sigma}$$

where σ and $\dot{\varepsilon}_p$ denote the stress and plastic strain rate tensors, $\dot{\lambda}$ is the plastic multiplier, and *G* is the Drucker-Prager function used in this model:

$$G = \sqrt{(\epsilon f_t tan\psi)^2 + \bar{q}^2} - \bar{p}tan\psi$$

When the potential plastic function shares the same shape as the yield surface, the flow is classified as "associated flow rule" (i.e. the plastic flow is connected with the yield criterion). If the associated rule is used, the plastic flow develops along the normal to the loading surface. However, the "non-associated flow rule" refers to the approach of using two separate functions, one of the plastic flow and the other for the yield surface. In this rule, the plastic flow develops along the normal to the plastic flow potential and not to the yield surface (26).
Referring to the Drucker-Prager function (figure 5.14):

- ψ is the dilation angle measured in the *p-q* plane at high confining pressure;
- ϵ is the eccentricity of the plastic flow potential surface;
- f_t is the uniaxial tensile strength of concrete.

In particular, the dilation angle and the eccentricity determine the shape of the flow potential surface: ψ represents the angle of inclination of the failure surface towards the hydrostatic axis in the meridian plan and ϵ adjusts the shape of the plastic potential eccentricity.
The eccentricity is a small positive value which defines the rate of approach of the plastic potential hyperbola to its asymptote: its length (measured along the hydrostatic axis) of the segment between the vertex of the hyperbola and the intersection of the asymptotes of this hyperbola (the centre of the hyperbola). Finally, it can be calculated as a ratio of tensile strength to compressive strength(27).

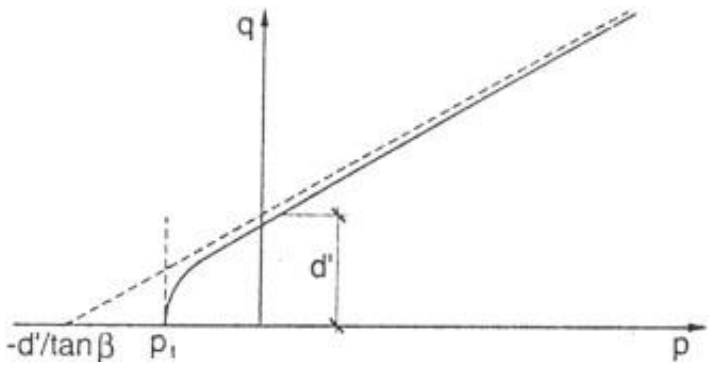

Figure 5.15 - *Drucker-Prager hyperbolic function of CDP flow potential and its asymptotes in the meridian plane* (27)

The concrete damaged plasticity model also requires a yield surface capable of determining the states of failure or damage. In particular, this model uses the yield function proposed by Lubliner et al. (18), with the modifications proposed by Lee and Fenves (19), which consider the different evolution of strength under compression and tension.
The yield surfaces in the plane stress and deviatoric plane conditions are depicted in figure 5.15(a-b). Furthermore, the yield function is defined in terms of effective stress as follows(25):

$$F = \frac{1}{1-\alpha}\left[\bar{q} - 3\alpha\bar{p} + \beta\left(\tilde{\varepsilon}_t^{pl}, \tilde{\varepsilon}_c^{pl}\right)\langle\hat{\bar{\sigma}}_{max}\rangle - \gamma\langle-\hat{\bar{\sigma}}_{max}\rangle\right] - \bar{\sigma}_c\left(\tilde{\varepsilon}_c^{pl}\right)$$

where:

$$\alpha = \frac{\left(\frac{\sigma_{b0}}{\sigma_{c0}}\right) - 1}{2\left(\frac{\sigma_{b0}}{\sigma_{c0}}\right) - 1}; \quad 0 \leq \alpha \leq 0.5$$

$$\beta = \frac{\bar{\sigma}_c\left(\tilde{\varepsilon}_c^{pl}\right)}{\bar{\sigma}_t\left(\tilde{\varepsilon}_t^{pl}\right)}(1-\alpha) - (1+\alpha); \qquad \gamma = \frac{3(1-K_c)}{2K_c - 1}$$

In these expressions:

- $\langle\hat{\bar{\sigma}}_{max}\rangle$ is the maximum principal effective stress;
- $\frac{\sigma_{b0}}{\sigma_{c0}}$ is the ratio of biaxial compressive yield stress to initial uniaxial compressive yield stress;
- $\bar{\sigma}_c\left(\tilde{\varepsilon}_c^{pl}\right)$ and $\bar{\sigma}_t\left(\tilde{\varepsilon}_t^{pl}\right)$ are cohesion values in compression and tension, depending on the compressive and tensile equivalent plastic strains, $\tilde{\varepsilon}_c^{pl}$ and $\tilde{\varepsilon}_t^{pl}$;
- γ represents a dimensionless material constant only for the stress states of triaxial compression;
- K_c controls the failure surface in the deviatoric cross-section and is the ratio of the second invariant on the tensile meridian and on the compressive meridian at any given value of the pressure invariant.

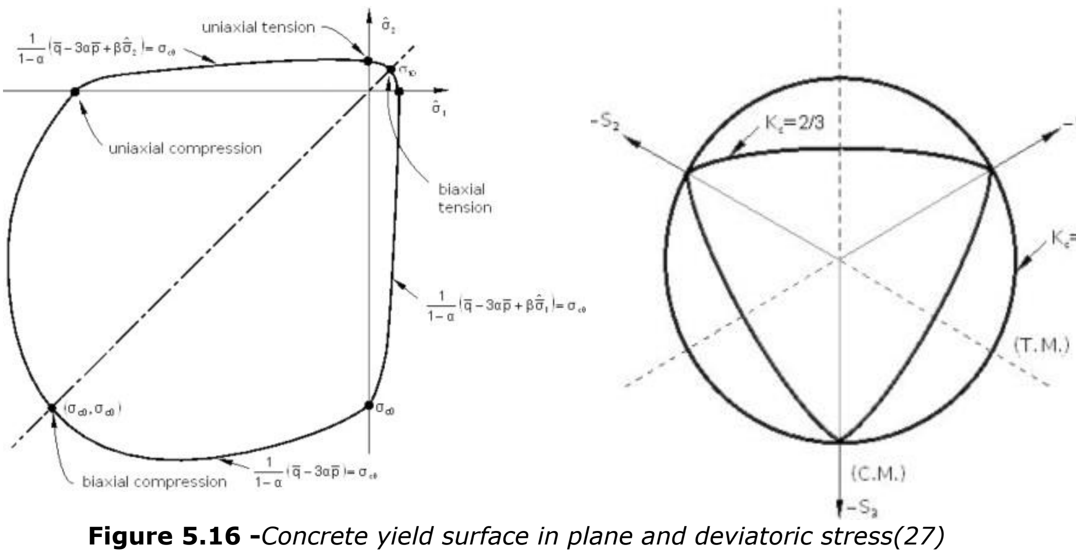

Figure 5.16 -*Concrete yield surface in plane and deviatoric stress(27)*

5.2.1.4 Damage evolution

In the CDP model, the degradation of stiffness, caused by microcracking, occurs in both tension and compression and becomes more significant as the strain increases(28). Under cyclic loading, the mechanism of stiffness degradation gets more complicated due to opening and closing of the microcracks and, in particular, the unloading response becomes weaker and degraded, and the modulus of elasticity is adopted to describe this degradation as expressed in Figure 5.16 (25).

Thus, the two main damage phenomena of the CDP model, the uniaxial tensile and compressive ones, can be possibly evaluated by defining two damage variables, namely d_c and d_t, which are used to characterise the degradation and the variation of the elastic stiffness (29).

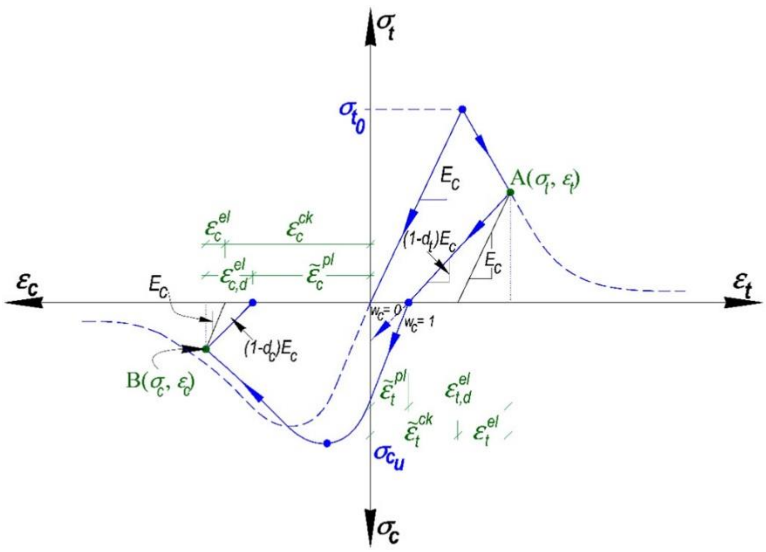

Figure 5.17 - *Definition of tensile and compressive damage (17,25)*

The compressive and tensile damage variable can be computed using the following relations(30):

$$d_c = 1 - \frac{\sigma_c}{\sigma_{cu}}$$

$$d_t = 1 - \frac{\sigma_t}{\sigma_{t0}}$$

Also, these variables can be defined differently: the tensile damage variable can be considered equal to the ratio of the cracking strain to the total tensile strain, and the compressive damage variable defined as the ratio of the crushing strain to the total compressive strain(31).

Thus, only when concrete enters in the softening phase in both tension and compression, the damage variables start to occur and increase their value(32).

Once the damage variables are found, it is possible to evaluate the equivalent plastic strain for crushed concrete and cracking concrete. In particular, The tensile damage variable can be defined as a tabular function of either the crack–opening displacement, $\tilde{u}_t^{pl}$, or the cracking strain, $\tilde{\varepsilon}_t^{pl}$(33):

$$\tilde{\varepsilon}_c^{pl} = \tilde{\varepsilon}_c^{in} - \frac{d_c}{1-d_c}\frac{\sigma_c}{E_0}$$

$$\tilde{\varepsilon}_t^{pl} = \tilde{\varepsilon}_t^{ck} - \frac{d_t}{1-d_t}\frac{\sigma_t}{E_0}$$

$$\tilde{u}_t^{pl} = \tilde{u}_t^{ck} - \frac{d_t}{1-d_t}\frac{\sigma_t l_0}{E_0}$$

where l_0 is the specimen length and it is assumed to be a unit length(34). Negative and/or decreasing plastic strains are indicative of incorrect damage evolutions, which leads to generate an error message in Abaqus, preventing the performing of the non-linear analysis. Furthermore, if no damage variable is specified for both tension and compression, the model become a classic plastic model (31).

5.2.1.5 Viscoplastic regularisation

The softening behaviour and stiffness degradation of some material models, in particular for concrete, often lead to severe convergence problems in implicit analysis programs, such as Abaqus/Standard. A common technique to solve these convergence issues is the use of a viscoplastic regularisation of the constitutive equations, which causes the consistent tangent stiffness of the softening material to become positive for sufficiently small time increments (21)

Viscoplasticity regularisation can be used in Abaqus/Standard for concrete damaged plasticity model: this technique allows the stresses to be outside of the yield surface.

The viscoplastic regularisation is based on the use of the Duvaut-Lions regularisation, according to which the viscoplastic strain rate tensor,$\tilde{\varepsilon}_v^{pl}$, is defined as:

$$\tilde{\varepsilon}_v^{pl} = \frac{1}{\mu}(\varepsilon^{pl} - \varepsilon_v^{pl})$$

where μ is the viscosity parameter representing the relaxation time of the viscoplastic system, ε_v^{pl} is the plastic strain evaluated in the inviscid solution and $\tilde{\varepsilon}_v^{pl}$ is the viscoplastic strain. In Abaqus, the default value of μ is zero, but when it is greater than zero the viscoplastic strain start increasing. Furthermore, when the viscoplastic strain is used, the viscous stiffness damage variable, $\dot{d}_v$ is introduced and expressed below:

$$\dot{d}_v = \frac{1}{\mu}(d - d_v)$$

where *d* is the damage variable of the inviscid solution. Thus, if the viscoplastic regularisation is used, the model output is based on elastic stiffness degradation and plastic strain values, d_v and ε_v^{pl}, respectively.

Using the viscoplastic regularisation with a small value for the viscosity parameter (small compared to the characteristic time increment) helps improve the rate of convergence of the model, without compromising results. Finally, if the value of μ approaches zero, the solution becomes a plastic response while if the viscosity parameter is assumed larger than the iteration time increment, the solution tends to be elastic(21)

5.2.2 Identification of constitutive parameters for CDP model

The plasticity modelling within the concrete damaged plasticity model is governed by the following fundamental parameters which identify the shape of the flow potential surface and the yield surface in the three-dimensional space of stresses:

- ψ , dilation angle;
- ϵ , is the eccentricity which is a parameter that defines the rate at which the function approaches the asymptote;
- $\frac{\sigma_{b0}}{\sigma_{c0}}$, the ratio of biaxial compressive yield stress to initial uniaxial compressive yield stress;
- K_c , the ratio of the second stress invariant on the tensile meridian to that on the compressive meridian for the yield function.

Usually, it is necessary to carry out a biaxial failure in-plane state of stress and a triaxial test of concrete to identify these parameters, while a uniaxial compression and uniaxial tension tests are needed to be carried out to describe the evolution of the stress-strain curves of concrete (the hardening and the softening rule in tension and compression).
In this thesis project, none of the parameters of the concrete damaged plasticity model was defined experimentally, but their definition was based on literature values and calibration parameter.
ψ is physically interpreted as a concrete internal friction angle, it represents the angle of inclination of the failure surface towards the hydrostatic axis, measured in the meridional plane (Figure 5.14). Various authors suggest different values of the dilation angle: Jankowiak (35) ,for his test, supposed ranges from 34° to 42°, while Kmiecik and Kamiński (27) indicated that a value of 40° is usually assumed in simulations. Zappitelli et al.(34) used a value of 20° for their concrete dam, Hafezolghorani et al. (30) proposed a value of 31° which was used on various CDP analysis performed on different concrete class and , finally, Vermeer and De Borst (36) proposed a value of 13°.
Each of these authors proposed and used a different value of dilation angle without improving a laboratory test: although, the values they proposed are based on their particular case of study and, thus, it might not be correct to choose a particular value randomly from these research topic because dilation angle values used for the same concrete class goes from 20° to 40°.
For this reason, a dilation angle calibration was performed to get the most accurate value to use for the non-linear analysis, as described in section 5.2.3.
The flow potential eccentricity ϵ ensures that the flow direction is always uniquely defined. According to the manual, the function approaches the linear Drucker-Prager flow potential asymptotically at high confining pressure stress and intersects the hydrostatic pressure axis at 90°.
The default flow potential eccentricity is assumed to be 0.1, which implies that the material has almost the same dilation angle over a wide range of confining pressure stress values. Increasing the value of provides more curvature to the flow potential, implying that the dilation angle increases more rapidly as the confining pressure decreases.
Moreover, values of eccentricity significantly lower than the default value may lead to convergence problems if the material is subjected to low confining pressures because of the very tight curvature of the flow potential locally where it intersects the p-axis(21). In particular, if it is considered an eccentricity value of $\epsilon = 0$ the flow potential tends to a straight line.
K_c is interpreted as a ratio of the distances between the hydrostatic axis and respectively the compression meridian and the tension meridian in the deviatoric cross section. Typical

values of K_c are between 0.64 and 0.8 (18). According to "Abaqus Analysis User's Manual" (21) is recommended to assume $K_c = 2/3$. This ratio must always higher than 0.5 and when the value of 1 is adopted, the deviatoric cross section of the failure surface becomes a circle (as in the classic Drucker-Prager strength hypothesis).
The term σ_{b0}/σ_{c0}, the ratio of biaxial compressive yield stress to initial uniaxial compressive yield stress. Various authors have worked on this topic and carried out experimental tests under various biaxial stress state, in particular, biaxial compressive test, giving their reference value and their considerations:

- Lubliner et al. (1989) reported a range of 1.10 to 1.16;
- Jankowiak (2005) indicated that σ_{b0}/σ_{c0} ratio is sensitive to the change of the dilation angle and the eccentricity;
- Kupfer et al., (1969) after several biaxial tests found out that the ratio range is approximately between 1.10 and 1.20;
- "Abaqus Analysis User's Manual,(vol3,") suggests a default value of 1.16.

After this brief, this theoretical description, according to an amount of research study previously mentioned, the fundamental parameters of yield surface and flow potential used in the analysis are defined as follows:

- ψ , dilation angle calibrated and discussed in section 5.2.3;
- ϵ , eccentricity value is 0.1;
- K_c value is 0.66
- σ_{b0}/σ_{c0} ratithe o of biaxial compressive yield stress to initial uniaxial compressive yield stress value is 1.16.

5.2.2.1 Compression behaviour

The properties of concrete subjected to uniaxial compression are usually obtained from a cylinder or cubic tests. In this project, no experimental results are available to perform an analysis using the stress-strain curve for the concrete. Thus, the expressions considered to describe the stress-strain curve are based on several studies in the literature.
The uniaxial compressive stress-strain curve, according to Eurocode 2(1) is depicted in figure 5.17.
The stress-strain curve is divided into three regions:

- linear elastic;
- non-linear plastic (hardening phase);
- post-peak stress (softening phase).

According to Eurocode 2 (EC2), concrete exhibits an elastic behaviour up to $0.4f_c$: at this level, which is almost 40% of the maximum uniaxial compressive strength, the specimen deformation is fully recoverable. In the pre-peak part of the stress-strain curve, the energy dissipation from all these meso-level mechanisms is small compared to the total energy stored in the specimen(38).

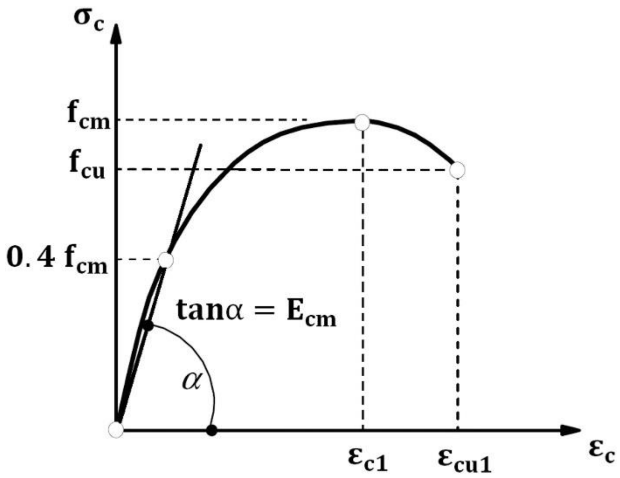

Figure 5.18 - *Schematic representation of the stress-strain relation*

In the plastic regime, the response of the concrete is characterised by stress hardening followed by strain softening beyond the peak stress f_{cm}.
In this physic phase, the deformation is no longer recoverable, and the stress-strain relation is no longer linear. Immediately after the peak stress, the concrete specimen displays strain softening and lateral expansions, which increase with the crack propagation: cracks start occurring and influencing the concrete behaviour once the peak stress is reached.
The softening curve of the stress-strain relations should be considered as the envelope to all possible stress-strain relations of concrete which tends to soften as a consequence of concrete micro-cracking: the descending part is strongly depending on the specimen or member geometry, the boundary conditions and the possibilities for load redistribution in the structure (1).
The uniaxial stress-strain curve was determined using the following expression(EC2, 2004):

$$\frac{\sigma_c}{f_{cm}} = \frac{k\eta - \eta^2}{1 + (k-2)\eta}$$

where:

- σ_c is the compressive stress;
- f_{cm} is the mean value of concrete cylinder compressive strength;
- $\eta = \varepsilon_c/\varepsilon_{c1}$;
- $\varepsilon_{c1} = 0.7 f_c^{0.31}$;
- $k = 1.05 E_{cm}\,|\varepsilon_{c1}|/f_{cm}$

This expression is valid for $0 < |\varepsilon_c| < |\varepsilon_{cu}|$ where $|\varepsilon_{cu}|$ is the nominal ultimate strain: a constant value of $\varepsilon_{cu} = 0.0035$ is provided by EC2 and it can be used for concrete with a characteristic value f_{ck} less than 55MPa. For characteristic value above the 55Mpa value, the ultimate strain value can be expressed as:

$$\varepsilon_{cu} = 2.8 + 27\,[(98 - f_c)/100]^4$$

Since the plasticity curve in EC2 consider the concrete behaviour only up to the ultimate strain ε_{cu} , limited to a value of 0.0035 which may lead to unrealistic overestimation of concrete strength (39), the descending branch was developed using the Pavlović et al. (40) curve.

Pavlović et al. suggested an extension of the compressive stress-strain curve beyond the EC2 ultimate strain: this extension is characterised by a sinusoidal descending curve between the corresponding EC2 ultimate strain ($\varepsilon_{cu1}, f_{cu1}$) and the ultimate strain ($\varepsilon_{cu2}, f_{cu2}$). The following expression defines the Pavlovic curve:

$$\sigma_c = f_c \left[\frac{1}{\beta} - \frac{\sin(\mu^{\alpha_{t1}}\,\alpha_{t2}\;\pi/2}{\beta\sin(\alpha_{t2}\;\pi/2)} + \frac{\mu}{\alpha}\right] \qquad \varepsilon_{cu1} < \varepsilon_c < \varepsilon_{cu2}$$

where:

$$\mu = \frac{(\varepsilon_c - \varepsilon_{cu1})}{(\varepsilon_{cu2} - \varepsilon_{cu1})} \qquad \beta = \frac{f_c}{f_{cu1}}$$

At the end of the descending part (ε_{cu2}), concrete strength was reduced to f_{cu2} by a factor$\beta = f_c/f_{cu2}$. They adopted a value of 20 and 0.03, for α and ε_{cu2}.The parameters α_{t1} and α_{t2} control tangents angles at the starting and end points of the sinusoidal curve and their value is set as 0.5 and 1. Table 5.3-5.4 summarizes the values of the stress-strain curve for C45/55 and C55/67, which were used for the CDP model and figure 5.18-5.19 depicts the final compressive stress-strain compression concrete response.

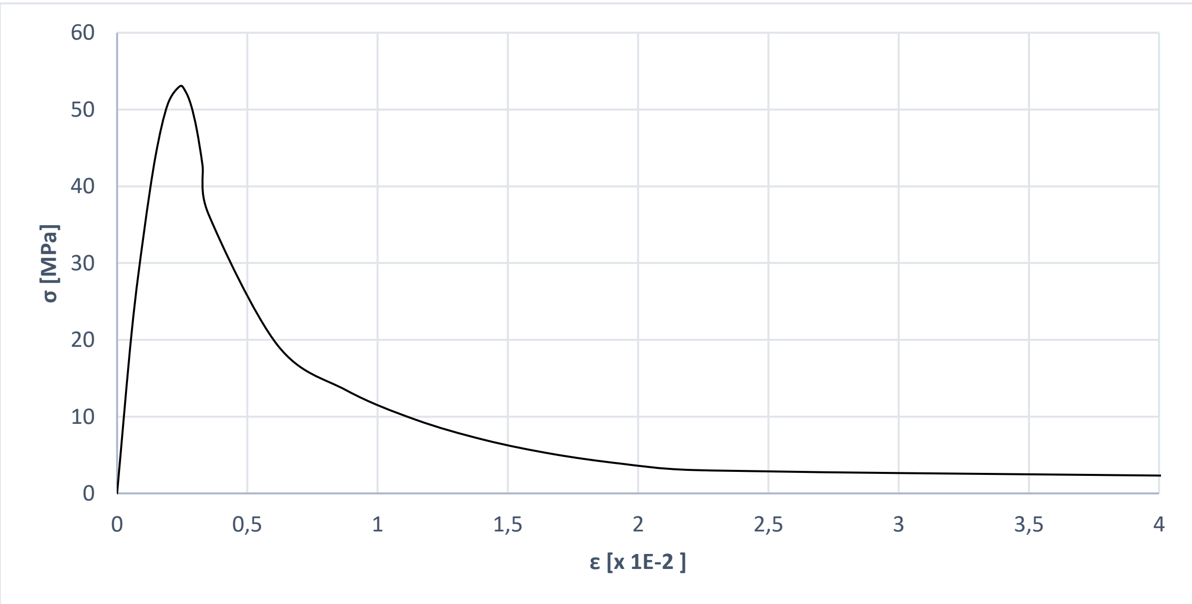

Figure 5.19 - *stress-strain curve EC2+Pavlovic – C45/55*

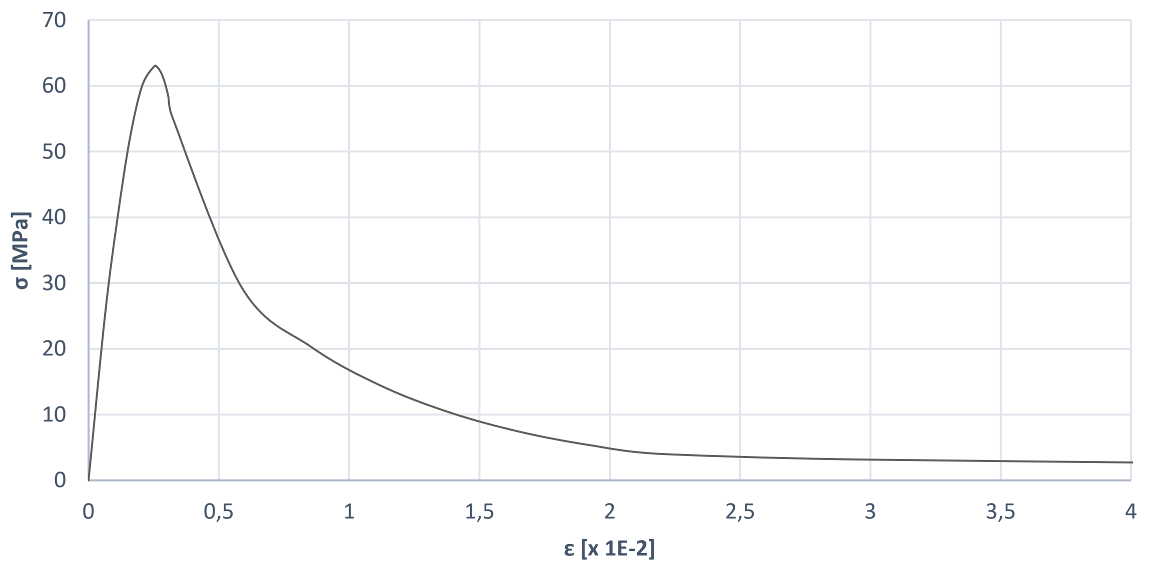

Figure 5.20 - *stress-strain curve EC2+Pavlovic – C55/67*

Total Strain	***Stress***	***Inelastic Strain***	***Damage***	***Plastic strain***
ε_c	$\sigma_c\ [MPa]$	$\tilde{\varepsilon}_c^{in}$	***d***	$\tilde{\varepsilon}_c^{pl}$
%	**-**	$\varepsilon_c - \varepsilon_{0c}^{el}$	$d_c = 1 - \frac{\sigma_c}{\sigma_{cu}}$	$\tilde{\varepsilon}_c^{pl} = \tilde{\varepsilon}_c^{in} - \frac{d_c}{1-d_c}\frac{\sigma_c}{E_0}$
0	*0*	-	-	-
0,000565551	*21,2*	*0*	*0*	*0*
0,001023352	*33,79206*	*0,000122*	*0*	*0*
0,001481153	*44,04778*	*0,000306*	*0*	*0*
0,001938954	*50,64749*	*0,000588*	*0*	*0*
0,002396755	*53*	*0,000983*	*0*	*0*
0,002617404	*52,40869*	*0,001219*	*0,011157*	*0,001204*
0,002838053	*50,56996*	*0,001489*	*0,04585*	*0,001424*
0,003058702	*47,37836*	*0,001795*	*0,106069*	*0,001645*
0,003279351	*42,71624*	*0,00214*	*0,194033*	*0,001865*
0,0035	*36,45189*	*0,002528*	*0,312228*	*0,002086*
0,00615	*19,34564*	*0,005634*	*0,634988*	*0,004736*

0,0088	*13,42983*	*0,008442*	*0,746607*	*0,007386*
0,01145	*9,613523*	*0,011194*	*0,818613*	*0,010036*
0,0141	*6,968166*	*0,013914*	*0,868525*	*0,012686*
0,01675	*5,115306*	*0,016614*	*0,903485*	*0,015336*
0,0194	*3,851043*	*0,019297*	*0,927339*	*0,017986*
0,02205	*3,048249*	*0,021969*	*0,942486*	*0,020636*
0,03	*2,65*	*0,029929*	*0,95*	*0,028586*
0,1	*0,4*	*0,099989*	*0,992453*	*0,098586*

Table 5.1 - *Compressive stress-strain curve values C45/55*

Total Strain	***Stress***	***Inelastic Strain***	***Damage***	***Plastic strain***
$\boldsymbol{\varepsilon_c}$	$\boldsymbol{\sigma_c\ [MPa]}$	$\boldsymbol{\tilde{\varepsilon}_c^{in}}$	***d***	$\boldsymbol{\tilde{\varepsilon}_c^{pl}}$
%	**-**	$\boldsymbol{\varepsilon_c - \varepsilon_{0c}^{el}}$	$\boldsymbol{d_c = 1 - \frac{\sigma_c}{\sigma_{cu}}}$	$\boldsymbol{\tilde{\varepsilon}_c^{pl} = \tilde{\varepsilon}_c^{in} - \frac{d_c}{1-d_c}\frac{\sigma_c}{E_0}}$
0	*0*	-	-	-
0,00063462	*25,2*	*0*	*0*	*0*
0,00110814	*39,798273*	*0,000106*	*0*	*0*
0,00158165	*51,895884*	*0,000275*	*0*	*0*
0,00205516	*59,992946*	*0,000544*	*0*	*0*
0,00252868	*63*	*0,000942*	*0*	*0*
0,00266294	*62,72932*	*0,001083*	*0,004297*	*0,001076387*
0,00279721	*61,887897*	*0,001239*	*0,017652*	*0,001210652*
0,00293147	*60,427973*	*0,00141*	*0,040826*	*0,001344916*
0,00306574	*58,296307*	*0,001598*	*0,074662*	*0,00147918*
0,0032	*55,433366*	*0,001804*	*0,120105*	*0,001613445*
0,00588	*29,331442*	*0,005141*	*0,534422*	*0,004293445*
0,00856	*20,247112*	*0,00805*	*0,678617*	*0,006973445*
0,01124	*14,355564*	*0,010878*	*0,772134*	*0,009653445*
0,01392	*10,244707*	*0,013662*	*0,837386*	*0,012333445*
0,0166	*7,3390204*	*0,016415*	*0,883508*	*0,015013445*
0,01928	*5,3284283*	*0,019146*	*0,915422*	*0,017693445*
0,02196	*4,0196054*	*0,021859*	*0,936197*	*0,020373445*
0,03	*3,15*	*0,029921*	*0,95*	*0,028413445*
0,1	*0,4*	*0,09999*	*0,993651*	*0,098413445*

Table 5.2 – *Compressive stress-strain curve values C55/67*

5.2.2.2 Tensile behaviour

The behaviour of concrete subjected to tensile loading is similar to the compressive behaviour previously described: in fact, even if the stress values are lower than the compressive case, the specimen shows a linear response, mostly up to 70% of the uniaxial tensile strength, followed by a softening stress-strain response in which are highlighted highly non-linear behaviour and the formation of micro-cracks. This softening behaviour, which is often ignored in design standards, becomes more critical and evident with increasing of strains: in particular, the tensile stress drops gradually with increasing deformations until a full crack is formed.
Finally, when the concrete specimen is unloaded from any point in the non-linear part, the response is weakened, and the material elastic stiffness appears to be damaged.
As for the compressive case, since no experimental results are available, the literature stress-strain tensile curves were used.
The concrete behaviour under uniaxial tension can be modelled by "tension stiffening" behaviour: this phenomenon describes the interaction and following stress transfer between the concrete and the reinforcement. As mentioned in section 5.2.1.2, there are three main methods for taking into account the effects of tension stiffening within Abaqus:

1. tensile stress-strain approach;
2. tensile stress-displacement (crack-opening displacement) approach;
3. using a fracture energy approach.

The first method consists in describing within Abaqus the tensile behaviour of concrete, both linear and nonlinear curves, defining a stress-strain relationship. In particular, Wang and T.C Hsu (41) proposed a model which was used in this the present study.
These authors divided concrete behaviour into two ascending and descending parts, the first describes the elastic phase while the second defines the softening stress-strain response, and the following expressions can express them:

$$\sigma_t = E_t \, \varepsilon_t \quad if \qquad \varepsilon_t \leq \varepsilon_{cr}$$

$$\sigma_t = f_t \left(\frac{\varepsilon_{cr}}{\varepsilon_t}\right)^n \varepsilon_t \quad if \qquad \varepsilon_t \geq \varepsilon_{cr}$$

Wang and T.C Hsu proposed a value of n=0.4, which is the rate of weakening. This curve shows a sharp change at cracking strain, which may lead to some problems during a finite element analysis: to avoid this problem; the authors suggested defining a short plateau at the peak point. Moreover, models implementing this technique might encounter major mesh sensitivity issues, especially when large regions of concrete has little or no reinforcement (21).
The tensile stress-strain curve adopted in the non-linear analysis is depicted in figure 5.2-5.3, and its values are shown in table 5.3-5.4.

Total Strain	***Stress***	***Cracking Strain***	***Damage***	***Plastic Strain***
$\boldsymbol{\varepsilon_t}$	$\boldsymbol{\sigma_t}$ $[\boldsymbol{MPa}]$	$\tilde{\boldsymbol{\varepsilon}}_t^{vk}$	***d***	$\tilde{\boldsymbol{\varepsilon}}_c^{pl}$
%	**-**	$\boldsymbol{\varepsilon_t - \varepsilon_{0t}^{el}}$	$\boldsymbol{d_t = 1 - \frac{\sigma_t}{\sigma_{tu}}}$	$\boldsymbol{\tilde{\varepsilon}_t^{pl} = \tilde{\varepsilon}_t^{ck} - \frac{d_t}{1-d_t}\frac{\sigma_t}{E_t}}$
0	*0*	*0*	*0*	*0*
0,00015	*3,795447*	*0,0000487*	*0*	*4,8749E-05*
0,00025	*3,0940222*	*0,00017*	*0,1848069*	*0,000148749*
0,00035	*2,704408*	*2,78E-04*	*0,2874599*	*0,000248749*
0,00045	*2,4457633*	*3,85E-04*	*0,355606*	*0,000348749*
0,00055	*2,2571185*	*4,90E-04*	*0,4053089*	*0,000448749*
0,00065	*2,1112229*	*5,94E-04*	*0,4437485*	*0,000548749*
0,00095	*1,813886*	*9,02E-04*	*0,522089*	*0,000848749*
0,00125	*1,6253071*	*1,21E-03*	*0,5717745*	*0,001148749*
0,00155	*1,491306*	*1,51E-03*	*0,6070803*	*0,001448749*
0,00185	*1,389411*	*1,81E-03*	*0,6339269*	*0,001748749*
0,00215	*1,3083503*	*2,12E-03*	*0,6552843*	*0,002048749*
0,00245	*1,2417467*	*2,42E-03*	*0,6728326*	*0,002348749*
0,00295	*1,1528442*	*2,92E-03*	*0,696256*	*0,002848749*
0,00345	*1,0828587*	*3,42E-03*	*0,7146953*	*0,003348749*
0,00395	*1,025795*	*3,92E-03*	*0,7297301*	*0,003848749*
0,00445	*0,9780373*	*4,42E-03*	*0,742313*	*0,004348749*
0,00495	*0,9372541*	*4,92E-03*	*0,7530583*	*0,004848749*
0,00575	*0,882739*	*5,73E-03*	*0,7674216*	*0,005648749*
0,00655	*0,8379207*	*6,53E-03*	*0,77923*	*0,006448749*
0,00735	*0,8001741*	*7,33E-03*	*0,7891753*	*0,007248749*
0,00815	*0,7677793*	*8,13E-03*	*0,7977104*	*0,008048749*
0,00915	*0,7330456*	*9,13E-03*	*0,8068619*	*0,009048749*
0,01015	*0,7032553*	*1,01E-02*	*0,8147108*	*0,010048749*
0,01115	*0,6773131*	*1,11E-02*	*0,8215459*	*0,011048749*
0,01615	*0,5840236*	*1,61E-02*	*0,8461252*	*0,016048749*
0,02115	*0,5242945*	*2,11E-02*	*0,8618623*	*0,021048749*
0,02615	*0,4816269*	*2,61E-02*	*0,873104*	*0,026048749*
0,03115	*0,4490722*	*3,11E-02*	*0,8816813*	*0,031048749*

Table 5.3 – *Tensile stress-strain curve values C45/55*

Total Strain	*Stress*	*Cracking Strain*	*Damage*	*Plastic Strain*
$\boldsymbol{\varepsilon_t}$	$\boldsymbol{\sigma_t}$ $[\boldsymbol{MPa}]$	$\boldsymbol{\tilde{\varepsilon}_t^{vk}}$	**d**	$\boldsymbol{\tilde{\varepsilon}_c^{pl}}$
%	-	$\varepsilon_c - \varepsilon_{0c}^{el}$	$d_c = 1 - \frac{\sigma_t}{\sigma_{tu}}$	$\tilde{\varepsilon}_t^{pl} = \tilde{\varepsilon}_t^{ck} - \frac{d_t}{1-d_t}\frac{\sigma_t}{E_t}$
0	*0*	*0*	*0*	*0*
0,00015	*4,2142936*	*0,0000439*	*0*	*4,38697E-05*
0,00025	*3,4354631*	*0,00016*	*0,1848069*	*0,00014387*
0,00035	*3,002853*	*2,74E-04*	*0,2874599*	*0,00024387*
0,00045	*2,7156656*	*3,82E-04*	*0,355606*	*0,00034387*
0,00055	*2,5062028*	*4,87E-04*	*0,4053089*	*0,00044387*
0,00065	*2,344207*	*5,91E-04*	*0,4437485*	*0,00054387*
0,00095	*2,0140574*	*8,99E-04*	*0,522089*	*0,00084387*
0,00125	*1,8046679*	*1,20E-03*	*0,5717745*	*0,00114387*
0,00155	*1,6558791*	*1,51E-03*	*0,6070803*	*0,00144387*
0,00185	*1,5427395*	*1,81E-03*	*0,6339269*	*0,00174387*
0,00215	*1,4527334*	*2,11E-03*	*0,6552843*	*0,00204387*
0,00245	*1,3787796*	*2,42E-03*	*0,6728326*	*0,00234387*
0,00295	*1,2800664*	*2,92E-03*	*0,696256*	*0,00284387*
0,00345	*1,2023576*	*3,42E-03*	*0,7146953*	*0,00334387*
0,00395	*1,1389967*	*3,92E-03*	*0,7297301*	*0,00384387*
0,00445	*1,0859687*	*4,42E-03*	*0,742313*	*0,00434387*
0,00495	*1,0406848*	*4,92E-03*	*0,7530583*	*0,00484387*
0,00575	*0,9801536*	*5,73E-03*	*0,7674216*	*0,00564387*
0,00655	*0,9303894*	*6,53E-03*	*0,77923*	*0,00644387*
0,00735	*0,8884773*	*7,33E-03*	*0,7891753*	*0,00724387*
0,00815	*0,8525076*	*8,13E-03*	*0,7977104*	*0,00804387*
0,00915	*0,8139409*	*9,13E-03*	*0,8068619*	*0,00904387*
0,01015	*0,7808631*	*1,01E-02*	*0,8147108*	*0,01004387*
0,01115	*0,752058*	*1,11E-02*	*0,8215459*	*0,01104387*
0,01615	*0,6484736*	*1,61E-02*	*0,8461252*	*0,01604387*
0,02115	*0,582153*	*2,11E-02*	*0,8618623*	*0,02104387*
0,02615	*0,5347769*	*2,61E-02*	*0,873104*	*0,02604387*
0,03115	*0,4986296*	*3,11E-02*	*0,8816813*	*0,03104387*

Table 5.4 – *Tensile stress-strain curve values C55/67*

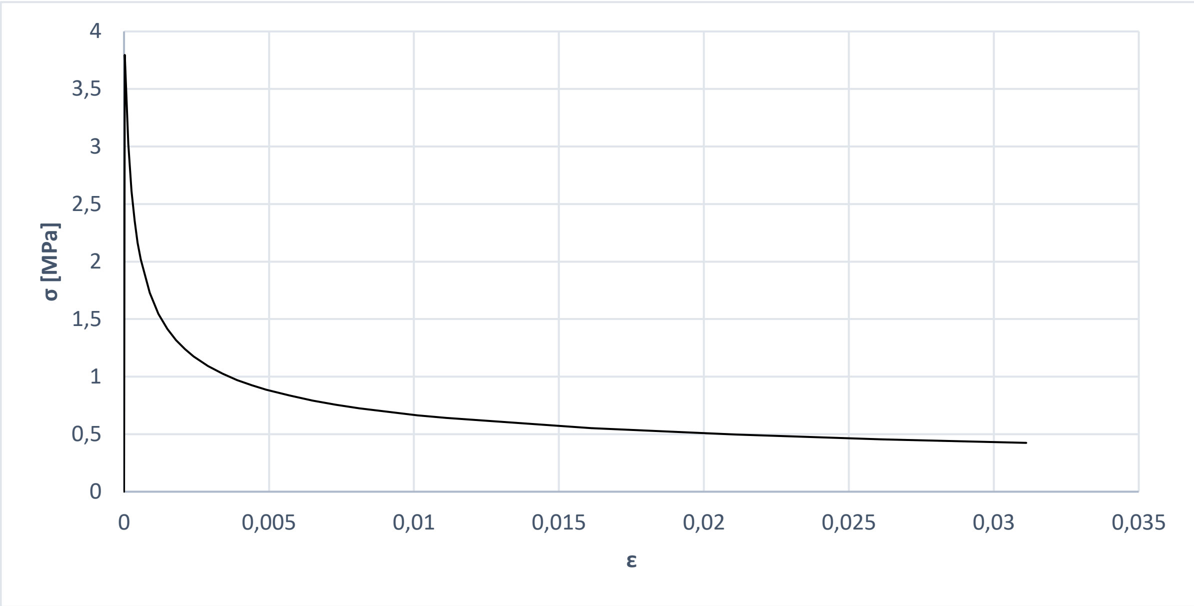

Figure 5.21 - *stress-strain curve - Whang & Hsu (41)– C45/55*

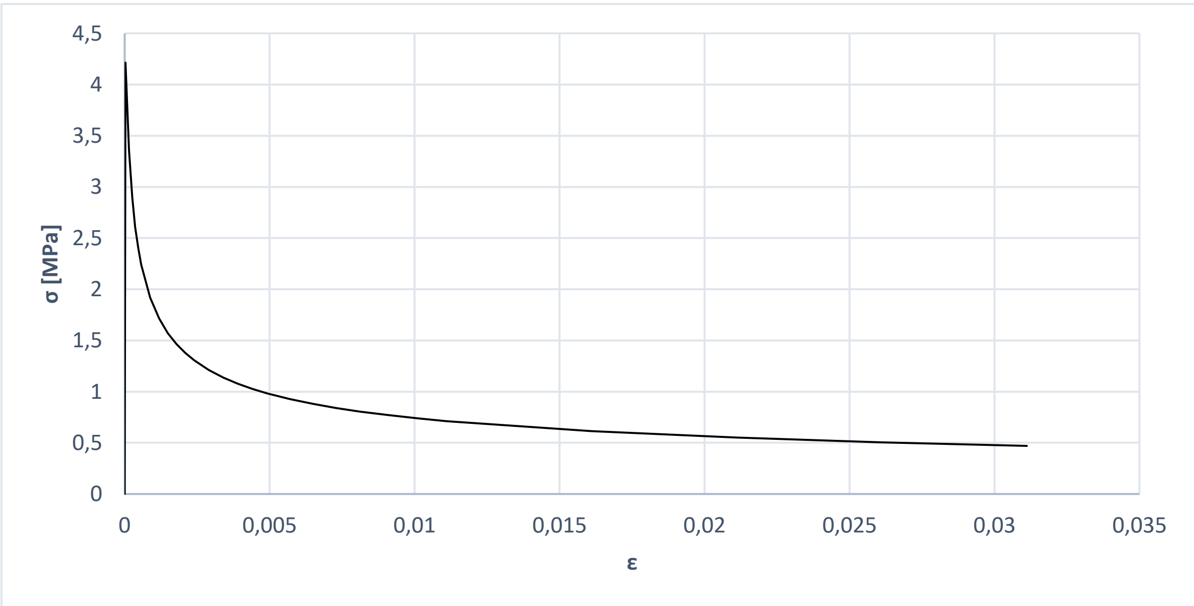

Figure 5.22 - *stress-strain curve - Whang & Hsu(41) – C55/67*

The last two methods are both based on the fracture energy criterion but are used differently in Abaqus: the post-failure stress can be specified whether as a tabular function of displacement or as fracture energy.
These methods are related to the energy balance approach developed by Hillerborg et al., (1976), which showed a reasonable agreement with results from a tensile laboratory test. Hillerborg et al. assumed that the response of concrete under tension is linear until the fracture surface is reached and then a linear softening branch (figure 5.22 - (25)) beyond cracking was adopted (39).

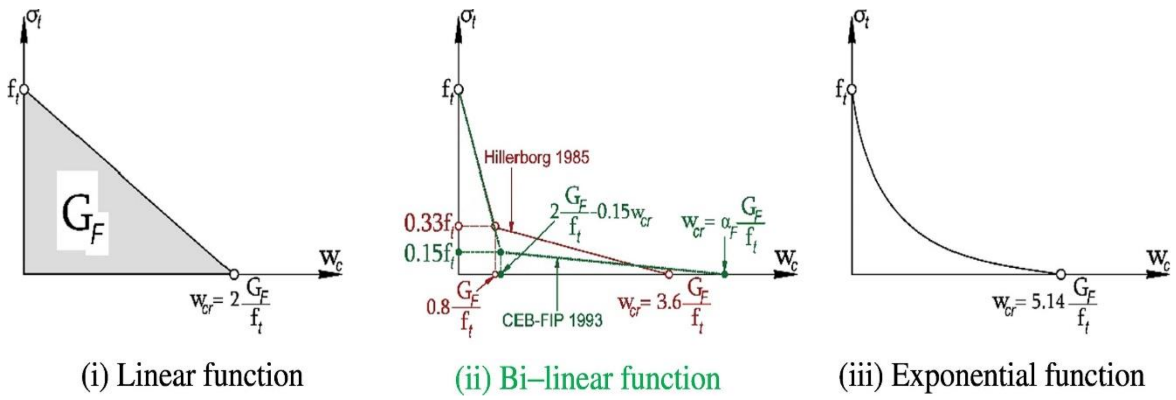

Figure 5.23 - *Concrete stress-crack opening curve: (i) Linear softening branch* (42) *, (ii) Bi-linear softening branch* (43);(44)*, (iii) Exponential softening branch (*(45)

Thus, concrete behaviour in this stage is controlled by this energy criterion based on the amount of energy absorbed by the formation of a unit area of crack surface.
In fracture mechanics theory, the fracture energy G_f is determined as the ratio of the total energy that is generated to fracture a specimen to the fractured cross-sectional area: in particular, fracture energy it is assumed to be the area under the stress-crack opening relation. The cohesive crack model, called a fictitious crack model by Hillerborg et al.,(1976) has been one of the essential tools in the analysis of the fracture of concrete and cement-based materials since its first application to structural analysis.
The fracture energy is defined, according to *Hillerborg et al., (1976)*, as:

$$Gf = \int \sigma dw$$

Different type of relationships, as depicted in figure 5.22, can be used. All these curves have standard essential features, as follows (46):

- it is non-negative and non-increasing;
- for zero crack openings, its value equals tensile strength;
- it tends to zero for large crack openings (complete failure, zero strength);
- it can be integrated over (0; ∞).

Assuming a linear approach to define the tensile cracking behaviour is the most straightforward approach: although, this approach tends to increase the stiffness of the concrete. Instead, a smoothest tension stiffening function, which is recommended, describe better the descending branch: in particular, can be used a bi-linear relationship, proposed from Hillerborg(1985)(43) and suggested by Model Code 1993-2010, or an exponential relationship provided by Cornelissen et al., (1986) and Hordijk,(1992). These formulations are the most used and cited in the literature: Furthermore, a predominantly debated in literature is about the location of the kink point.

As depicted in figure 5.22, Hillerborg (1985)(43) proposed the coordinates of the kink point at:

$$(0.33f_t\,,0.8G_f/f_t)$$

while the coordinates suggested by CEB-FIP (1993) were:

$$(0.15f_t\,,\frac{2G_f}{f_t}-0.15w_{cr})$$

where $w_{cr}=\frac{\alpha_f G_f}{f_t}$, G_f is the total fracture energy and α_f a dimensionless coefficient, both depending on the aggregate size. Instead, as shown in the following figure, with the new Model Code, these coordinates of the kink point were changed into:

$$(0.2f_t\,,\frac{G_f}{f_t})$$

Also the cracking displacement w_{cr} at which complete loss of strength takes place is defined differently:

$$w_{cr}=2\frac{G_f}{f_t}\qquad (\text{“Abaqus Analysis User's Manual, vol3,”})$$

$$w_{cr}=\frac{\alpha_f G_f}{f_t}\qquad (Model\ Code, 1993)$$

$$w_{cr}=5\frac{G_f}{f_t}\qquad (Model\ Code, 2010)$$

$$w_{cr}=3.6\frac{G_f}{f_t}\qquad (\text{Hillerborg}, 1985)$$

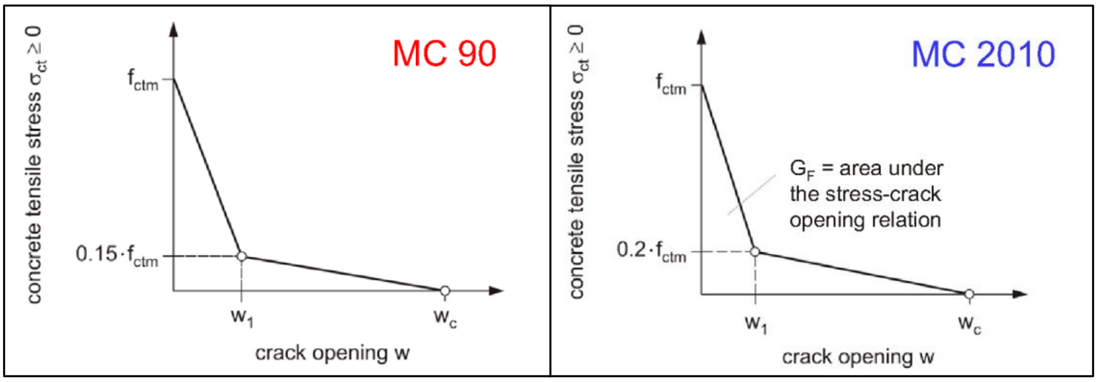

Figure 5.24 - *Bi-linear softening curve Model Code 1993-2010*

It can be noted that the tail of the exponential law is 1.5 longer than that of Hillerborg, (1985) bi-linear law: however, the predict remains unaffected, and the numerical response is expected to be similar (25).
In this project, in order to explore take advantage of all the tools provided by the concrete damaged plasticity model, the linear softening relationship and the exponential softening

relationship were adopted: in particular, the linear response was used into Abaqus to improve "the fracture energy approach", while the Cornelissen's exponential curve was used for the "crack-opening displacement approach" as described in section 5.2.1.2 and 5.2.2.2.

The bi-linear softening curve was not used due to some computational errors within Abaqus.

The exponential law of Cornelissen et al. (1986) has the following expression:

$$\frac{\sigma_t}{f_t} = \left[1 + (c_1 \frac{w_t}{w_{cr}})\right] \exp\left(-c_2 \frac{w_t}{w_{cr}}\right) - \frac{w_t}{w_{cr}} (1 + c_1^3) \exp(-c_2)$$

$$w_{cr} = 5.14 \frac{G_f}{f_t}$$

where σ_t is the tensile stress normal to the crack direction, f_t is the concrete uniaxial tensile strength, w_c is the crack-opening displacement, w_{cr} is the crack-opening displacement at the complete release of stress or fracture energy, c_1 and c_2 are material constants taken as 3.00 and 6.93, respectively. G_f is the fracture energy of concrete required to create a stress-free crack over unit surface.

The tensile curve adopted in the non-linear analysis is depicted in figure 5.24-5.25, and its values are shown in table 5.5-5.6.

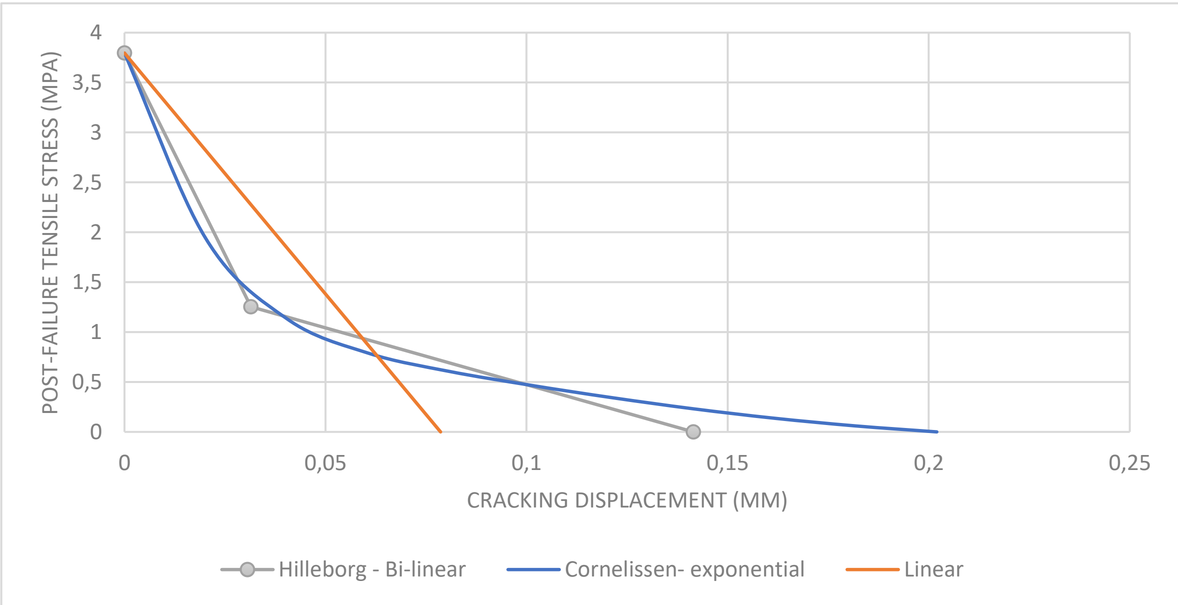

Figure 5.25 – *Linear, bi-linear and exponential curve - concrete class C45/55*

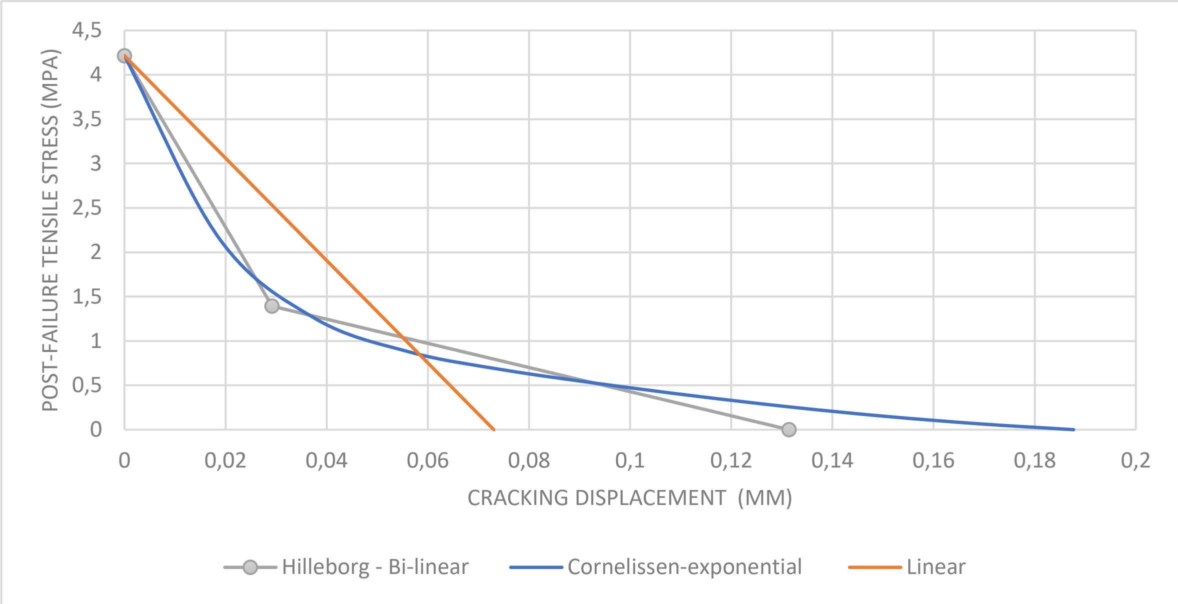

Figure 5.26 – *Linear,bi-linear and exponential curve - concrete class C55/67*

Cracking displacement	***Stress***	***Damage***	***Plastic displacement***
$\tilde{u}_t^{ck}$	$\sigma_t\ [MPa]$	***d***	$\tilde{u}_t^{pl}$
-	**-**	$d_t = 1 - \frac{\sigma_t}{\sigma_{tu}}$	$\tilde{u}_t^{pl} = \tilde{u}_t^{ck} - \frac{d_t}{1-d_t}\frac{\sigma_t l_0}{E_0}$
0	*3,795446994*	*0,0000*	-
0,020201923	*1,938855441*	*0,4892*	*0,020152394*
0,040403845	*1,133368652*	*0,7014*	*0,040332829*
0,060605768	*0,78947287*	*0,7920*	*0,060525578*
0,080807691	*0,605930956*	*0,8404*	*0,080722604*
0,101009614	*0,467323469*	*0,8769*	*0,100920829*
0,121211536	*0,343161151*	*0,9096*	*0,12111944*
0,141413459	*0,231817849*	*0,9389*	*0,141318392*
0,161615382	*0,136891344*	*0,9639*	*0,161517783*
0,181817304	*0,059984793*	*0,9842*	*0,181717654*

Table 5.5 – *Exponential curve values C45/55*

Cracking displacement	***Stress***	***Damage***	***Plastic displacement***
$\tilde{u}_t^{ck}$	$\sigma_t\ [MPa]$	***d***	$\tilde{u}_t^{pl}$
-	-	$d_t = 1 - \frac{\sigma_t}{\sigma_{tu}}$	$\tilde{u}_t^{pl} = \tilde{u}_t^{ck} - \frac{d_t}{1-d_t}\frac{\sigma_t l_0}{E_0}$
0	*4,214293618*	*0,0000*	*0*
0,018769058	*2,152817869*	*0,4892*	*0,018717143*
0,037538117	*1,258441571*	*0,7014*	*0,037463679*
0,056307175	*0,876595164*	*0,7920*	*0,056223121*
0,075076234	*0,672798478*	*0,8404*	*0,074987047*
0,093845292	*0,518894959*	*0,8769*	*0,09375223*
0,112614351	*0,381030706*	*0,9096*	*0,112517816*
0,131383409	*0,257400112*	*0,9389*	*0,131283761*
0,150152468	*0,15199799*	*0,9639*	*0,150050165*
0,168921526	*0,066604416*	*0,9842*	*0,168817073*

Table 5.6 - *Exponential curve values C55/67*

Cracking displacement	***Stress***	***Damage***	***Plastic displacement***
$\tilde{u}_t^{ck}$	$\sigma_t\ [MPa]$	***d***	$\tilde{u}_t^{pl}$
-	-	$d_t = 1 - \frac{\sigma_t}{\sigma_{tu}}$	$\tilde{u}_t^{pl} = \tilde{u}_t^{ck} - \frac{d_t}{1-d_t}\frac{\sigma_t l_0}{E_0}$
0	*3,79544699*	*0*	*0*
0,003	*3,50692199*	*7,60E-02*	*0,002898749*
0,008240447	*3,21839699*	*1,52E-01*	*0,008139196*
0,013480894	*2,92987199*	*2,28E-01*	*0,013379643*
0,018721341	*2,64134699*	*3,04E-01*	*0,01862009*
0,023961788	*2,35282199*	*3,80E-01*	*0,023860537*
0,029202234	*2,06429699*	*4,56E-01*	*0,029100983*
0,037062905	*1,77577199*	*5,32E-01*	*0,036961654*
0,044923575	*1,48724699*	*6,08E-01*	*0,044822324*
0,052784245	*1,19872199*	*6,84E-01*	*0,052682994*
0,060644916	*0,91019699*	*7,60E-01*	*0,060543665*
0,068505586	*0,62167199*	*8,36E-01*	*0,068404335*
0,078606703	*0,33314699*	*9,12E-01*	*0,078505452*

Table 5.7 - *Linear curve values C45/55*

Cracking displacement	*Stress*	*Damage*	*Plastic displacement*
$\tilde{u}_t^{ck}$	$\sigma_t\ [MPa]$	d	$\tilde{u}_t^{pl}$
-	-	$d_t = 1 - \frac{\sigma_t}{\sigma_{tu}}$	$\tilde{u}_t^{pl} = \tilde{u}_t^{ck} - \frac{d_t}{1-d_t}\frac{\sigma_t l_0}{E_0}$
0	*4,2143*	*0*	*0*
0,003	*3,925775*	*6,85E-02*	*0,00289387*
0,007868757	*3,63725*	*1,37E-01*	*0,007762627*
0,012737514	*3,348725*	*2,05E-01*	*0,012631384*
0,017606271	*3,0602*	*2,74E-01*	*0,017500141*
0,022475028	*2,771675*	*3,42E-01*	*0,022368898*
0,027343785	*2,48315*	*4,11E-01*	*0,027237655*
0,034646921	*2,194625*	*4,79E-01*	*0,03454079*
0,041950057	*1,9061*	*5,48E-01*	*0,041843926*
0,049253192	*1,617575*	*6,16E-01*	*0,049147062*
0,056556328	*1,32905*	*6,85E-01*	*0,056450197*
0,063859463	*1,040525*	*7,53E-01*	*0,063753333*
0,073031356	*0,752*	*8,22E-01*	*0,072925225*

Table 5.8 - *Linear curve values C55/67*

5.2.3 Dilation angle calibration

In this section is investigated the role of one other fundamental parameter of the concrete damaged plasticity model: the dilation angle ψ. This value describe also the level of volum change experienced by the concrete as crack occur and slip occurs along crack surfaces (48).
A sensitivity analysis on dilation angle was performed to investigate its influence on the response of the structure in terms of CDP model variables output: the calibration of this parameter is very common and recommended in the research field even because in most of the case, real results from a laboratory test are not available.
Furthermore, Abaqus doesn't provide a standard value for the dilation angle. Various researches topic analyse this problem, and different values of the dilation angle are used. Usually, for concrete, a range between 31° to 42° of the dilation angle parameter is recommended (49): this is also confirmed according to various studies performed by different authors (19), (50) and (51).
Besides, it was found out that low dilation angle values produce brittle behaviour while higher values produce a more ductile behaviour(52) and in particular, decreasing values of the dilation angle reduces the stiffness of the structure in the non-linear stage(53).

The dilation angle ψ calibration was performed on the two local models, having the following characteristics:

- a mesh size of 75 mm for the entire model except for the parts where it is expecting that cracks occur: in particular, the bottom concrete part and the surfaces where the saddle lays on. These parts are meshed using a finer mesh of 50 mm;
- loads, in particular, SLS combination, and boundary conditions (section 3 - 4.3.4);
- compressive behaviour described in section 5.2.2.1;
- tensile behaviour, in particular, the softening branch, is described using the stress-strain curve(section 5.2.2.2 – table 5.3,5.4);
- $\epsilon = 0.1$ (section 5.2.2)
- $\frac{\sigma_{b0}}{\sigma_{c0}} = 1.16$ (section 5.2.2);
- $K_c = 0.66$ (section 5.2.2);
- μ viscotity parameter value is of 0.001 (section 5.2.2);
- elastic-perfectly plastic behaviour for reinforcement (section 2.4 – 4.3.2).

Even if in the previous section, after the mesh sensitivity analysis, a 50 mm mesh size was recommended, this value could not be adopted because using that mesh size the computational time became extremely long (almost 24 hours); instead, using two different value, one coarser for the entire model (75 mm) and one finer for the most sensitive crack parts (50 mm), helped decreasing the computational time. The values of eccentricity, σ_{b0}/σ_{c0}, (ratio of biaxial compressive yield stress to initial uniaxial compressive yield stress), K_c and μ were set according to the research study of (54).
Finally, to investigate the dilation angle influence, this particular model was analysed with three different dilation angle values: 20°, 30° and 40°.
Abaqus offers a variety of output variables for the concrete damaged plasticity model, among which ("Abaqus Analysis User's Manual, vol3," 2010):

- DAMAGEC - compressive damage variable d_c;
- DAMAGET - tensile damage variable d_t;
- PEEQ - compressive equivalent plastic strain $\tilde{\varepsilon}_c^{pl}$;
- PEEQT - tensile equivalent plastic strain $\tilde{\varepsilon}_t^{pl}$;
- SDEG - stiffness degradation variable, d.
- ALLDMD - energy dissipated in the whole (or partial) model by damage;
- ALLPD - energy dissipated plastic deformation.

A first check was carried out on reference point 9 and 10, which are both located at the bottom concrete part of the model: in particular, for both points, the maximum principal plastic strain (PE, MAX.PRINCIPAL), the tensile damage variable (DAMAGET) and the stiffness degradation variable (SDEG) were plotted with the time (analysis time *t_0=0 – t_1=1, step incrementation time = 0,05).*
The maximum principal plastic strain was checked because it is the leading indicator of cracking initiation in concrete damage plasticity model, and it is a powerful tool to visualise the direction of cracking. Cracks are supposed to initiate when the tensile equivalent plastic strain is greater than zero ($\tilde{\varepsilon}_t^{pl} > 0$) and the maximum principal plastic strain is positive(18). In addition, the orientation of cracks is assumed to be perpendicular to the maximum principal plastic strains.

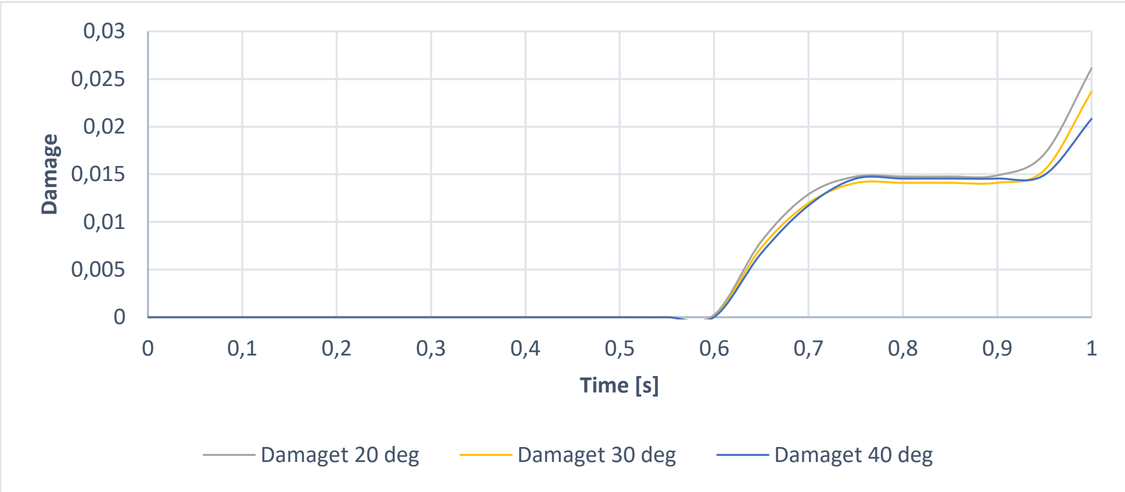

Figure 5.27 - *DAMAGET - Reference point 9 (ψ =* $\mathbf{20°}$ *,* $\mathbf{30°}$*,* $\mathbf{40°}$*)*

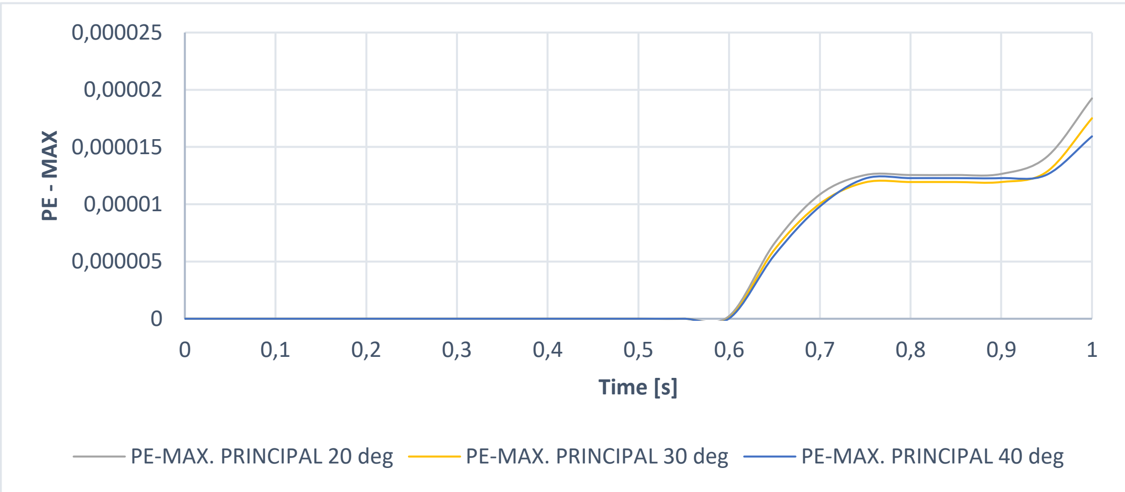

Figure 5.28 - *Maximum principal plastic strain - Reference point 9 (ψ=20°, 30°, 40°)*

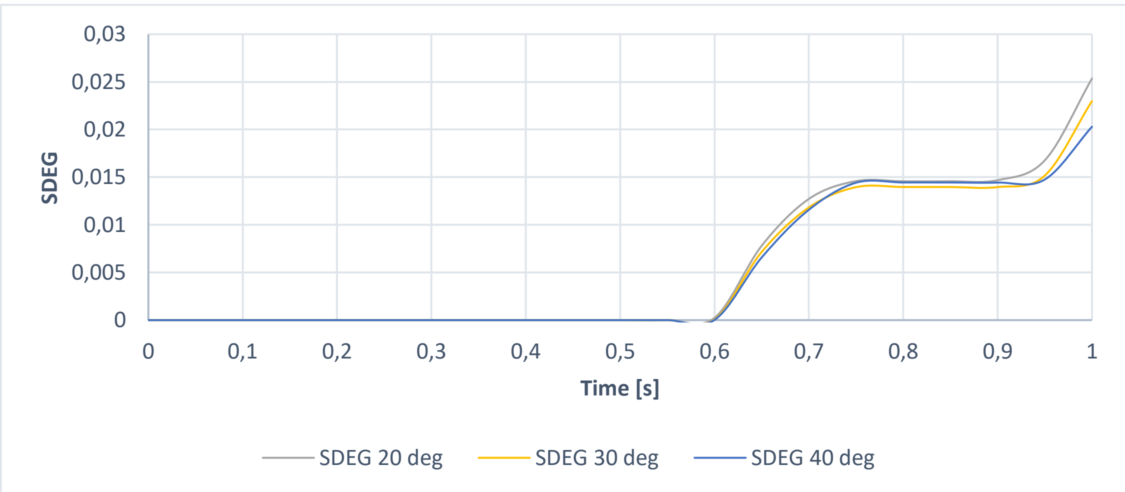

Figure 5.29 - *Stiffness degradation variable - Reference point 9 (ψ=20°, 30°, 40°)*

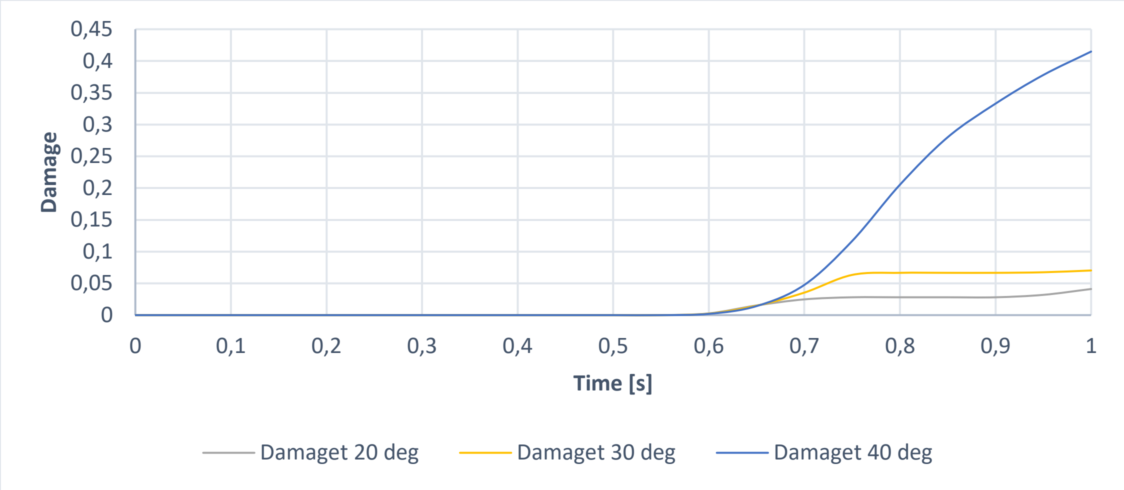

Figure 5.30 - *DAMAGET - Reference point 10 (ψ=20°, 30°, 40°)*

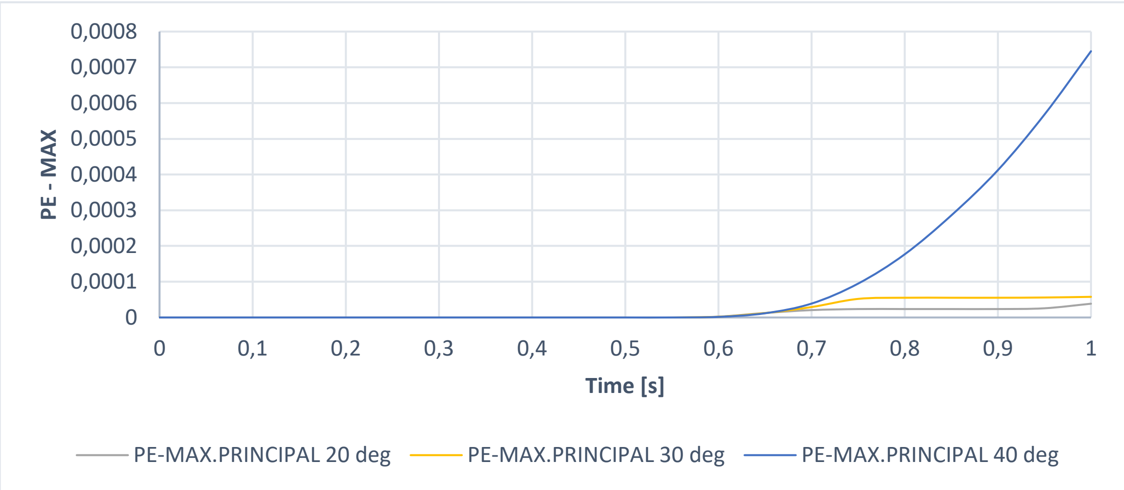

Figure 5.31 - *Maximum principal plastic strain - Reference point 10 (ψ=20°, 30°, 40°)*

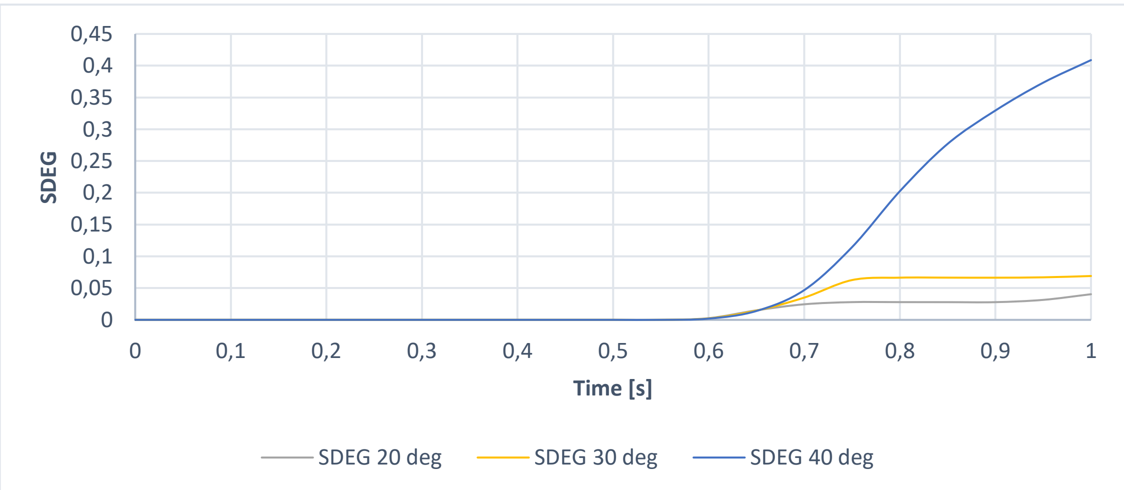

Figure 5.32 - *Stiffness degradation variable - Reference point 10 (ψ=20°, 30°, 40°)*

From the previous graphs, it is possible to give an interpretation of the influence of the dilation angle. The reference point 9-10 show a behaviour which is not the one indicated in the literature: as described before, when using higher values of the dilation angle, concrete becomes stiffer and whether the damage and the maximum principal plastic strain decrease. Instead, it seems that these points, in particular, RP 9, tend to exhibit a different behaviour which is characterised by increasing value of the damage and the plastic strain with high dilation angle value, as shown in figure 5.26-5.27-5.28: furthermore, the reference point 10 shows an entirely different behaviour (fig.5.29-5.30-5.31).
Thus, these two points are not accurate enough to describe the influence of the dilation angle and, for this reason, a more suitable parameter for the check must be identified.
In particular, a linear path (fig.5.32), perpendicular to the cracks pattern, was defined within Abaqus: the previous output variables were plotted along this path. The following figure shows where the path is located (results from CDP analysis with $\psi = 20°$).

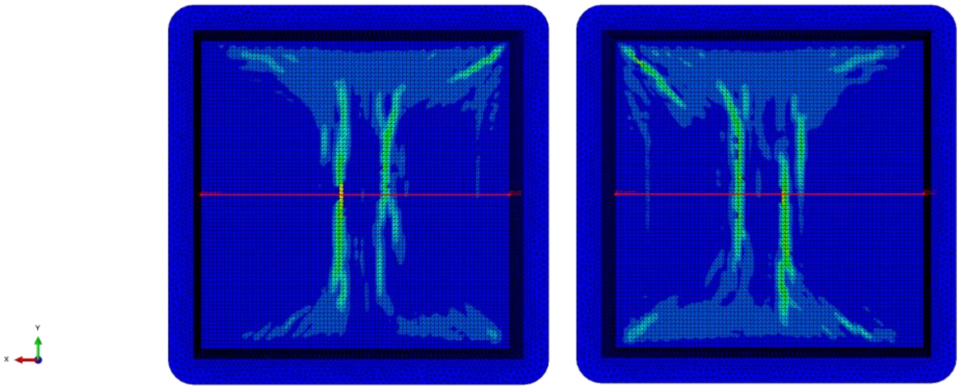

Figure 5.33 - *Linear path - local model #1(RH)-#2(LH)*

It was observed that using different and higher values of this parameter, the pattern of the cracks tend to evolve as the stiffness increase: in particular, this alteration causes that the two main cracks, showed above, start getting closer to each other and, thus, the reference points 9-10 got directly involved. This might be the reason why these two points showed a behaviour in terms of stiffness and damage, which is not easy to compare to the literature (fig.5.30-5.31).
From the following graphs (5.33-5.38), in which the three output variables (damage, maximum principal stresses and stiffness degradation) are plotted along the path, it is possible to understand this situation better. In particular, it was noticed that:

- as expected, along the path, output curve created with higher values $(30° - 40°)$ of the dilatation angle tends to be lower than the other related to lower values of $\psi(20°)$; in particular, this is clear in the external zone before the peaks, which indicate the presence of the main current cracks;
- between the peaks, higher values of $\psi\,(30°, 40°)$ define curve which are located above the one with $\psi = 20°$. This behaviour seems to be a demonstration of what described before, so that using higher values of the dilation angle, the two cracks get closer. Thus, in this case, it is likely that for values of ψ greater than $40°$, the crack pattern would be define only by one main crack.
- in correspondence with the cracks, the values of $30°, 40$ produce higher peak because stiffer model tends to have the damage concentrated in some parts while in brittle model, the damage is more scattered, as can be seen from the figure 5.43.

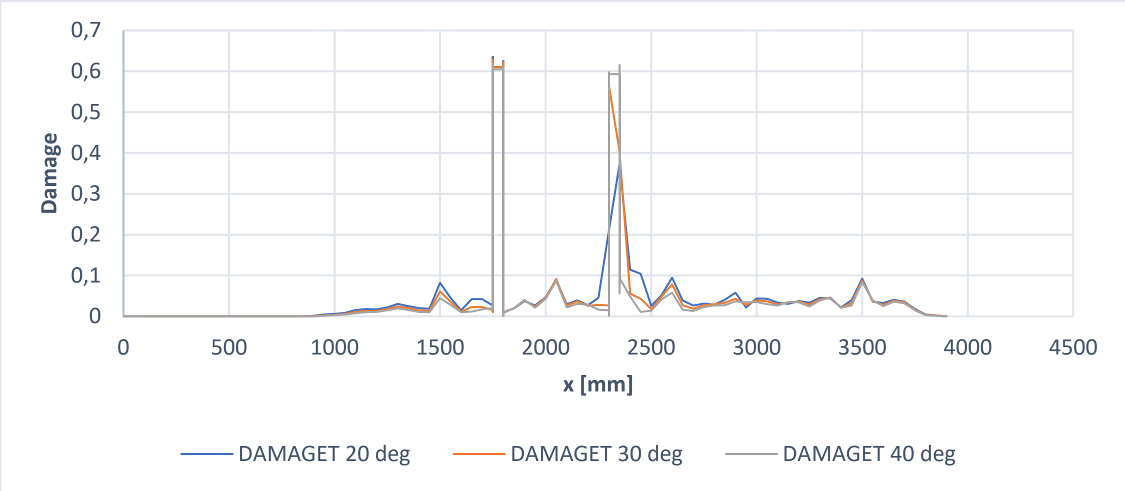

Figure 5.34 - *Damage - x (local model #1)*

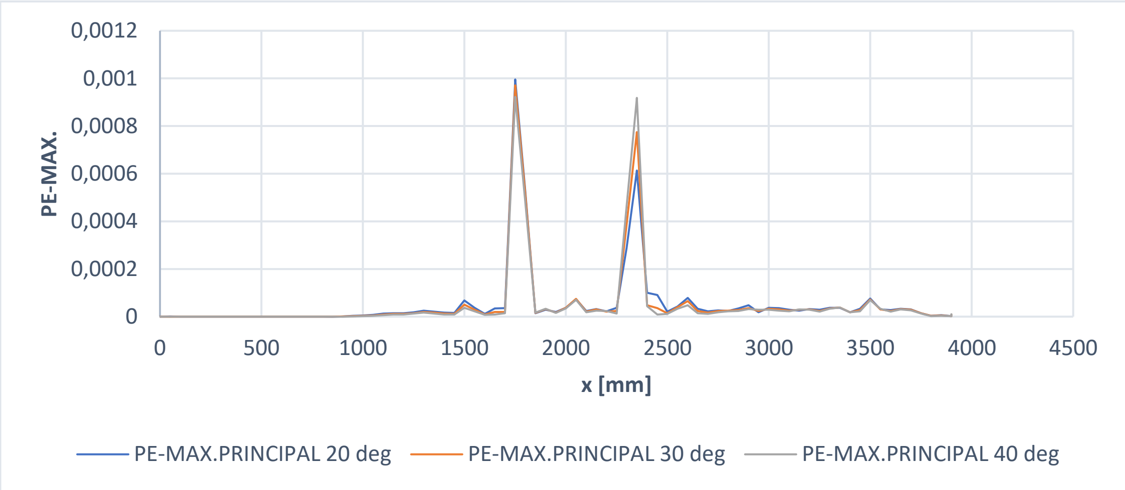

Figure 5.35 - *Maximum principal plastic strain - x (local model #1)*

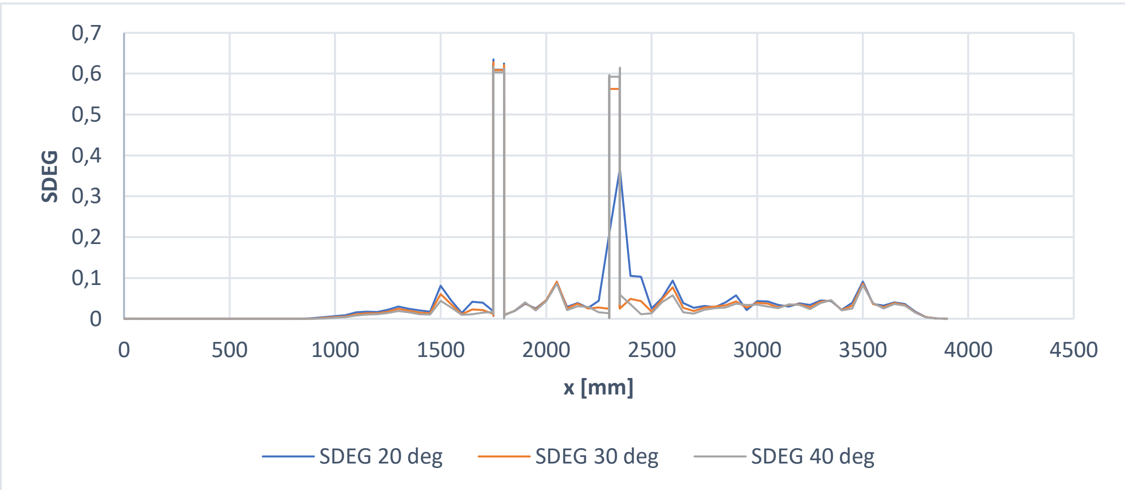

Figure 5.36 - *Stiffness degradation variable - x (local model #1)*

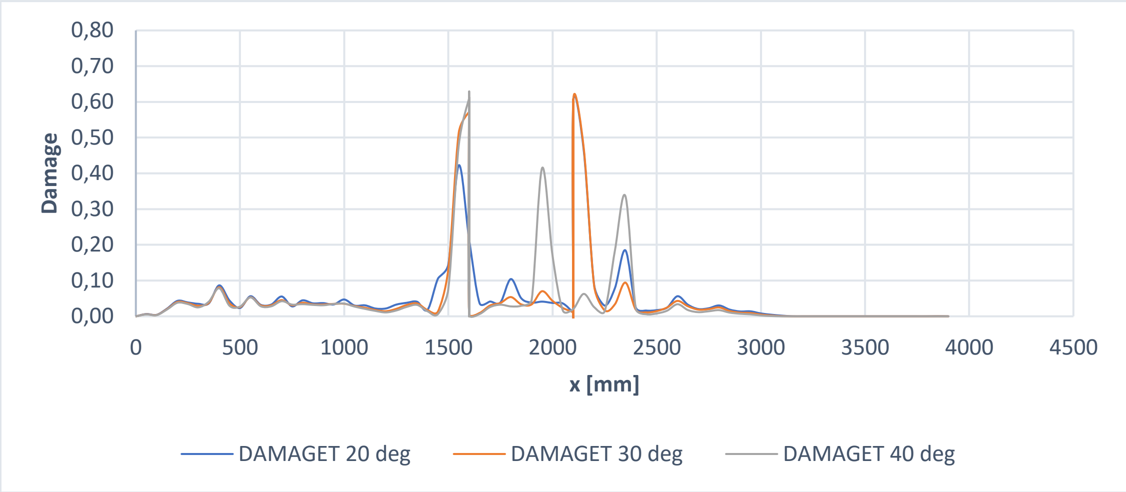

Figure 5.37 - *Damage - x (local model #2)*

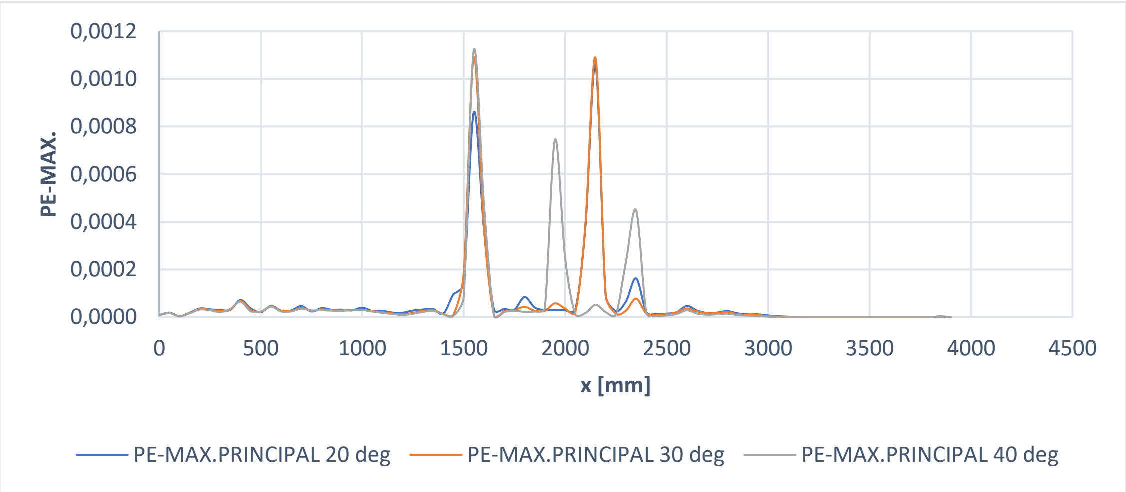

Figure 5.38 - *Maximum principal plastic strain - x (local model #2)*

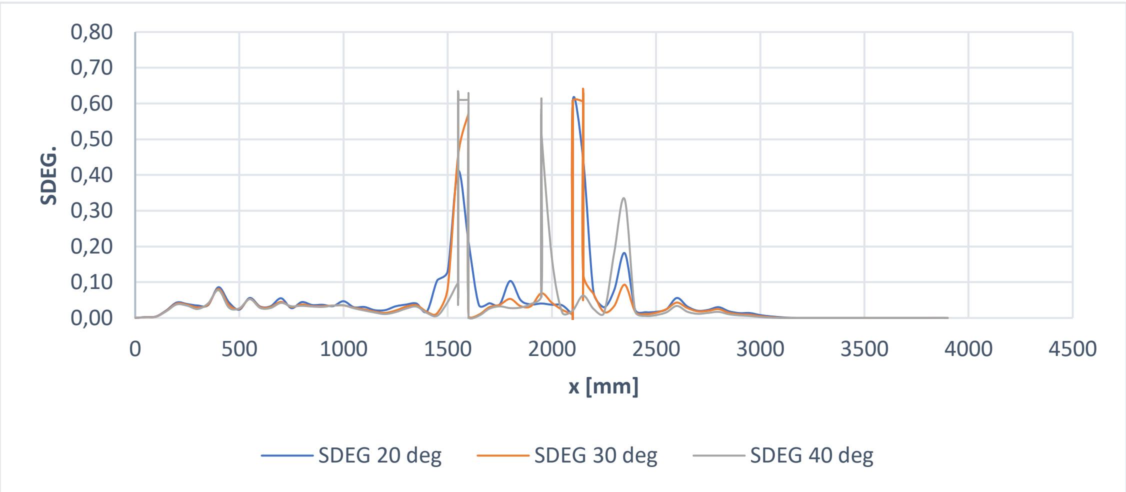

Figure 5.39 - *Stiffness degradation variable - x (local model #2)*

Finally, a further check, based on the energy, was performed. In particular, the attention was focused on the energy dissipated in the model by damage (ALLDMD) and the energy dissipated by plastic deformation (ALLPD). As depicted in the following figure 5.39-5.42, the model show without any doubt the classical behaviour described in literature: corresponding to higher value of the dilation angle, since the reinforced concrete is stiffer, it produce less energy and, so, the plastic strains and the damage in the whole model generate lower quantities of energy. This behaviour can be evicted by the following graphs, in which only the last step of the analysis was taken into account.

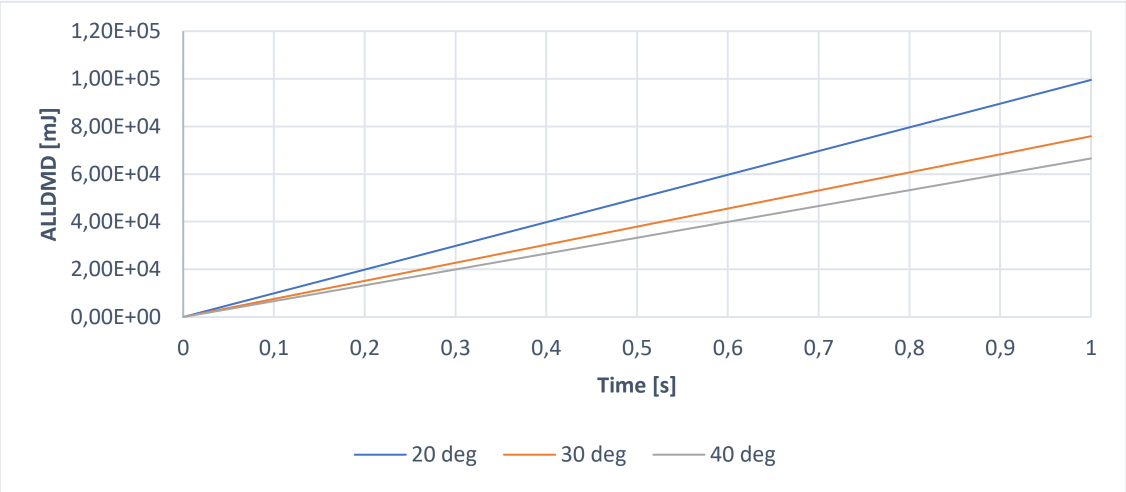

Figure 5.40 - *Energy dissipated by damage (local model #1)*

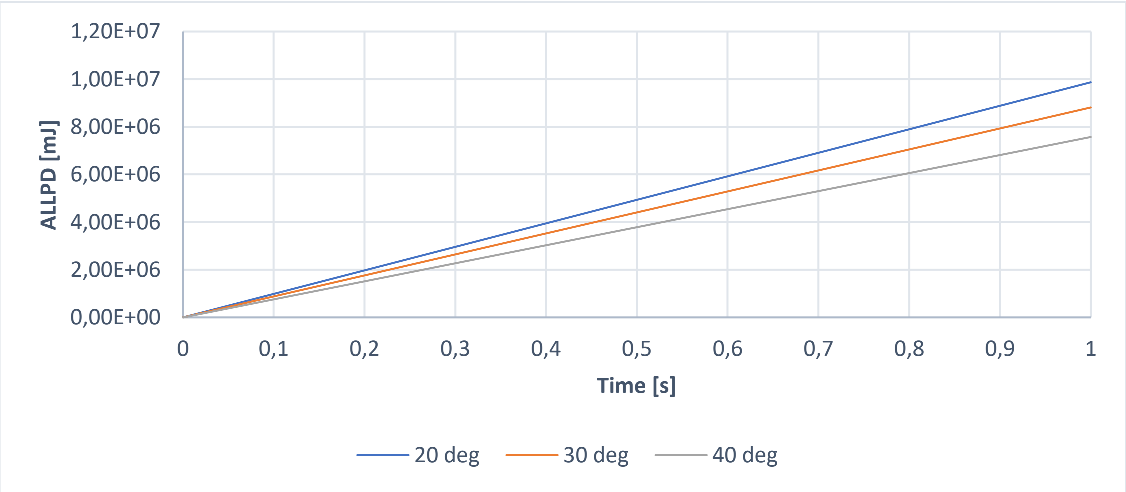

Figure 5.41 - *Energy dissipated by plastic deformations (local model #1)*

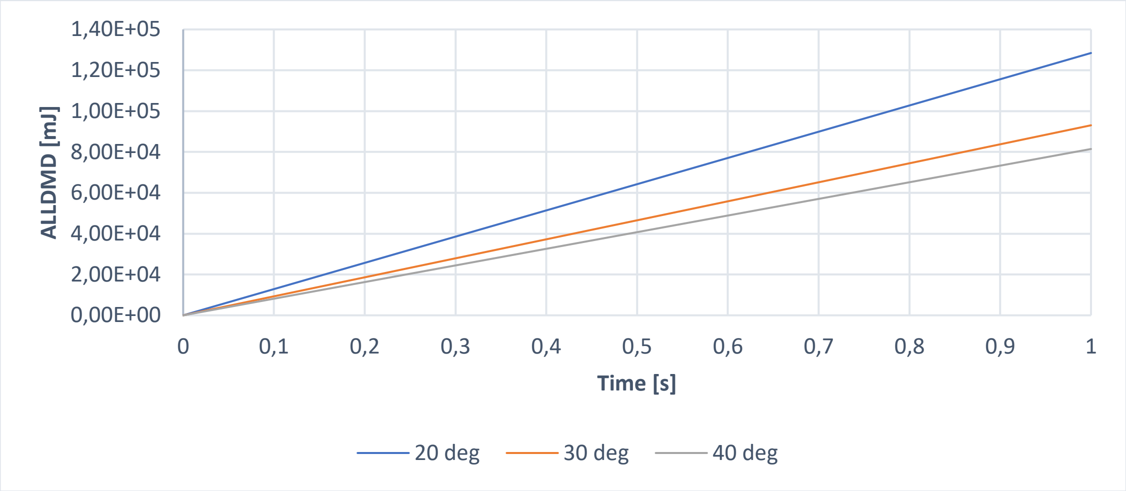

Figure 5.42 - *Energy dissipated by damage (local model #2)*

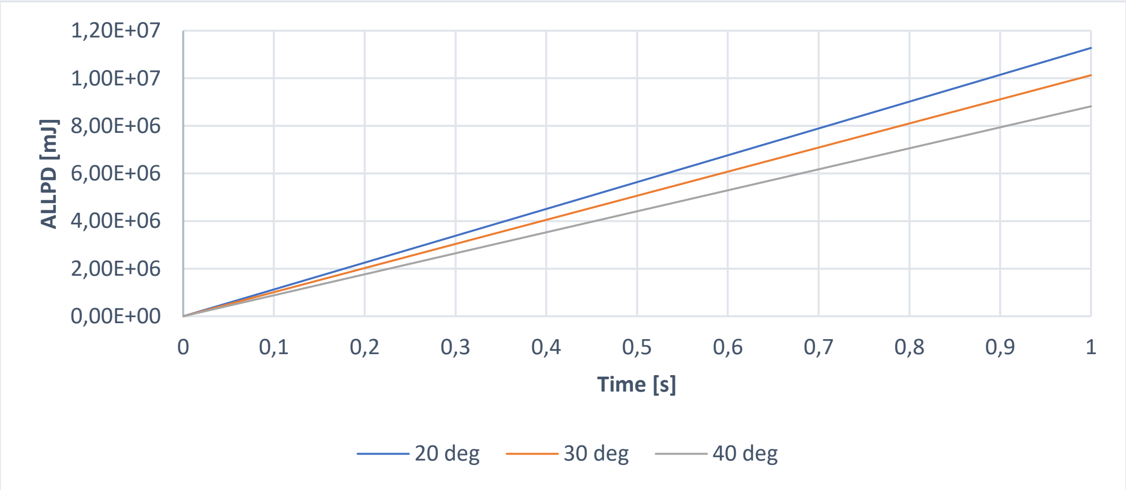

Figure 5.43 - *Energy dissipated by plastic deformations (local model #2)*

Moreover, figure 5.34 depict the damage result for both models within Abaqus: it is shown that the damage tends to decrease as the dilation angle increase and, it is also possible to see how the crack pattern evolves.
Besides, the two parts of the top tower are not perfectly symmetrical (tower #2 shows a hollow part which leads to a different reinforcement distribution) thence the pattern of the cracks is quite bit different. In the following figure, it is also possible to identify with the red point the location of reference point 9 and reference point 10 (fig.5.34).
Therefore, it is reasonable to declare that even if the values in terms of damage, plastic strain and stiffness degradation are likely similar to each other, each value of dilation angle defines a particular behaviour in terms of crack pattern. Usually, a dilation angle calibration, according to the literature, is compared with laboratory test curve or literature curve (load-displacement beam for example) but in this case, none of this was available. Thus, since a range value between $31° - 42°$ is often used in literature after the influence of ψ was investigated, it was chosen to define a dilation angle value of $\psi = 31°$, according to the research paper of Hafezolghorani (30), which used this value for testing B50 concrete class.

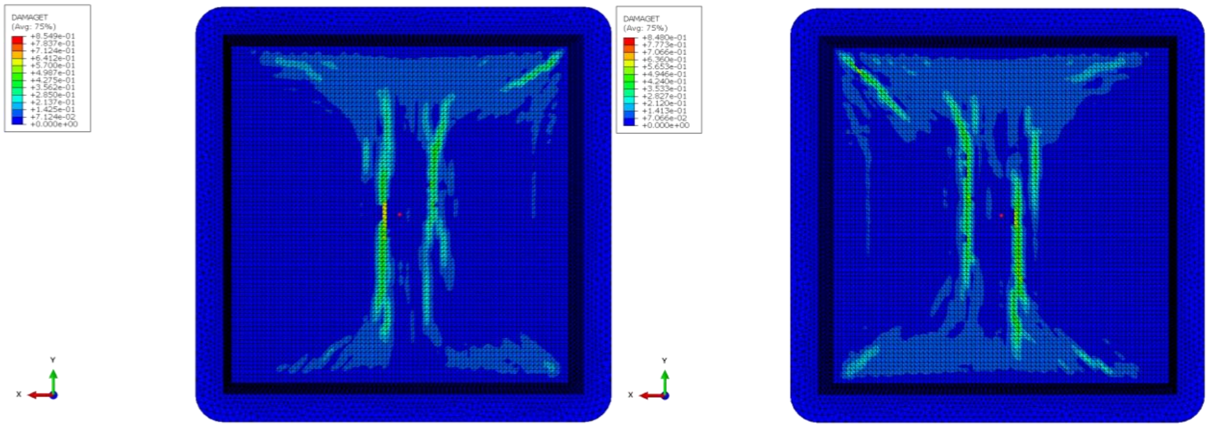

$(\psi = 20°)$

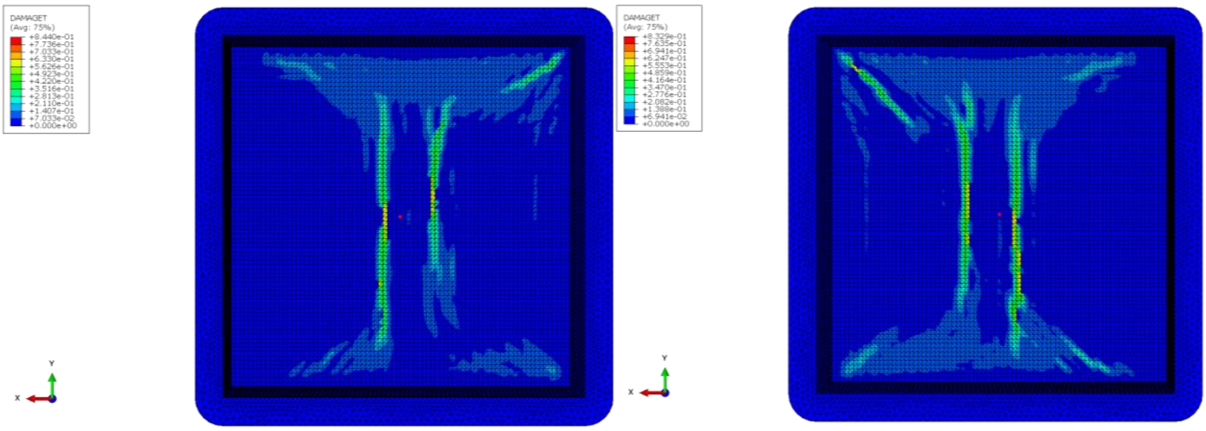

$(\psi = 30°)$

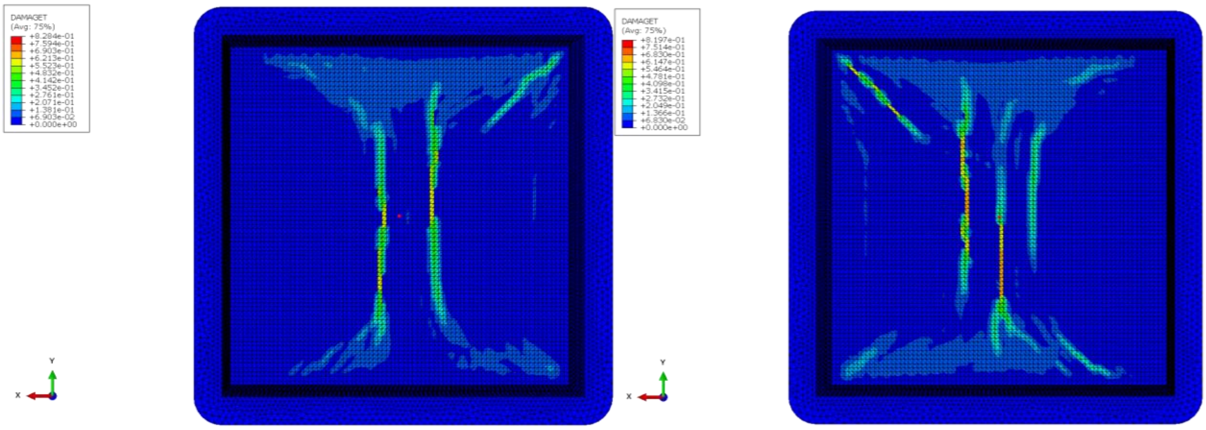

$(\psi = 40°)$

Figure 5.44 - *DAMAGET - local model#1 (LH) -#2(RH)*

5.2.4 Influence of Tension stiffening

In this section, the influence of the different models used to describe the tension stiffening effect was investigated. As previously described in section 5.2.2.2, Abaqus allows the user to execute the tension stiffening in three different ways:

- stress-strain curve $(\sigma - \varepsilon)$;
- stress- cracking displacement curve $(\sigma - w)$;
- fracture energy.

The analysis of the two local models were carried out using the value of the dilation angle found in the previous section ($\psi = 31°$) and the tension stiffening relations described in section 5.2.2.2. For a better and clearer understanding, these models are going to be identified as: "*stress-strain model*", "*stress-displacement model", "stress-fracture energy model".*

The results obtained from the analysis show different behaviours: in particular, the model implemented with the stress-strain curve seems to simulate better the non-linear phase. Indeed, since the information about the real behaviour of this structure were not available, this model was supposed to be the most accurate mainly because it is more capable than the other of providing further details about the crack pattern. This assumption was forced by the fact that whether laboratory test data for the material and real cracking analysis were missing.

The differences between these three different models are about their accuracy to represent the areas in which the tensile concrete strength has been reached. In particular, as depicted in figure 5.51, when the stress and the damage are given in terms of cracking displacement, the results are different. It was observed that, first, the models based on the fracture energy approach (*"stress-displacement model" and "stress-fracture energy model")* tend to overestimate the after-peak concrete response: this observation is proven by the fact that the damage variable (DAMAGET) and the energy dissipated by the damage (ALLDMD) are lower than the "stress-strain" case.

Damage variable (DAMAGET) was checked considering the two most damaged element laying on the two main cracks reported by the "*stress-strain model*": in particular, they are identified as element n.834185 and n.306495, for local model #1-#2 respectively; moreover, these elements was chosen not only for being the most damaged but also for being those with the highest values of plastic strain (whether maximum principal strain and plastic strain in x-direction) and stiffness degradation.

For these elements, the maximum principal stresses and the total strain were also plotted and investigated: furthermore, the total strain was calculated, adding up whether the elastic and plastic strain. Naturally, plastic strain values are zero until the elastic limit is reached.

As can be seen from the following graphs and images, it was observed that the models using the fracture energy approach give insufficient results: in particular, whether globally that locally these models produce very low values compared to the "*stress-strain model*"; this situation is described in figure 5.44-5.45, in terms of energy dissipated by the whole model and, in figure 5.46-5.47, in terms of damage for a single element.

Moreover, as depicted in figure 5.48-5.49, the stress-strain response given by these three different tension stiffening approach is different: in particular, while the response is identical up to the peak (linear field), it totally changes in the non-linear field, where, the stresses and strains given by the *stress-displacement model" and "stress-fracture energy model"* are quite limited. Thus, it seems that these two models simulate the behaviour of concrete after the tensile peak as if it did not lose stiffness. This deduction is demonstrated

by the fact that the values of damage are very low and the damaged is not localised but it is spread out: in particular, it can also be evicted by figure 5.50 in which PEEQT variable output is depicted. It was chosen to depict the tensile plastic strain (PEEQT) instead of the damage (DAMAGET) because further and different information needed to be given in order to confirm this discussion of the results.
Instead, the "stress-strain" model seems to be capable in representing the reduction of stiffness and strength of the concrete.
Finally, these different behaviour expressed by these model may also be ascribed to their conditions of use within Abaqus: indeed, the specification of tension stiffening using the stress-strain relation may lead to convergence problem due to mesh sensitivity: this problem occurs typically in the case with little or missing reinforcement(42). Instead, the models based on the fracture energy can also be used in case of no reinforcement, but their implementation requires the definition of a characteristic length associated with an integration point: this definition of the characteristic crack length is used because the direction in which cracking occurs is not known in advance. Abaqus assumes by default this length value as 1.

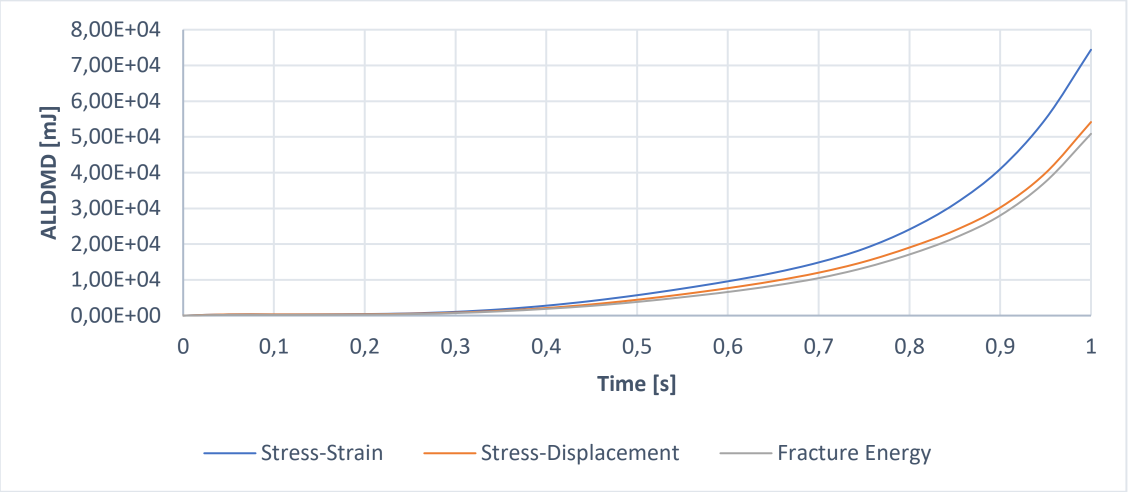

Figure 5.45 - *Energy dissipated by damage (local model #1)*

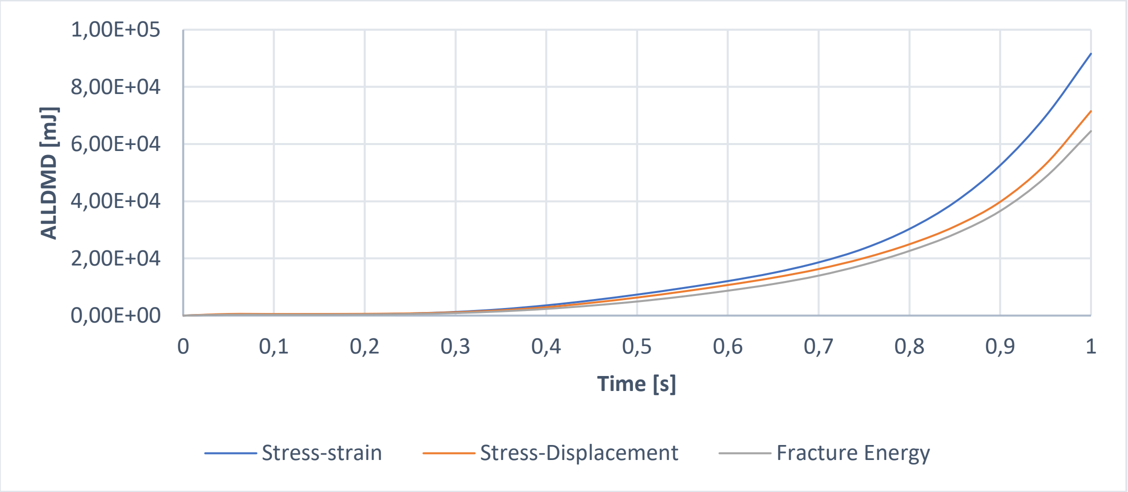

Figure 5.46 - *Energy dissipated by damage (local model #2)*

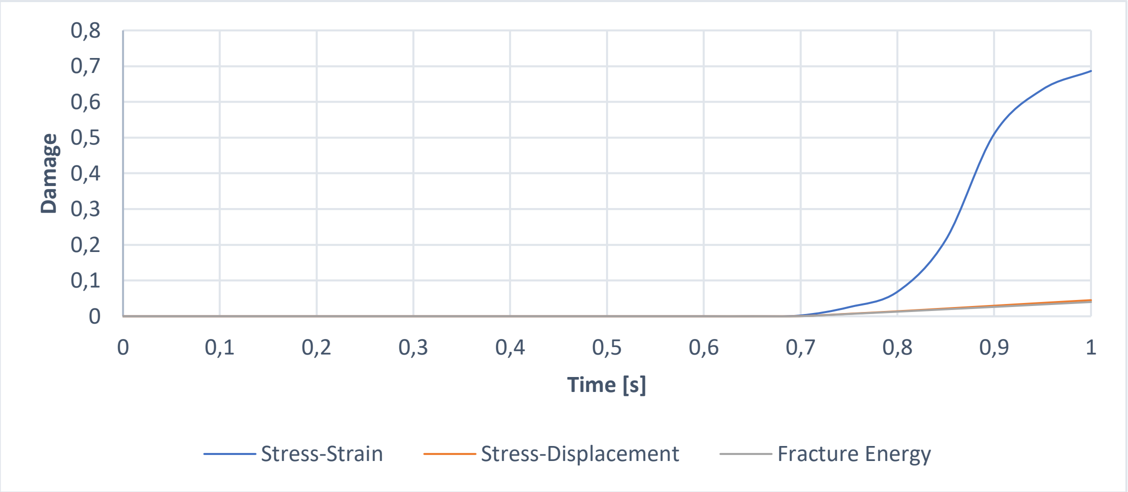

Figure 5.47 - *DAMAGET – E: 834185*

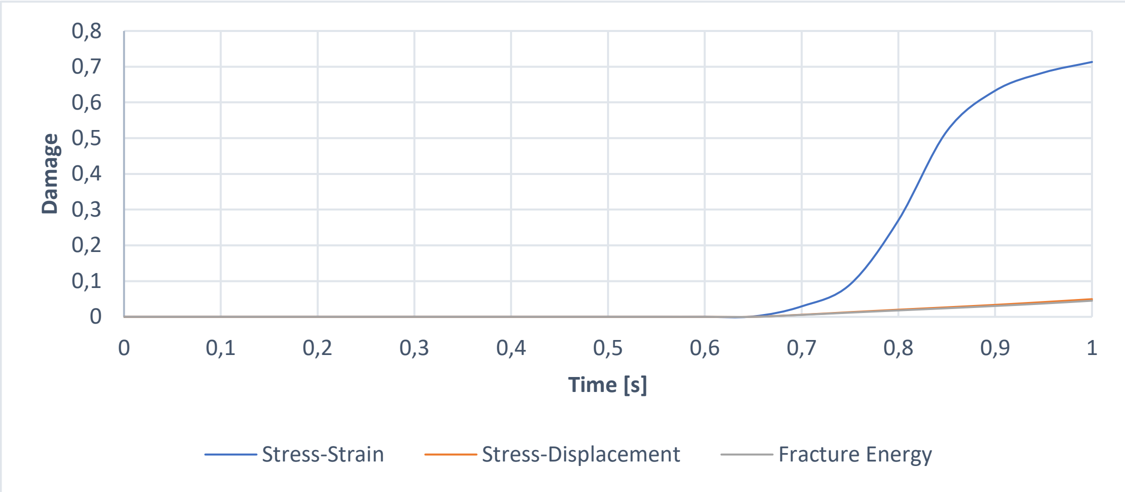

Figure 5.48 - *DAMAGET – E: 306495*

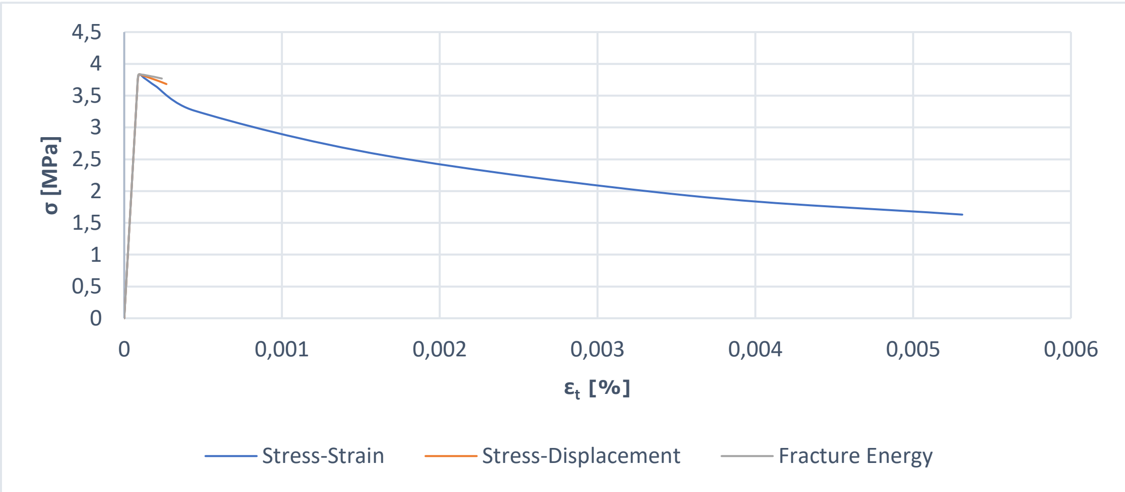

Figure 5.49 - *Maximum Principal stress-Total strain E: 834185*

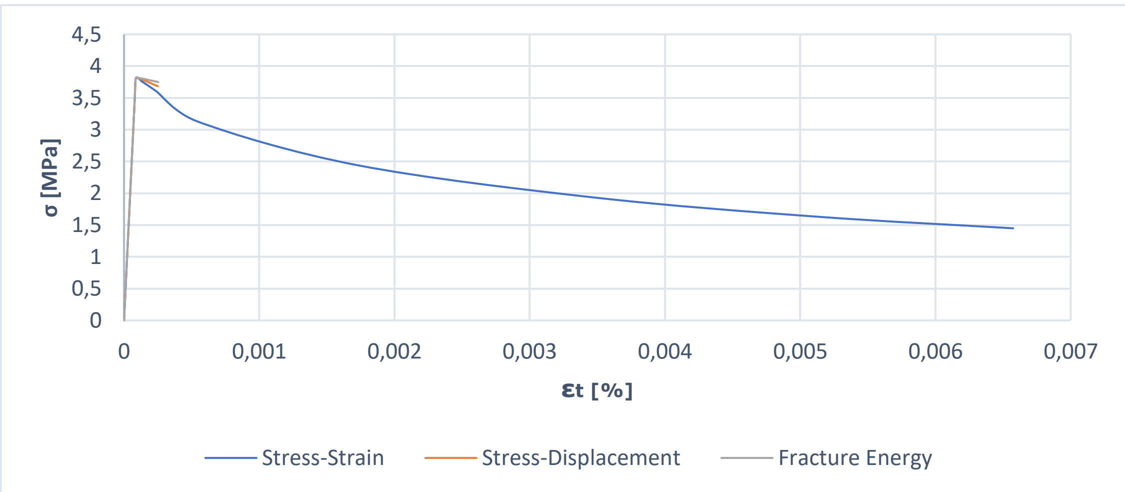

Figure 5.50 - *Maximum Principal stress-Total strain E: 306495*

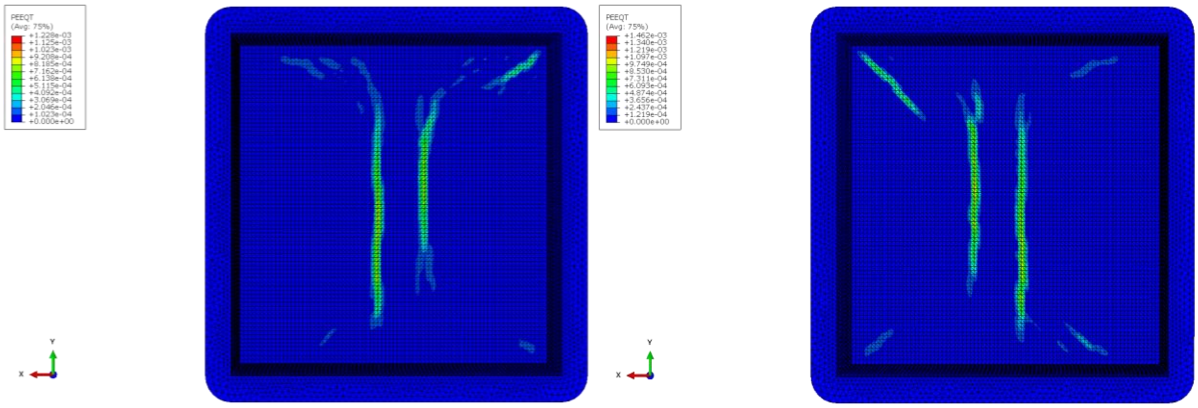

$("Stress - Strain\ model")$

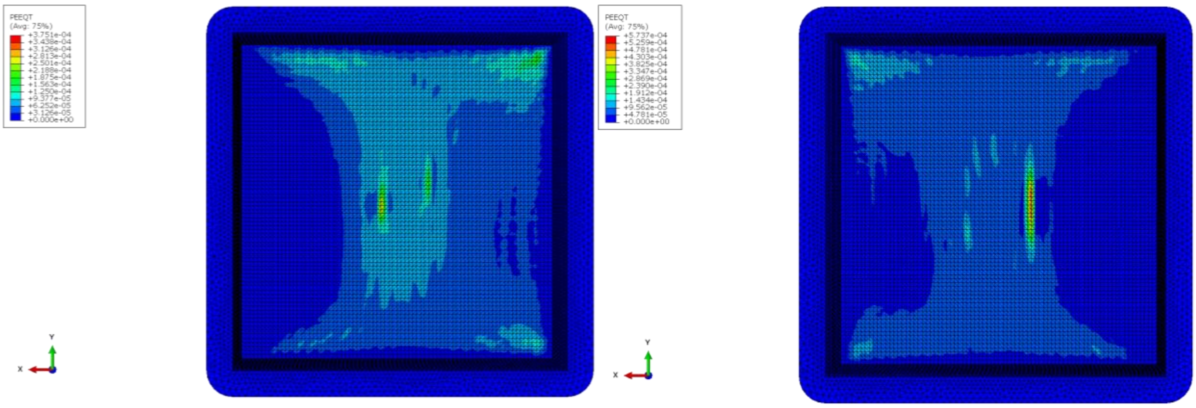

$("Stress - Displacement\ model")$

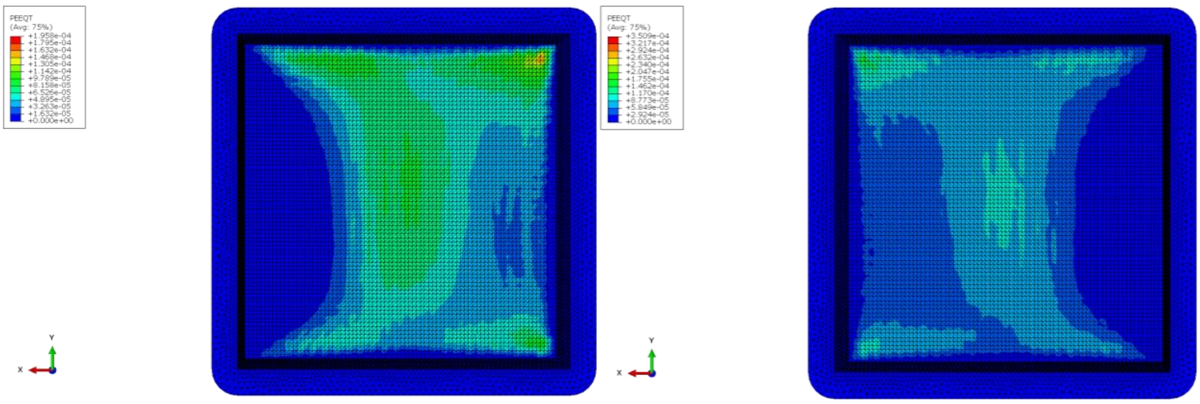

$(Fracture\ Energy\ model")$

Figure 5.51 - *PEEQT - local model#1 (LH) -#2(RH)*

6 Verification of serviceability (SLS)

6.1 Cracking on reinforced structures

Cracks in reinforced concrete are a common occurrence when it is subjected to bending, shear, torsion or tension loading. In particular, a reinforced concrete structure develops cracks whenever stress in the component exceeds its tensile strength. Cracks may also be caused by externally applied forces, imposed deformations and other phenomena such as shrinkage or thermal strains. Furthermore, the presence of these fractures may also lead to accelerated reinforcement corrosion in severe environments (55). Nevertheless, cracks are not always an indicator of a lack of serviceability or durability: in reinforced concrete structures, cracking due to tension, bending, shear, torsion is often inevitable and does not necessarily impair serviceability or durability.
The design codes pay much attention to this problem, in particular, for the serviceability limit state (SLS). This limit state aims to give the structures the ability to maintain the functionality characteristics during the design working life. Thus, in order to certify that the structure and/or the structural elements perform adequately in regular use, the serviceability limit state must be verified.
The verifications suggested by Eurocode 2 for the serviceability limit state are about:

- stress limitation;
- limit state of cracking;
- limit states of deformation;
- vibrations.

In this project, only the limit state of cracking was examined. Especially, in this section, using the cracks pattern information gained thanks to the concrete damaged plasticity model, a limitation of crack width was performed.
This verification was done following various standards:

- Eurocode 2 EN 1992-1-1:2004 (1);
- Eurocode 2 EN 1992-1-1:2018 (Draft Version) (56);
- Fib Bulletin 66: Model Code 2010, Final Draft- Volume 2(57).

All of these codes suggest the same way to carry out a limitation of crack width, but some parameters change from one version to another, and so the final value of the crack width. In particular, the codes suggest that the crack width has to satisfy the following conditions:

$$w_d \leq w_{lim}$$

where:

- w_d is the design crack width considered at the concrete surface;
- w_{lim} is the nominal limit value of crack width considered at the concrete surface.

The nominal limit value of crack width is specified for cases of expected functional, appearance related or in some cases durability related consequences of cracking. Instead, the design crack width is a value which depends on the maximum crack spacing $S_{r,max}$ and from the difference between the mean strain in the reinforcement (including the effect of

imposed deformations and taking into account the effects of tension stiffening) and the mean strain in the concrete between the cracks, $\varepsilon_{sm} - \varepsilon_{cm}$. Furthermore, in order to evaluate the relative mean strain $\varepsilon_{sm} - \varepsilon_{cm}$, it is necessary to define the effective area of concrete in tension surrounding the reinforcement $A_{c,eff}$ of depth $h_{c,eff}$ (figure 6.1).
This parameter $h_{c,eff}$ is assumed to be the lesser of these values for each standard:

$$h_{c,eff} = \min \begin{cases} 2,5\ (h - d) \\ (h-x)/3 \\ h/2 \end{cases} \qquad \text{Eurocode } 2 - 2004(1), \mathit{Draft}\ 2018(56)$$

$$h_{c,eff} = \min \begin{cases} 2,5\ (c + \Phi/2) \\ (h-x)/3 \end{cases} \qquad \text{Model Code } 2010(57)$$

where:

- *c* is the cover concrete, $7\ mm$;
- *Φ* is the diameter of the rebar $32\ mm$;
- *x* is the depth of the neutral axis, $\approx 1000\ mm$;
- *d* is the effective depth;
- *h* is the height of the section,$3650\ mm$.

In this case, since there are four layers of reinforcement at different heights in the effective area, the effective depth *d* was calculated in relation to the level of steel centroid, using the following equation:

$$d = \frac{\sum_i A_i * d_i}{A_{tot}} = 3355\ mm$$

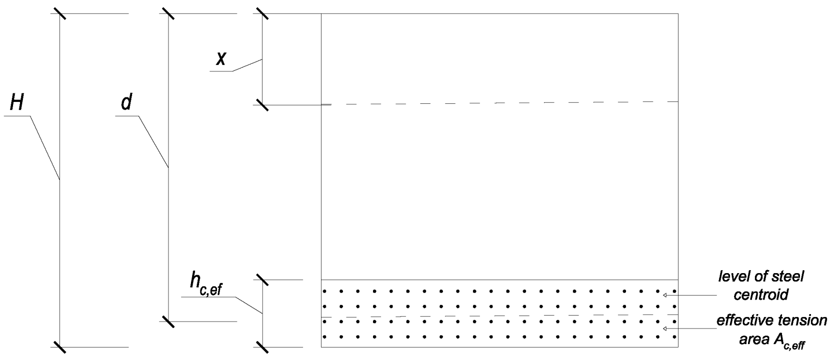

Figure 6.1 - *Effective tension area*

The evaluation of the maximum crack spacing $S_{r,max}$ and the relative mean strain $\varepsilon_{sm} - \varepsilon_{cm}$, and consequently the design crack width are reported in the following table.

<table>
<tr><td colspan="7">EUROCODE EN 1992-1-1:2004</td></tr>
<tr><td rowspan="2">w_{max} $[mm]$</td><td rowspan="2">XS 1</td><td colspan="5">Reinforced members - Quasi - permanent load combination</td></tr>
<tr><td colspan="5">0,3</td></tr>
<tr><td>w_k $[mm]$</td><td colspan="6">$s_{r,max}\,(\varepsilon_{sm} - \varepsilon_{cm})$</td></tr>
<tr><td colspan="2">$s_{r,max} = k_3 c + k_1 k_2 k_4 \dfrac{\Phi}{\rho_{eff}}$</td><td colspan="5">$(\varepsilon_{sm} - \varepsilon_{cm}) = \dfrac{\sigma_s - K_t \dfrac{f_{ct}}{\rho_{eff}}(1+\alpha\rho_{eff})}{E_s} \geq 0{,}6\dfrac{\sigma_s}{E_s}$</td></tr>
<tr><td>ρ_{eff} [%]</td><td>0,024593801</td><td>σ_s [MPa]</td><td colspan="4">60</td></tr>
<tr><td>c [mm]</td><td>70</td><td>f_{ctm} [MPa]</td><td colspan="4">3,795447</td></tr>
<tr><td>K_1</td><td>0,8</td><td>d [mm]</td><td colspan="4">3355</td></tr>
<tr><td>K_2</td><td>0,5</td><td>α</td><td colspan="4">5,335390945</td></tr>
<tr><td>K_3</td><td>3,4</td><td>K_t</td><td colspan="4">0,4</td></tr>
<tr><td>K_4</td><td>0,425</td><td>E_S [MPa]</td><td colspan="4">200000</td></tr>
<tr><td>Φ</td><td>32</td><td>E_C [MPa]</td><td colspan="4">37485,538</td></tr>
<tr><td>$S_{r,max}$ [mm]</td><td>459,1939509</td><td>h_c [mm]</td><td>737,5</td><td>737,5</td><td>883,33</td><td>1825</td></tr>
<tr><td colspan="2" rowspan="5">$w_k = s_{r,max}\,(\varepsilon_{sm} - \varepsilon_{cm}) = 0{,}082\ mm$</td><td>$A_{c,eff}$ $[mm^2]$</td><td colspan="4">2876250</td></tr>
<tr><td>A_s $[mm^2]$</td><td colspan="4">70737,92</td></tr>
<tr><td>ρ_{eff} [%]</td><td colspan="4">0,024593801</td></tr>
<tr><td>0,6*σ_s/E_S [%]</td><td colspan="4">0,02%</td></tr>
<tr><td>$\varepsilon_{sm} - \varepsilon_{cm}$ [%]</td><td colspan="4">-0,005%</td></tr>
</table>

Table 6.1 - *Calculation of crack width (EN 1992-1-1:2004-7.3.4)* (1)

<table>
<tr><td colspan="7">MODEL CODE 2010 – FINAL DRAFT – VOLUME 2</td></tr>
<tr><td rowspan="2">$w_{lim}\ [mm]$</td><td rowspan="2">XS 1</td><td colspan="5">Reinforced members - Quasi - permanent load combination</td></tr>
<tr><td colspan="5">0,2</td></tr>
<tr><td>$w_{max}\ [mm]$</td><td colspan="6">$2l_{s,max}\,(\varepsilon_{sm} - \varepsilon_{cm})$</td></tr>
<tr><td colspan="2">$l_{s,max} = kc + \frac{1}{4}\frac{f_{ctm}}{\tau_b}\frac{\Phi}{\rho_{eff}}$</td><td colspan="5">$(\varepsilon_{sm} - \varepsilon_{cm}) = \frac{\sigma_s - \beta\frac{f_{ct}}{\rho_{eff}}(1+\alpha\rho_{eff})}{E_s}$</td></tr>
<tr><td>ρ_{eff} [%]</td><td>0,084362457</td><td>σ_s [MPa]</td><td colspan="4">60</td></tr>
<tr><td>c [mm]</td><td>70</td><td>f_{ctm} [MPa]</td><td colspan="4">3,795447</td></tr>
<tr><td>K</td><td>1</td><td>d [mm]</td><td colspan="4">3355</td></tr>
<tr><td>f_{ctm}</td><td>3,795447</td><td>α</td><td colspan="4">5,335390945</td></tr>
<tr><td>τ_b</td><td>6,8318046</td><td>β</td><td colspan="4">0,4</td></tr>
<tr><td>Φ</td><td>32</td><td>E_S [MPa]</td><td colspan="4">200000</td></tr>
<tr><td>$l_{s,max}$ [mm]</td><td>122,68</td><td>E_C [MPa]</td><td colspan="4">37485,538</td></tr>
<tr><td colspan="2" rowspan="5">$w_{max} = 2l_{s,max}\,(\varepsilon_{sm} - \varepsilon_{cm}) = 0{,}041\ mm$</td><td>$h_c$ [mm]</td><td>215</td><td>215</td><td>883,33</td><td>-</td></tr>
<tr><td>$A_{c,eff}\ [mm^2]$</td><td colspan="4">838500</td></tr>
<tr><td>$A_s\ [mm^2]$</td><td colspan="4">70737,92</td></tr>
<tr><td>ρ_{eff} [%]</td><td colspan="4">0,084362457</td></tr>
<tr><td>$\varepsilon_{sm} - \varepsilon_{cm}$ [%]</td><td colspan="4">0,02%</td></tr>
</table>

Table 6.2 - *Calculation of crack width (Model Code 2010, Final Draft- Volume 2)* (57)

<table>
<tr><td colspan="6">EUROCODE EN 1992-1-1:2018</td></tr>
<tr><td rowspan="2">w_{max} [mm]</td><td rowspan="2">XS 1</td><td colspan="2">Reinforced members – Limit for appearance</td><td colspan="2">Reinforced members – Limit for durability</td></tr>
<tr><td colspan="2">0,3</td><td colspan="2">0,4</td></tr>
<tr><td>w_k [mm]</td><td colspan="5">$s_{r,max}\,(\varepsilon_{sm} - \varepsilon_{cm})$</td></tr>
<tr><td colspan="2">$s_{r,max} = 2c + 0{,}35k_b \frac{\Phi}{\rho_{eff}}$</td><td colspan="4">$(\varepsilon_{sm} - \varepsilon_{cm}) = \frac{\sigma_s - K_t \frac{f_{ct}}{\rho_{eff}}(1 + \alpha\rho_{eff})}{E_s} \geq 0{,}6\frac{\sigma_s}{E_s}$</td></tr>
<tr><td>ρ_{eff} [%]</td><td>0,024593801</td><td>σ_s [MPa]</td><td colspan="3">60</td></tr>
<tr><td>c [mm]</td><td>70</td><td>f_{ctm} [MPa]</td><td colspan="3">3,795447</td></tr>
<tr><td>K_b</td><td>0,8</td><td>d [mm]</td><td colspan="3">3355</td></tr>
<tr><td>Φ</td><td>32</td><td>α</td><td colspan="3">5,335390945</td></tr>
<tr><td>$S_{r,max}$ [mm]</td><td>459,1939509</td><td>K_t</td><td colspan="3">0,4</td></tr>
<tr><td colspan="2" rowspan="8">$w_k = s_{r,max}\,(\varepsilon_{sm} - \varepsilon_{cm}) = 0{,}091\,mm$</td><td>$E_S$ [MPa]</td><td colspan="3">200000</td></tr>
<tr><td>E_C [MPa]</td><td colspan="3">37485,538</td></tr>
<tr><td>h_c [mm]</td><td>737,5</td><td>737,5</td><td>883,33 | 1825</td></tr>
<tr><td>$A_{c,eff}$ [mm^2]</td><td colspan="3">2876250</td></tr>
<tr><td>A_s [mm^2]</td><td colspan="3">70737,92</td></tr>
<tr><td>ρ_{eff} [%]</td><td colspan="3">0,024593801</td></tr>
<tr><td>0,6*σ_s/E_S [%]</td><td colspan="3">0,02%</td></tr>
<tr><td>$\varepsilon_{sm} - \varepsilon_{cm}$ [%]</td><td colspan="3">-0,005%</td></tr>
</table>

Table 6.3 - *Calculation of crack width (EN 1992-1-1:2004-7.3.4)* (56)

7 Discussion

The results achieved in this project have given many compelling issues about the non-linear behaviour of the structure.
In this section, some aspects of the results obtained in chapter 5 and 6 were analysed.
As described in section 5.2.4, the *"stress-strain model"* was assumed to be the most capable of representing the non-linear behaviour of the concrete. In particular, it was noticed that the model indicate the presence of two main longitudinal cracks pointed in the y-direction (figure 5.50): this non-linear model also indicate the presence of other damaged zones (figure 7.1-7.2).

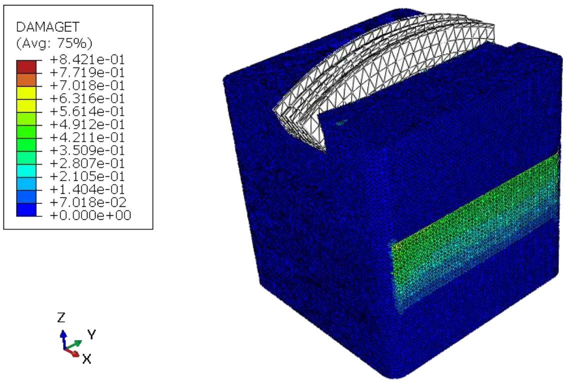

Figure 7.1 - *DAMAGET - local model#1 - Iso view n.1*

These damaged zones shown in the figures were not taken into account because:

- the damage spread over the external surface of the tower, as depicted in figure 7.1, is due to the boundary conditions ("*BC3*"-section 4.3.4) which were applied to deal with the absence of the cross-beam. The presence of these boundary conditions (*U1, U2, U3, UR1, UR2, UR3=0)* causes an increase of localised stress, which lead to a damaged state. Thus, it is unlikely that this kind of situation would reflect the real behaviour in that zone.

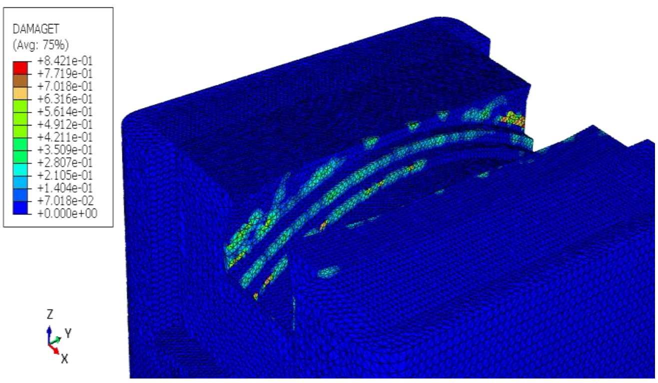

Figure 7.2 - *DAMAGET - local model#1 - Iso view n.2*

- the damage, figure 7.2, is due to excessive contact pressure between the steel saddle and the concrete part. These damaged regions, even if they may be more realistic than the other described above, were not considered. These regions were not considered because the interaction properties, which were modelled in the contact parts, were set in a non-realistic way: in fact, only, normal contact was assumed between the steel saddle and the concrete surface. Usually, in order to describe the real behaviour of this type of contact zone, the influence of the shear bolts and the presence of the friction should have been modelled.

Instead, for what concerns the two main cracks highlighted by the "*stress-strain model*", it is possible to understand how the damage and, so, the cracking, propagate into the solid model with the height. In figure 7.3, it is evident that plastic strains *11* (perpendicular to the cracks) start to arise below the first row of reinforcement and as the height decrease down to the cover concrete, the plastic strains increase their value and spread over the bottom of the concrete part. In particular, even if the plastic strains are spread over the surface, the highest values are localised in correspondence of the two main microcracks (figure 7.3-RH).

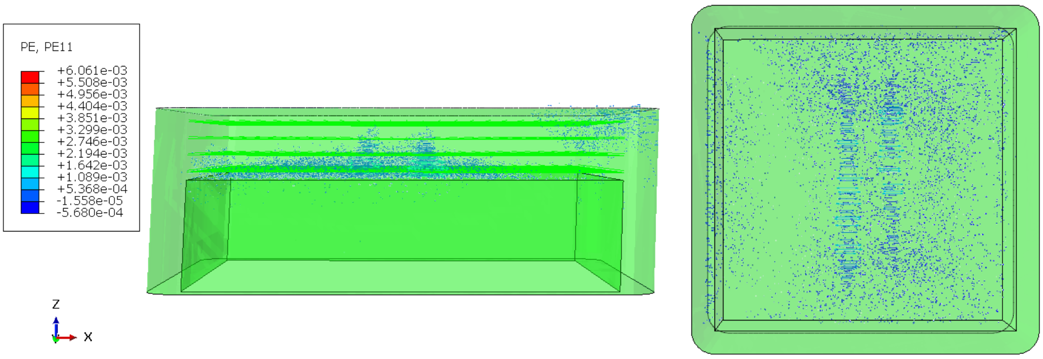

Figure 7.3 - *Plastic strains-PE11 – Front view (LH) - Bottom view (RH)*

Also, from figure 7.4, it is possible to understand how the damage caused by the cracking evolve along with the height. The following figure was realised making a vertical cut in correspondence of one of the two main cracks. In terms of strain, stress and damage, the situation in both cracks is almost identical, so for simplicity, the following considerations are made regarding only one of them. It is evident that the damage is localised along the crack and its value increase progressively up to the concrete cover: in particular, damage values start from 0,07 (blue region) up to 0,6≈0,7 (yellow region).

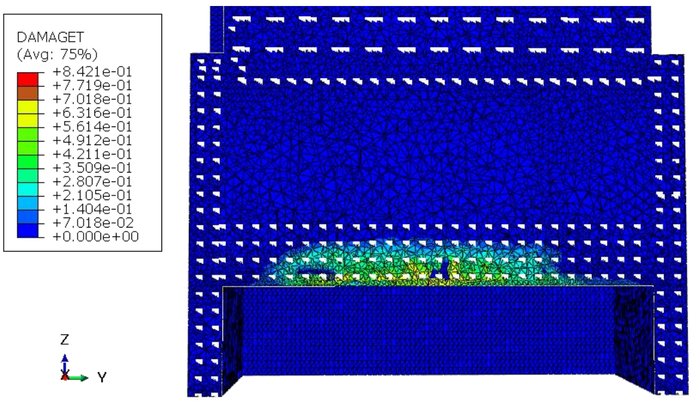

Figure 7.4 - *Damaget - Vertical cut view*

Then, the stress state of the rebar was checked: as depicted in figure 7.5, the last layer of reinforcement, in correspondence with the crack, show the highest values of tensile stress. In particular, the maximum stress in the reinforcement is almost 60 MPa, which means that the steel is still in the elastic stage, and it is not yielded. Moreover, the whole reinforcement of the model is not yielded.

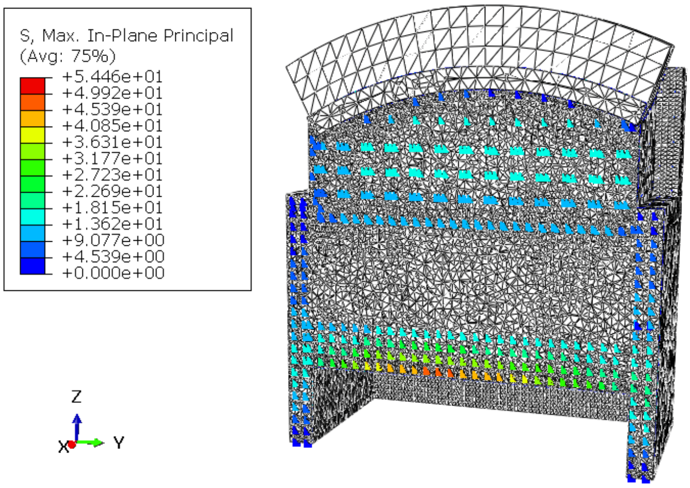

Figure 7.5 - *Maximum Principal stress - Rebar*

Finally, another check on the stresses was performed: the normal stresses $\sigma_{11} - \sigma_{22}$ were plotted along a vertical axis (as section 5.1) and, then, compared to the stress distributions of the linear case (figure 7.7-7.9). It was observed that the compression values of both case, linear and non-linear, are quite similar but in the tensile zone it can be observed a relevant difference of values. In particular, for both local models, the normal stresses in x-the direction (σ_{11}), show lower values than the linear case: it can be noticed that in correspondence with almost 3 m of height, the stresses reach the tensile strength and then decrease. Thus, the elements between almost 3 m and 3.5 m of height are charachterised by a post-elastic behaviour (softening) which is why the tensile value are lower than the linear case.
Finally, in order to complete this stress verification, the vertical stress σ_{33} in the concrete part below the saddle was analyzed: this verification was carried out taking in exam, for both local models, the three reference point below the saddle (RP 2,4,7 for local model #1 and RP 1,3,8 for local model #2). It was observed that for each reference point, the compressive stress value are lower than the compressive strength of concrete. Reference points are described in section 4.3.6. Compressive values are indicated in terms of absolute value.

Reference points local model #1	
RP 2	*29 MPa*
RP 4	*31 MPa*
RP 7	*21 MPa*

Reference points local model #2	
RP 1	*30,8 MPa*
RP 3	*33 MPa*
RP 8	*22 MPa*

Table 7.1 – *Normal stress σ_{33} –Reference point*

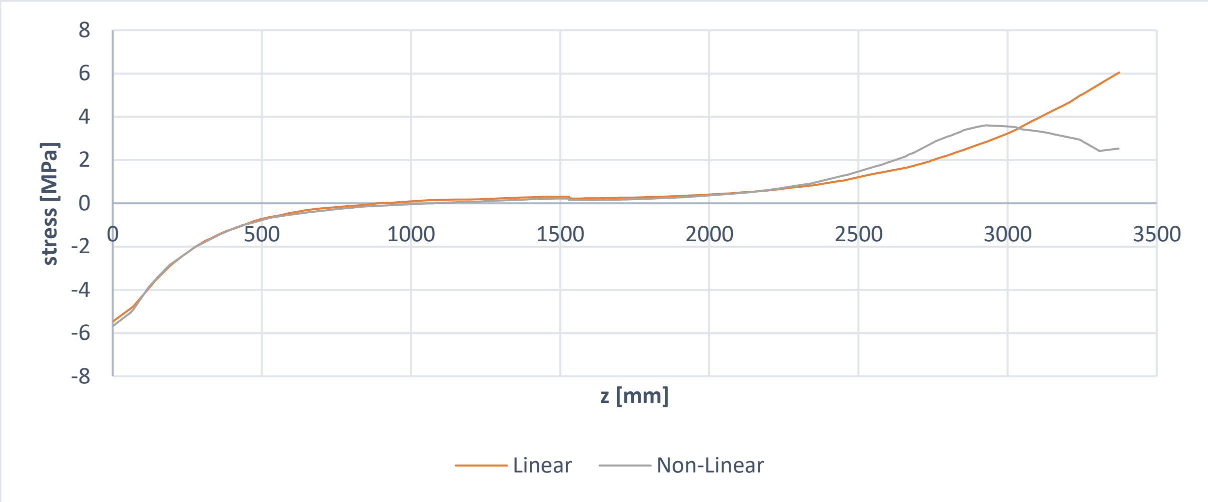

Figure 7.6 - *Normal stress - σ_{11} -z (local model #1)*

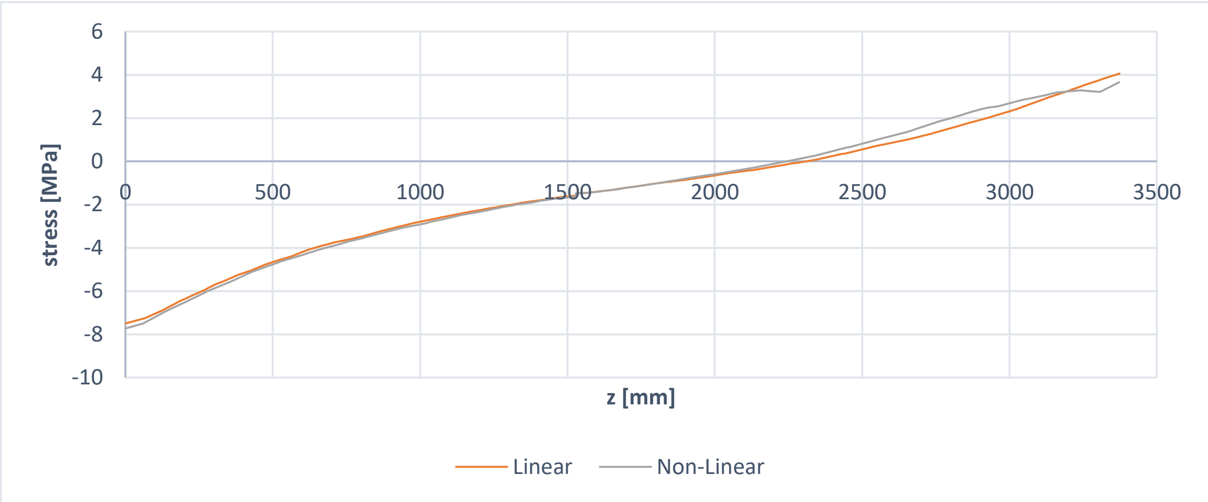

Figure 7.7 - *Normal stress - σ_{22} -z (local model #1)*

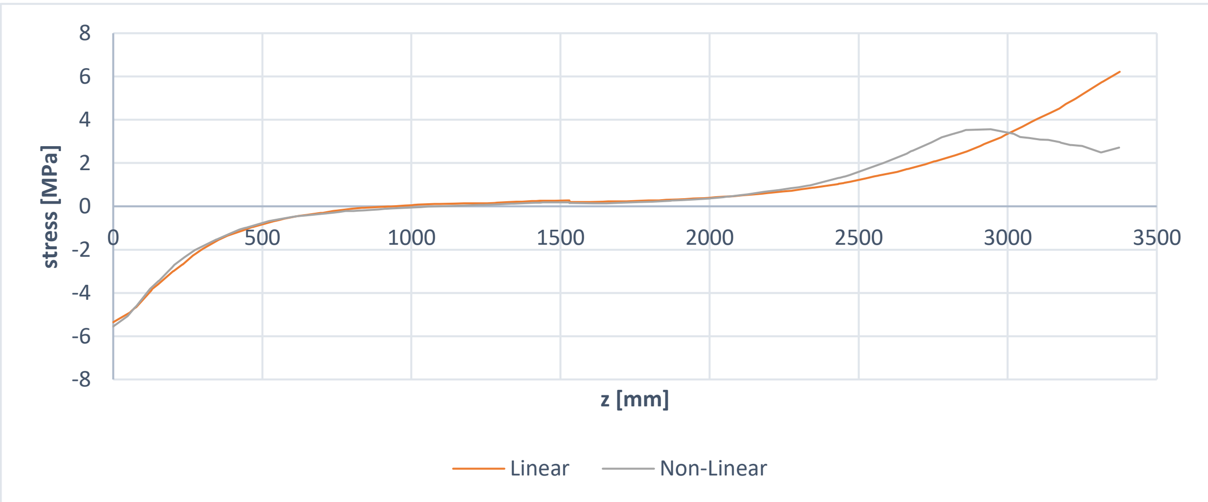

Figure 7.8 - *Normal stress - σ_{11}-z (local model #2)*

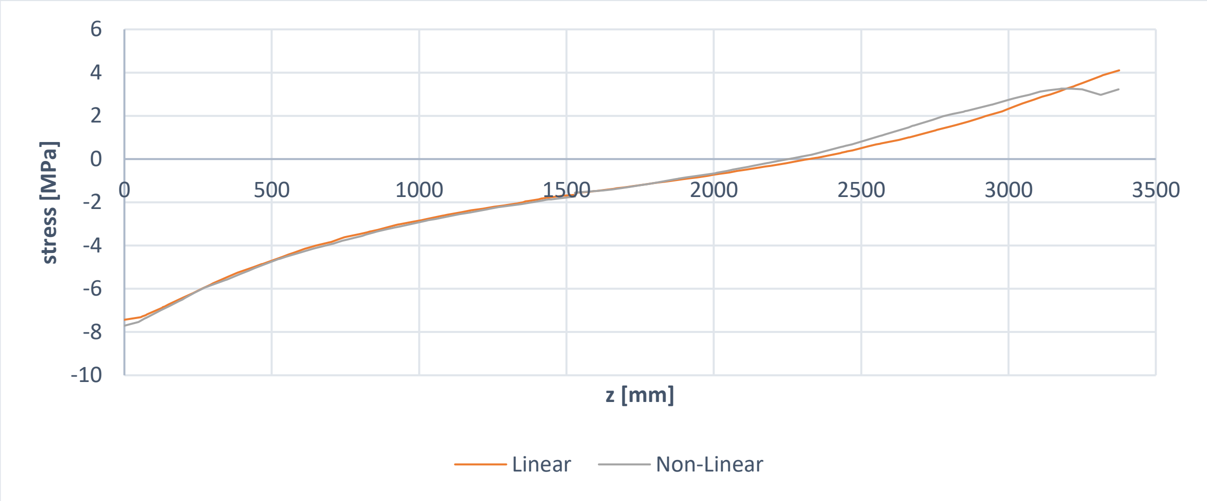

Figure 7.9 - *Normal stress – σ_{22}-z (local model #2)*

Finally, as described in chapter 6, starting from the results of the non-linear analysis, the width of the cracks was calculated, according to different standards. Even if, for each code (Eurocode 2-2004/2010- and Model Code 2010)both the design and the limit crack width were different, the verification was satisfied. It was observed that using different standards, the parameters that significantly changed more than the others, were the maximum crack spacing S_r and the depth of the effective area, $h_{c,eff}$.
In particular, the draft of the Model Code 2010 tends to give the lower value of the maximum cracking spacing S_r and of $h_{c,eff}$: in particular, since in section 6.1 the effective depth was calculated in the "slab-case"(figure 8-b), it was tried to evaluate the effective depth according to the "beam-case"(figure 8-a) suggested by Model Code 2010 (figure 8).

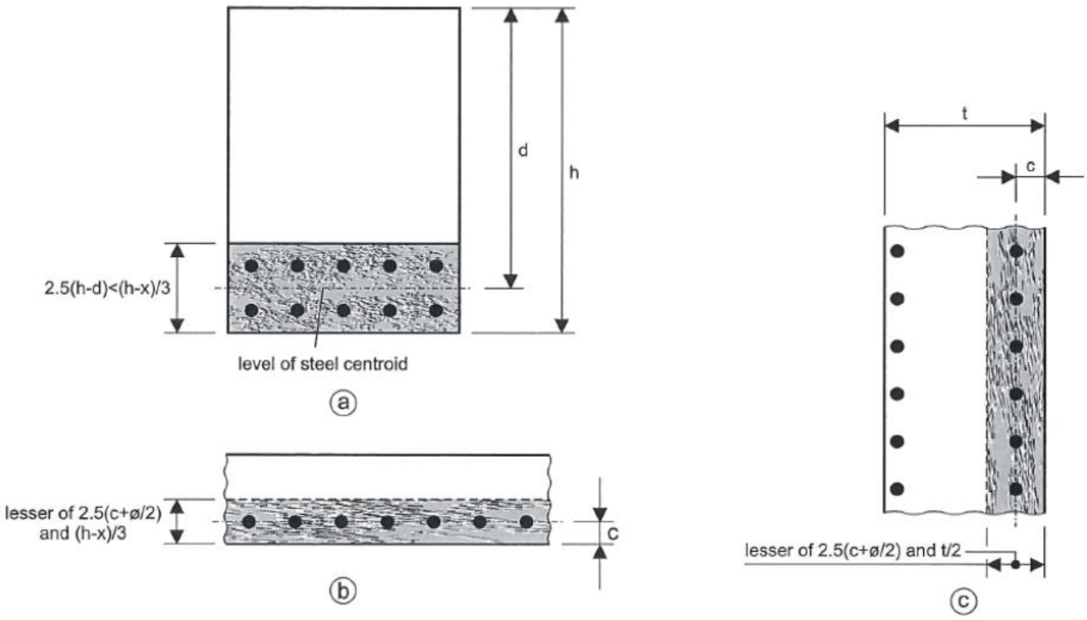

Table 7.2 - *Effective tension area of concrete $A_{c,eff}$ for: (a) beam;(b) slabs; (c) member in tension (shaded area)* - (57)

In the following table, it is possible to observe the differences between these parameters using different standards.

	Eurocode 2004	*Eurocode 2008*	*Model Code – Draft - 2010*	
			beam(a)	*slab(b)*
$h_{c,eff}$ *[mm]*	*737,5*	*737,5*	*737,5*	*215*
$S_{r,max}$ *[mm]*	*459,19*	*504,39*	*250,7*	*122,68*
w_k *[mm]*	*0,08*	*0,09077*	*0,09025*	*0,041*

Table 7.3 – *Comparison of crack width values*

The result is that the crack width value, computed in the slab case according to Model Code 2010, is almost half of the value calculated using the Eurocode.

It can be concluded that concrete damaged plasticity model has been a useful tool to investigate the non-linear behaviour of the top tower. It allowed developing many exciting considerations, from structure behaviour up to crack verification), which may be useful to improve the knowledge of these particular structures.

8 Conclusions

This master thesis project aimed to provide information about the non-linear behaviour of this particular reinforced concrete structure, including the presence of cracking. Each chapter of this project contributed to creating a complete overview of all the characteristics of the structure.

Concrete damage plasticity (CDP) model appeared to be a useful tool to complete the task of this project. CDP was found to be promising for the nonlinear analysis of reinforced concrete structural systems.

This model also showed the importance of an accurate modelling: in fact, in order to obtain high-quality results from this model, each aspect had to be widely examined, starting from material properties up to the modelling approach. Furthermore, the presented results of the analysis showed that a proper choice of CDP model parameters should be made very carefully, possibly examining the assumed values with the experimental results (section 5.2.3 – 5.2.4). This stage of modelling of reinforced concrete structures seems to be the most critical and crucial for obtaining realistic results.

It has been shown that the concrete damaged plasticity model is capable of:

- detecting the regions where the concrete tensile strength has been reached;
- providing information about the crack pattern and its evolution during loading;
- estimating the level of damage in compression and tension;
- describing the stiffness reduction in concrete.

Based on the results of the non-linear analysis, it can be concluded that the main goal of the project has been achieved: considering the assumptions made, a complete overview of the most likely non-linear behaviour of this structure was obtained.

9 Recommendations for Further Work

The final results are conditioned by the assumptions made. For example, the lacking information related both to material laboratory test and the real post-cracking behaviour of the structure influence the accuracy of the concrete damaged plasticity model. In particular, the choice of the most suitable tension-stiffening model is important.

In addition to this, both type of analysis, linear and non-linear static, were influenced by various executive details, such as prestressed reinforcement or shear bolts, which was decided to not implement in the Abaqus models. However, these results about the crack pattern and crack width are influenced by various factors.

The first factor is the tension-stiffening model chosen for the analysis. Even if the stress-strain relation used to describe this phenomenon, gave acceptable results, it is strongly affected by the mesh-sensitivity problem. The solution to this problem, as suggested in the Abaqus manual, would be changing the tension-stiffening model. However, if the "stress-strain" model has to be used, in order to obtain acceptable estimations of the tension stiffening effect, it should be paid attention to the density of reinforcement, the quality of the bond between rebar and the concrete, the relative size of the concrete aggregate compared to the rebar diameter, and the mesh. Thus, improving these factors, the quality of the results would increase, and the mesh-sensitivity would be less of a concern.

The second factor which influences the results is neglecting the prestressed reinforcement. This is left out because it was chosen not to model the cross-beam, which is a prestressed beam and contains prestressed reinforcement. Moreover the presence of the prestressed cable would have improved the strength of the structure, decreasing the probability of cracking: it is reasonable to assume that the prestressing would have introduced in the tensile zone (which is where these cables are anchored), compressive stresses that would have decreased the tensile value at the bottom of the concrete part.

Furthermore, for the analysis, the real modulus of elasticity of concrete was used, instead of the effective modulus $E_{c,ef}$ suggested by the standars. The effective modulus is, in fact, reduced in order to take into account the long term effects of shrinkage. Finally, creep and thermal effects were not considered.

These considerations and assumptions may be a suitable starting point for further works: realising a model with all these aspects would improve the accuracy of the results, making them as similar as possible to the real case.

The creation of a FEM model, implemented with all these aspects, may be a helpful tool for the bridge designing: an accurate model would also help predicting and controlling the non-linear behaviour of these particular structures.

References

1. European Committee for Standardisation. EN 1992-1-1: Eurocode 2: Design of concrete structures - Part 1-1: General rules and rules for buildings [Internet]. 2004 [cited 2019 May 26]. 227 p. Available from: http://archive.org/details/en.1992.1.1.2004

2. Hardanger Bridge - bridgeinfo.net [Internet]. [cited 2019 Jun 3]. Available from: http://bridgeinfo.net/bridge/index.php?ID=106

3. The Hardanger bridge [Internet]. Statens vegvesen. [cited 2019 Jun 1]. Available from: https://www.vegvesen.no/vegprosjekter/Hardangerbrua/InEnglish/the-hardanger-bridge

4. Hardanger Bridge - MT Højgaard [Internet]. [cited 2019 Jun 1]. Available from: https://mth.com/Our-Projects/Hardanger-bridge

5. NY EUROPEISK BETONGSTANDARD [Internet]. [cited 2019 May 7]. Available from: https://fabeko.no/assets/Ny_eur_betongstandard-juli_2004.pdf

6. 14:00-17:00. ISO 4991:2015 [Internet]. ISO. [cited 2019 Jun 15]. Available from: http://www.iso.org/cms/render/live/en/sites/isoorg/contents/data/standard/05/92/59267.html

7. BS EN 10293:2005 - Steel castings for general engineering uses – BSI British Standards [Internet]. [cited 2019 May 24]. Available from: https://shop.bsigroup.com/ProductDetail/?pid=000000000030188308

8. Vaidyanathan R, Perumal P. Structural Analysis Vol II. Laxmi Publications; 2004. 348 p.

9. Abaqus Analysis User's Guide, vol4. :1128.

10. Börgesson L. ABAQUS. In: Stephansson O, Jing L, Tsang C-F, editors. Developments in Geotechnical Engineering [Internet]. Elsevier; 1996 [cited 2019 May 15]. p. 565–70. (Coupled Thermo-Hydro-Mechanical Processes of Fractured Media; vol. 79). Available from: http://www.sciencedirect.com/science/article/pii/S0165125096800472

11. What is a Mesh? — SimScale Documentation [Internet]. [cited 2019 May 15]. Available from: https://www.simscale.com/docs/content/simwiki/preprocessing/whatisamesh.html

12. Abaqus Analysis User's Guide (6.13) [Internet]. [cited 2019 May 24]. Available from: http://dsk.ippt.pan.pl/docs/abaqus/v6.13/books/usb/default.htm?startat=pt05ch26s07abm69.html#usb-mat-cusermat

13. Bathe K-J, Walczak J, Welch A, Mistry N. Nonlinear analysis of concrete structures. Comput Struct. 1989 Jan 1;32(3):563–90.

14. Koh CG, Teng M, Wee TH. A Plastic-Damage Model for Lightweight Concrete and Normal Weight Concrete. In 2008.

15. Menetrey P, Willam KJ. Triaxial Failure Criterion for Concrete and its Generalization. Struct J. 1995 May 1;92(3):311–8.

16. Jason L, Huerta A, Pijaudiercabot G, Ghavamian S. An elastic plastic damage formulation for concrete: Application to elementary tests and comparison with an isotropic damage model. Comput Methods Appl Mech Eng. 2006 Nov 1;195:7077–92.

17. Abaqus Theory Manual. :1172.

18. Lubliner J, Oliver J, Oller S, Oñate E. A plastic-damage model for concrete. Int J Solids Struct. 1989 Jan 1;25(3):299–326.

19. Lee Jeeho, Fenves Gregory L. Plastic-Damage Model for Cyclic Loading of Concrete Structures. J Eng Mech. 1998 Aug 1;124(8):892–900.

20. Hamad WI, Owen JS, Hussein MFM. Modelling the degradation of vibration characteristics of reinforced concrete beams due to flexural damage: VIBRATION CHARACTERISTICS OF DAMAGED REINFORCED CONCRETE BEAMS. Struct Control Health Monit. 2015 Jun;22(6):939–67.

21. Abaqus Analysis User's Manual, vol3. 2010;679.

22. Ian Gilbert R. Tension Stiffening in Lightly Reinforced Concrete Slabs. J Struct Eng. 2007 Jun 1;133(6):899–903.

23. International Federation for Structural Concrete, editor. Model Code 2010: final draft. Vol. 1: ... Lausanne: International Federation for Structural Concrete; 2012. 311 p. (Bulletin / International Federation for Structural Concrete Draft model code).

24. Hillerborg A, Modéer M, Petersson P-E. Analysis of crack formation and crack growth in concrete by means of fracture mechanics and finite elements. Cem Concr Res. 1976 Nov 1;6(6):773–81.

25. Earij A, Alfano G, Cashell K, Zhou X. Nonlinear three–dimensional finite–element modelling of reinforced–concrete beams: Computational challenges and experimental validation. Eng Fail Anal. 2017 Dec;82:92–115.

26. Gálvez JC, Červenka J, Cendón DA, Saouma V. A discrete crack approach to normal/shear cracking of concrete. Cem Concr Res. 2002 Oct;32(10):1567–85.

27. Kmiecik P, Kamiński M. Modelling of reinforced concrete structures and composite structures with concrete strength degradation taken into consideration. Arch Civ Mech Eng. 2011 Jan;11(3):623–36.

28. Omidi O, Lotfi V. Finite Element Analysis of Concrete Structures Using PlasticDamage Model in 3-D Implementation. 2010;8(3):17.

29. Burlion N, Gatuingt F, Pijaudier-Cabot G, Daudeville L. Compaction and tensile damage in concrete: constitutive modelling and application to dynamics. Comput Methods Appl Mech Eng. 2000 Mar;183(3–4):291–308.

30. Hafezolghorani M, Hejazi F, Vaghei R, Jaafar MSB, Karimzade K. Simplified Damage Plasticity Model for Concrete. Struct Eng Int. 2017 Feb;27(1):68–78.

31. Wahalathantri B, Thambiratnam D, Chan T, Fawzia S. A Material Model for Flexural Crack Simulation in Reinforced Concrete Elements Using ABAQUS. 2011 Apr 28;

32. Tao Y, Chen JF. Concrete Damage Plasticity Model for Modeling FRP-to-Concrete Bond Behavior. J Compos Constr. 2015 Feb;19(1):04014026.

33. Sümer Y, Aktaş M. Sümer | Defining parameters for concrete damage plasticity model. Chall J Struct Mech. 2015;7.

34. Zappitelli MP, Villa EI, Fernández-Sáez J. Application of the concrete damaged plasticity model to analyze cracking development in concrete gravity dams under dynamic loading. 2014;7.

35. Jankowiak T. IDENTIFICATION OF PARAMETERS OF CONCRETE DAMAGE PLASTICITY CONSTITUTIVE MODEL. 2005;17.

36. Vermeer PA, De Borst R. Non-Associated Plasticity for Soils, Concrete and Rock. HERON 29 3 1984 [Internet]. 1984 [cited 2019 May 26]; Available from: http://resolver.tudelft.nl/uuid:4ee188ab-8ce0-4df3-adf5-9010ebfaabf0

37. Kupfer H, Hilsdorf HK, Rusch H. BEHAVIOR OF CONCRETE UNDER BIAXIAL STRESSES. Am Concr Inst J Proc [Internet]. 1969 Aug [cited 2019 May 26]; Available from: https://trid.trb.org/view/101925

38. Mihashi H, Rokugo K. Fracture Properties and Parameters. :24.

39. Kassem F. Reliability of reinforced concrete structures : Case of slabs subjected to impact. 2015 Nov 4 [cited 2019 May 24]; Available from: https://tel.archives-ouvertes.fr/tel-01339833

40. Pavlović M, Marković Z, Veljkovic M, Buđevac D. Bolted shear connectors vs. headed studs behaviour in push-out tests. J Constr Steel Res. 2013 Sep 1;88:134–149.

41. Wang T, T.C Hsu T. Nonlinear finite element analysis of concrete structures using new constitutive models. Comput Struct. 2001 Dec 1;79:2781–91.

42. Abaqus Analysis User’s Manual, vol3. 2010;679.

43. Hillerborg A. The theoretical basis of a method to determine the fracture energyG F of concrete. Mater Struct. 1985 Jul;18(4):291–6.

44. béton fib F internationale du. CEB-FIP Model Code 1990: Design Code. fib Fédération internationale du béton; 1993. 462 p.

45. Cornelissen HAW, Hordijk DA, Reinhardt HW. Experimental determination of crack softening characteristics of normalweight and lightweight concrete. 1986;

46. Khezrzadeh H. Interpretation of Tensile Softening in Concrete, Using Fractal Geometry. Sci Iran. 2008;Vol. 15:8.

47. Hordijk DA. Tensile and tensile fatigue behaviour of concrete; experiments, modelling and analyses. Heron. 1992 Jan 1;37:1–79.

48. Gebreyohaness AS, Clifton GC, Butterworth JW. Finite element modeling of non-ductile RC walls. 2012;10.

49. Najafgholipour M, DEHGHAN S, Dooshabi A, Niroomandi A. Finite Element Analysis of Reinforced Concrete Beam-Column Connections with Governing Joint Shear Failure Mode. Lat Am J Solids Struct. 2017 May 26;14:1200–25.

50. Wu JY, Li J, Faria R. An energy release rate-based plastic-damage model for concrete. Int J Solids Struct. 2006 Feb 1;43(3):583–612.

51. Voyiadjis GZ, Taqieddin ZN. Elastic Plastic and Damage Model for Concrete Materials : Part I - Theoretical Formulation. Int J Struct Chang Solids. 2009;1(1):31–59.

52. Malm R. Predicting shear type crack initiation and growth in concrete with non-linear finite element method. 2009.

53. Demir A, Öztürk H, Bogdanovic A, Stojmanovska M, Edip K. Sensitivity of Dilation Angle in Numerical Simulation of Reinforced Concrete Deep Beams. 2017 Jul 1;6:33.

54. Dere Y. Nonlinear FE Modeling of Reinforced Concrete. Int J Struct Civ Eng Res. 2017;71–4.

55. Löfgren I. Calculation of crack width and crack spacing. 2007;12.

56. EN 1992-1-1: Eurocode 2 :Design of concrete structures - Part1-1 - 2018 (Draft Version).

57. International Federation for Structural Concrete, editor. Model Code 2010: final draft. Vol. 2: ... Lausanne: International Federation for Structural Concrete; 2012. 331 p. (Bulletin / International Federation for Structural Concrete Draft model code).

Appendices

- K440;
- K441;
- K445;
- K652;
- K680;
- K681.

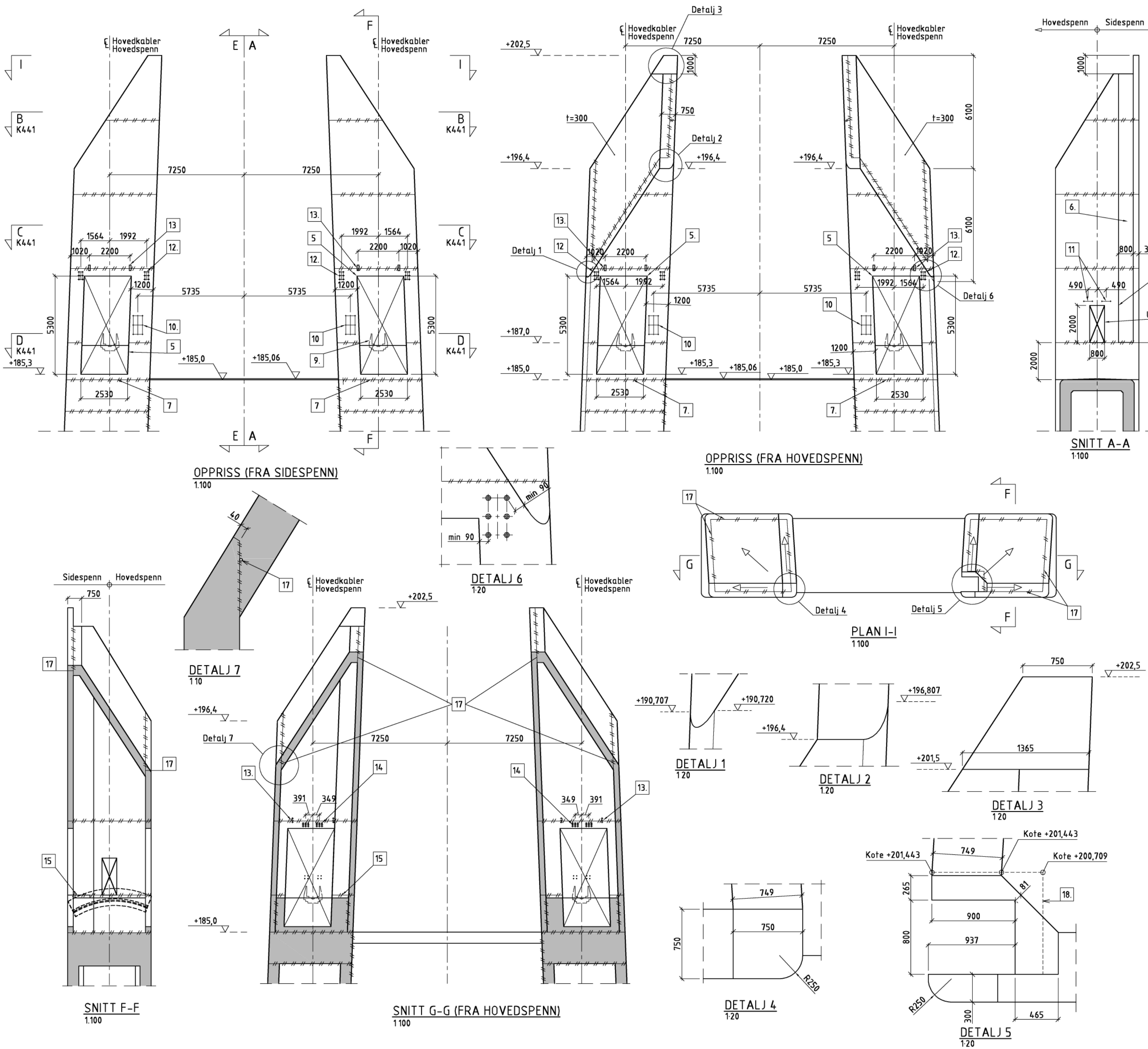

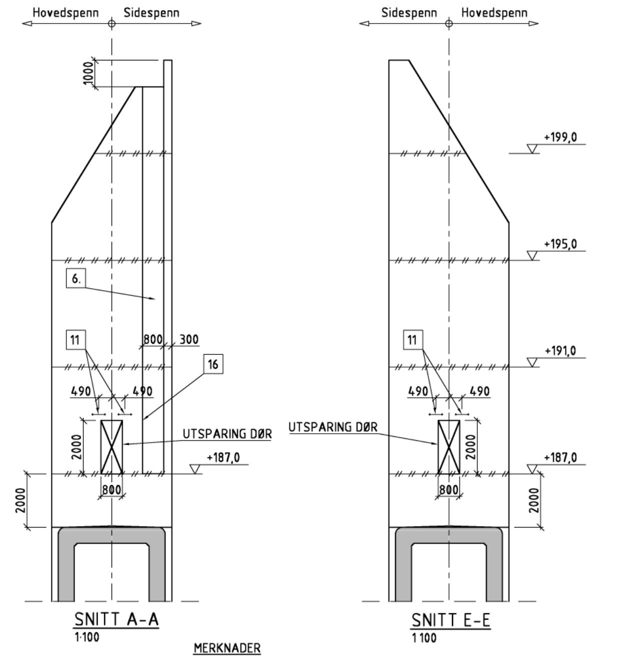

MERKNADER

1 Kontrollklasse: Utvidet kontroll iht NS 3465

2. Betongkvalitet. Sadel understøp mellom kote 185 og 186,85 utføres med B55 SV-40. Øvrige deler utføres med B45 SV-40.

3 Synlige hjørner avfases 30 mm, hvis ikke annet er angitt

5 Utsparing for spinning av hovedkabler

6 Sliss 900x800 for leider.

7 Injeksjonsslange i horisontal støpeskjøt på kote 185

8 Dørutsparinger på kote 187,1 forberedes for karm som vist på K901

9 Tårnsadel, se tegning K651, K652 og K653

10 Innstøpt boltegruppe for plattform 004, se tegning nr.K443

11 Innstøpt boltegruppe for plattform 005, se tegning nr K443

12 Innstøpt boltegruppe for spinneutstyr 001, se tegning nr K443
Innstøpningshylser må ikke stå nærmere enn 90 mm fra kant utsparing eller kant skrå takflate - toleranser inkludert Se detalj 6
Teoretisk mål 1564 mm tillates avveket ±50 mm for å oppnå dette.
Tilpasning må ikke gå på bekosting av innbyrdes avstand i gruppen.
Prinsippet gjelder samtlige boltegrupper med teoretisk avstand 1564 mm.

13 Utsparinger for spinneutstyr 004, se tegning nr. K443
Angitt mål 1020 gjelder uk utsparing.

14 Innstøpt boltegruppe for spinneutstyr 002, se tegning nr K443

15 Innvendig lokal forhøyning til kote +187,145 som gulv for sliss,se tegn K441

16 ø50 rørutsparing for elektro, se tegning K441.

17 Injeksjonsslange SikaFuko VT1 eller tilsv i støpeskjøt mellom vegger og tak Seksjonering og mateslanger etter nærmere avtale med byggherren

18 Stiplet linje med kotehøyder angir teoretisk skjæring mellom sliss for leider og utvendig takflate.

HENVISNINGER
Tegning K401, Tårn Bu, Form
Tegning K441, Tårn Bu, Tårntopp, Detaljer og 3D-perspektiv, Form
Tegning K443, Tårn, Innstøpningsgods tårntopp
Tegning K942, Utstyr, Dør til tårntopp Bu øst og Vallavik vest
Tegning K943, Utstyr, Dør til tårntopp Bu vest og Vallavik øst
Tegning K905, Utstyr, Topprigler og tårntopper, Tilkomstutstyr
Tegning K930, Merking for fly- og skipstrafikk
Tegning K931, Utstyr, Feste for flysikringslys

Tegn nr	K440	Rev	SB

Rev	Revisjonen gjelder	Prosj.	Kontr.	Dato
SB	Som bygd	AGK	IMJ	20 06 2014
F	Detalj 5, Merknad 18	AGK	BI	29.04.2011
E	Detalj 7, Merknad 17	AGK	BI	08.03.2011
D	Detalj 6, Merknad 12 og 15, Henvisninger, Støpeskjøter	AGK	MBR	03 02 2011
C	Merknad 13, 16, Snitt A-A, støpeskjøter	AGK	MBR	23 12 2010
B	Generell revisjon 3D-modell, detalj 1-5, Merknad 15	MBR	AGK	10 12 2010
A	Arbeidstegning	MBR	AGK	04 10 2010

Godkjent som arbeidstegning i notat fra Vegdirektoratet — Saksnr. 2010/011531-035

Statens vegvesen

Prosj.	RBJ
Tegner	RBJ
Dato.	25 06 2007
Prosj.leder	Bjørn Isaksen
PROFnr.	12r0013b_015
Målestokk	1:100, 1:20, 1:10 (A1)
Byggv. nr	12-2950
Tegn. nr.	K440
Rev.	SB

Rv 7 / Rv 13
12-2950 HARDANGERBRUA
Tårn Bu
Tårntopp, Plan og oppriss
Form

Prosjektert av Statens vegvesen Vegdirektoratet, Bruseksjonen

SNITT B-B, kote 199,45
1:50

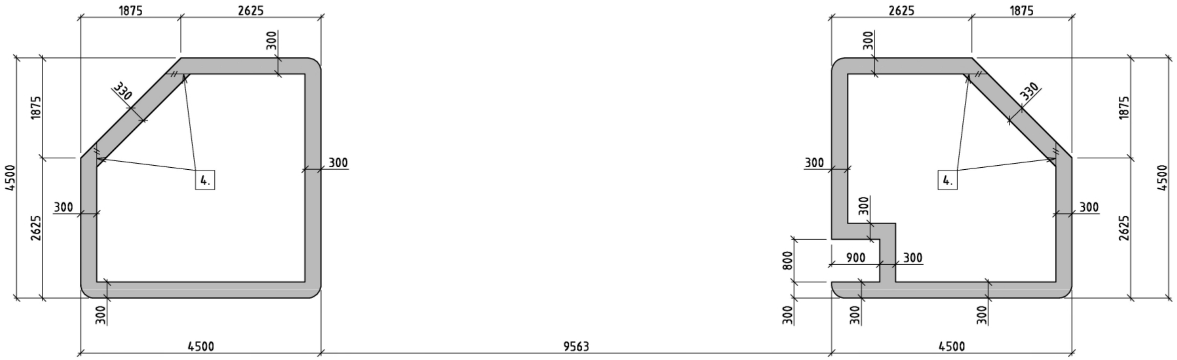

SNITT C-C, kote 193,35
1:50

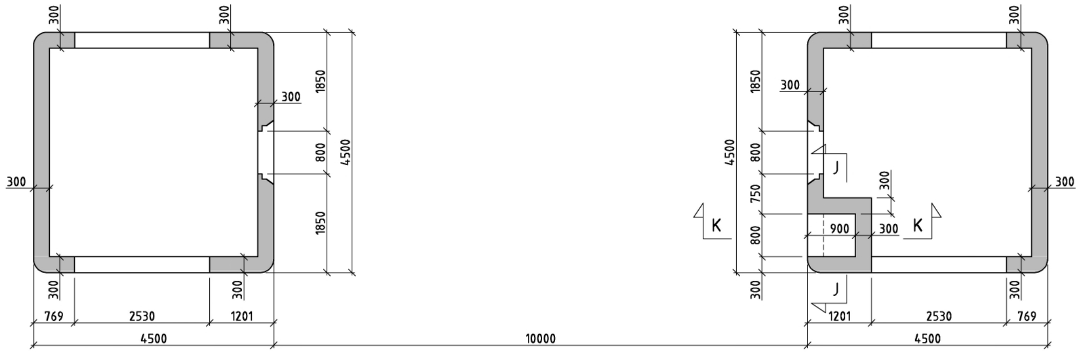

SNITT D-D, kote 187,5
1:50

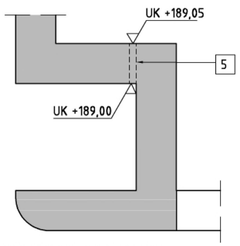

RØRUTSPARING FOR ELEKTRO KOTE +189
1:20

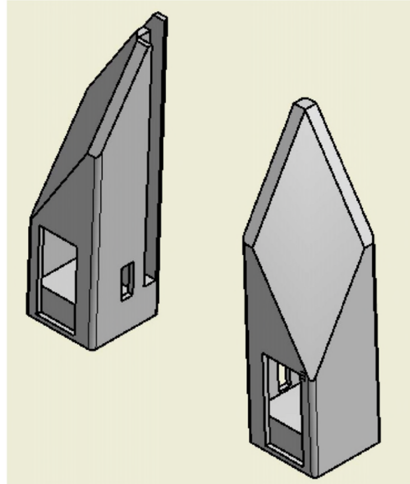

3D-perspektiv tårntopp øst og vest sett fra hovedspenn

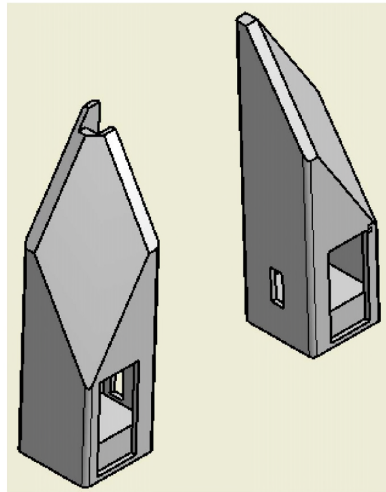

3D-perspektiv tårntopp øst og vest sett fra hovedspenn

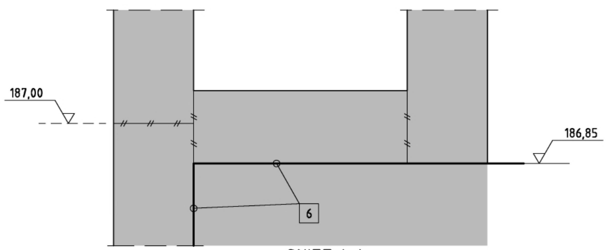

SNITT J-J
1:10

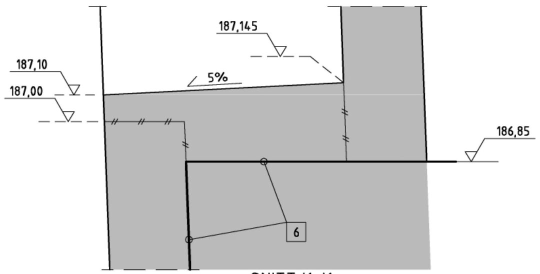

SNITT K-K
1:10

MERKNADER

1. Kontrollklasse. Utvidet kontroll iht. NS 3465
2. Betongkvalitet B45 SV-40
3. Synlige hjørner avfases 30 mm hvis ikke annet er angitt.
4. Injeksjonsslange SikaFuko VT1 eller tilsv. i støpeskjøt mellom vegger og tak. Seksjonering og mateslanger etter nærmere avtale med byggherren
5. Rørutsparing ved bruk av plastrør med innvendig diameter ø50. Fall utover som vist.
6. Ett lag asfaltpapp mot vegger og under sliss for leider

HENVISNINGER

Tegning K401, Tårn Bu, Form
Tegning K440, Tårn Bu, Tårntopp, Plan og oppriss, Form
Tegning K443, Tårn, Innstøpningsgods tårntopp
Tegning K942, Utstyr, Dør til tårntopp Bu øst og Vallavik vest
Tegning K943, Utstyr, Dør til tårntopp Bu vest og Vallavik øst
Tegning K905, Utstyr, Topprigler og tårntopper, Tilkomstutstyr
Tegning K930, Merking for fly- og skipstrafikk
Tegning K931, Utstyr, Feste for flysikringslys

SB	Som bygd	AGK	IMJ	20.06.2014
C	3D-perspektiv, Merknad 4	AGK	BI	08.03.2011
B	Hjørner Snitt B-B og C-C, Dørutsparing, Snitt J-J og K-K	AGK	MBR	03.02.2011
A	Arbeidstegning	AGK	MBR	17.01.2011
Rev	Revisjonen gjelder	Prosj	Kontr.	Dato

Godkjent som arbeidstegning i notat fra Vegdirektoratet

Saksnr. 2010/011531-041

Statens vegvesen

Prosj.	AGK	Dato
Tegner	IMJ	07.01.2011
Prosjleder	Bjørn Isaksen	
PROFnr.	12r0013b_015	
Målestokk	1:50 (A1)	
Byggv. nr.	12-2950	
Tegn. nr.	K441	Rev SB

Rv 7 / Rv 13
12-2950 HARDANGERBRUA
Tårn Bu
Tårntopp detaljer og 3D-perspektiv
Form

Prosjektert av Statens vegvesen Vegdirektoratet, Bruseksjonen

Tegn nr K441 Rev SB

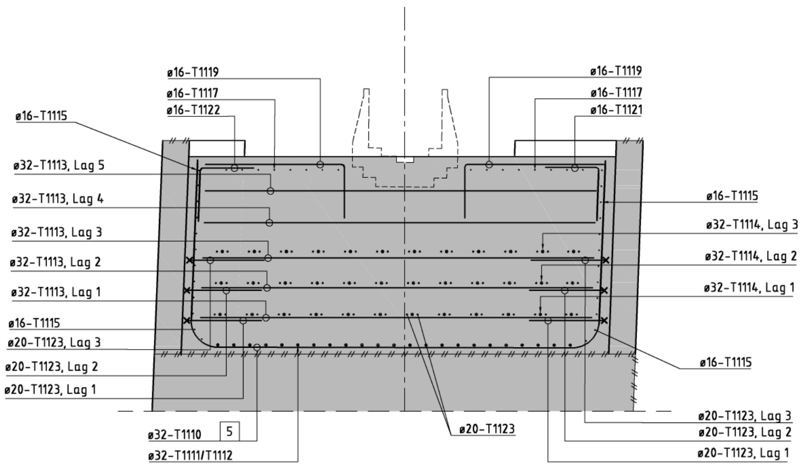

SNITT A-A
1:25

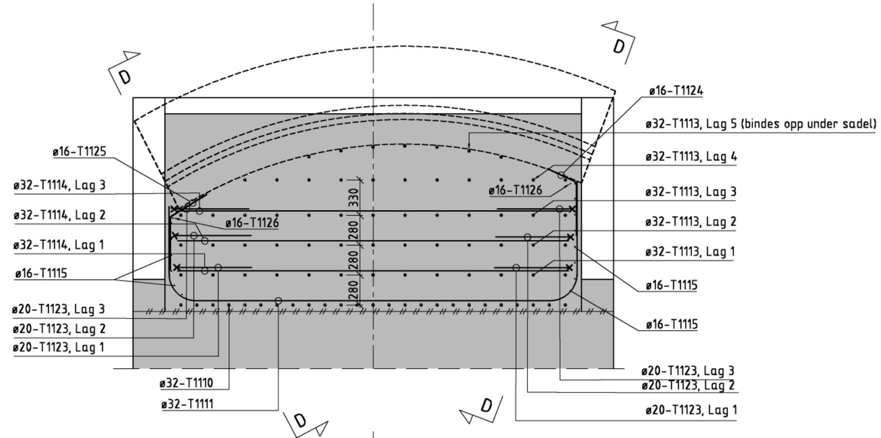

SNITT B-B
1:25

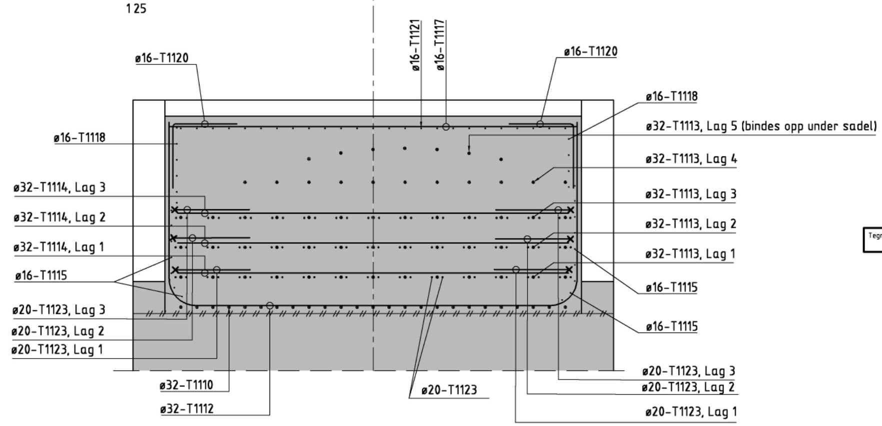

SNITT C-C
1:25

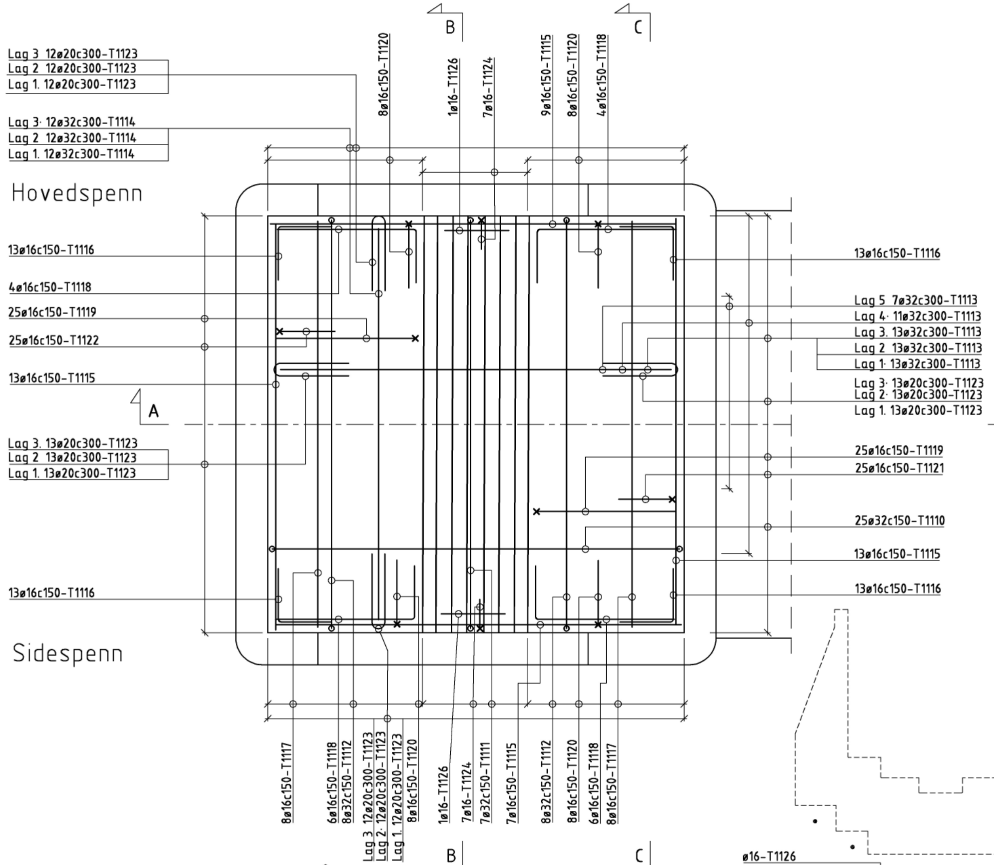

PLAN TÅRNTOPP
1:25

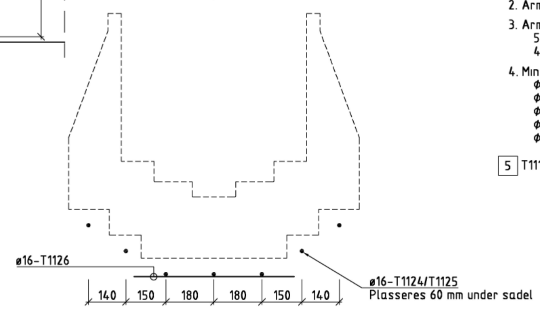

SNITT D-D, Plassering T1124/T1125/T1126
1:10

MERKNADER

1. Kontrollklasse Utvidet kontroll iht NS 3465
2. Armering Kamstenger teknisk klasse B500NC iht. NS 3576-3
3. Armeringsoverdekning.
   55±15 mm til konstruktiv armering
   40±5 mm til ø12 monteringsstenger
4. Minimum omfaringslengde
   Φ12 = 400 mm
   Φ16 = 500 mm
   Φ20 = 600 mm
   Φ25 = 800 mm
   Φ32 = 1000 mm

5 T1110 monteres med armeringsstol som bygger ca 40mm

HENVISNINGER

Tegning K401, Tårn Bu, Form
Tegning K402, Tårn Bu, Støpeetapper
Tegning K436, Tårn Bu, Tårnbein oversikt kt +131-185, Armering
Tegning K438, Tårn Bu, Tårnbein detaljer ved topprigel, Armering
Tegning K439, Tårn Bu, Tårnbein snitt kt +173, Armering
Tegning K444, Tårn Bu, Tårntopp vegger kt. +185-187, Armering

Bøyeliste side T111 - T112

Rev	Revisjonen gjelder	Prosj.	Kontr.	Dato
SB	Som bygd	AGK	IMJ	20 06 2014
C	T1124/T1125/T1126, Snitt D-D	AGK	MBR	22 02 2011
B	T1123, lag 3	AGK	MBR	17.01.2011
A	Arbeidstegning	AGK	MBR	23 12 2010

Godkjent som arbeidstegning i notat fra Vegdirektoratet
Saksnr. 2010/011531-035

Statens vegvesen

Prosj.	AGK	Dato
Tegner	GH	26 11 2010
Prosjleder	Bjørn Isaksen	
PROFnr.	12r0013b_015	
Målestokk	1:25 (A1)	
Byggnr.	12-2950	

Rv 7 / Rv 13
12-2950 HARDANGERBRUA
Tårn Bu
Tårntopp understøp sadel
Armering

Tegn nr K445 Rev SB

Prosjektert av Statens vegvesen Vegdirektoratet, Bruseksjonen

Tegn nr K445 Rev SB

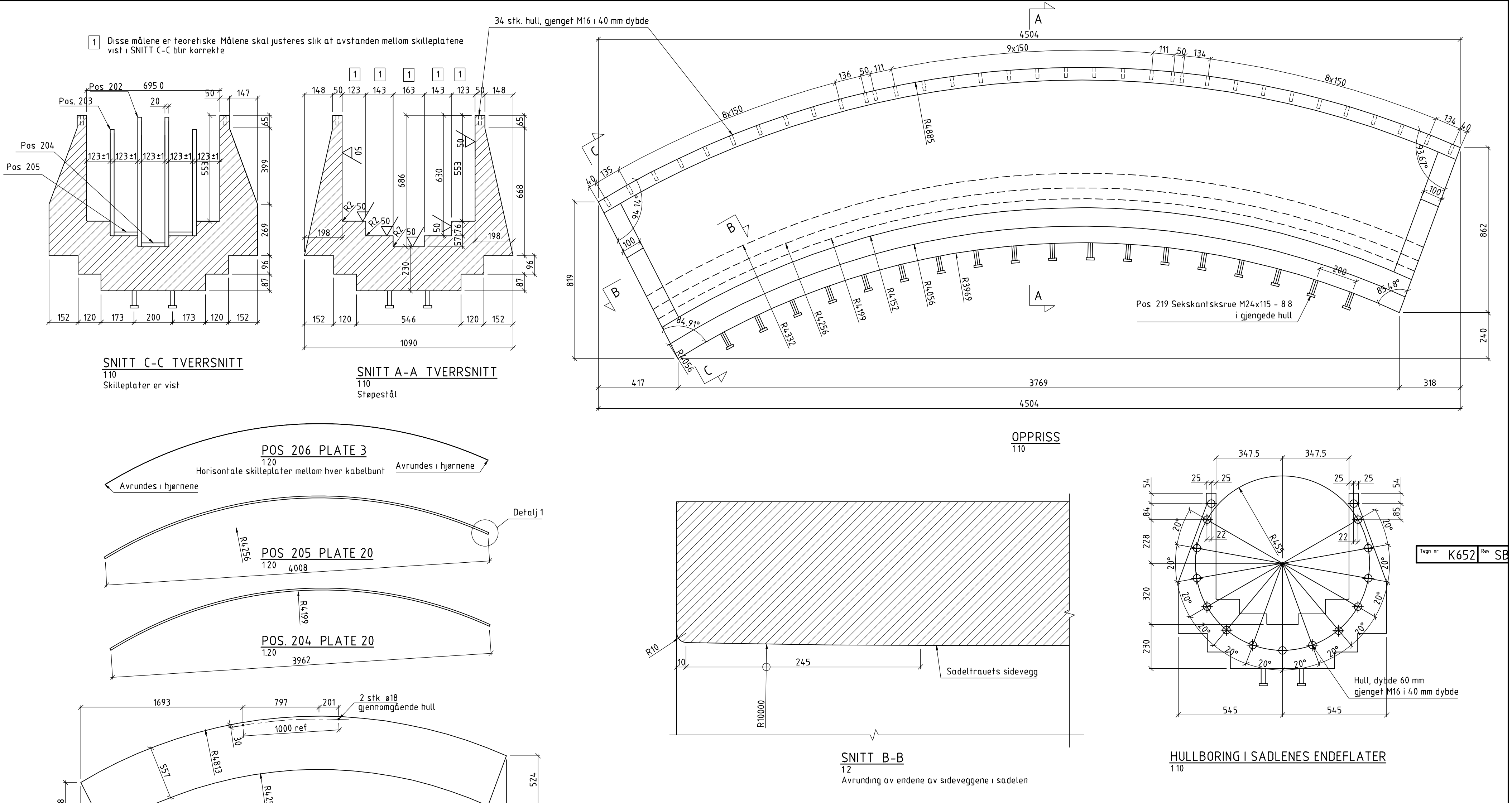

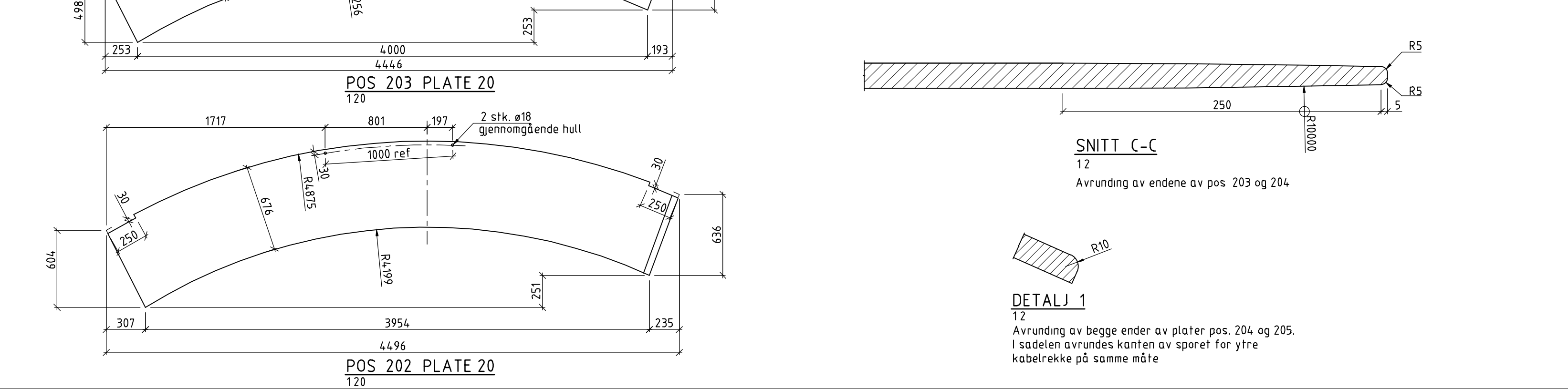

HENVISNING

Materialliste D51 Tårn- og spredesadler

Rev	Revisjonen gjelder	Prosj.	Kontr.	Dato
SB	Som bygd	GAG	IMJ	20.06.2014
K	Hull ø18 vist	GAG	BI	06.05.2011
J	Skruehull i ende av sadel endret	GAG	AGK	08.04.2010
I	Utsparinger i pos. 202 påført	GAG	AGK	26.02.2010
H	Radiusmålsetting påført pos. 205	GAG	AGK	27.01.2010
G	Skruehull i topp sadel målsatt	GAG	AGK	04.12.2009
F	Skruehull i ende av sadel korrigert	GAG	AGK	29.10.2009
E	Målsetting korrigert	GAG	AGK	07.10.2009
D	Bredden av kabelsporene endret	GAG	AGK	23.09.2009
C	Arbeidstegning BRU-01, BRU-02	GAG	BI	28.08.2009
B	Skruehull i topp av sadelvegger tilføyd	GAG		17.08.2009
A	Arbeidstegning	GAG	AGK	17.06.2009

Statens vegvesen

Rv. 7 / Rv. 13

12-2950 HARDANGERBRUA

Tårnsadler
Detaljer

Prosj.	GAG
Tegner	GAG
Dato	22.06.2007
Prosjleder	Bjørn Isaksen
PROFnr	12r0013b_015
Målestokk	1:20, 1:10, 1:2 (A1)
Byggv. nr.	12-2950
Tegn nr	K652
Rev	SB

Prosjektert av Statens vegvesen Vegdirektoratet, Bruseksjonen

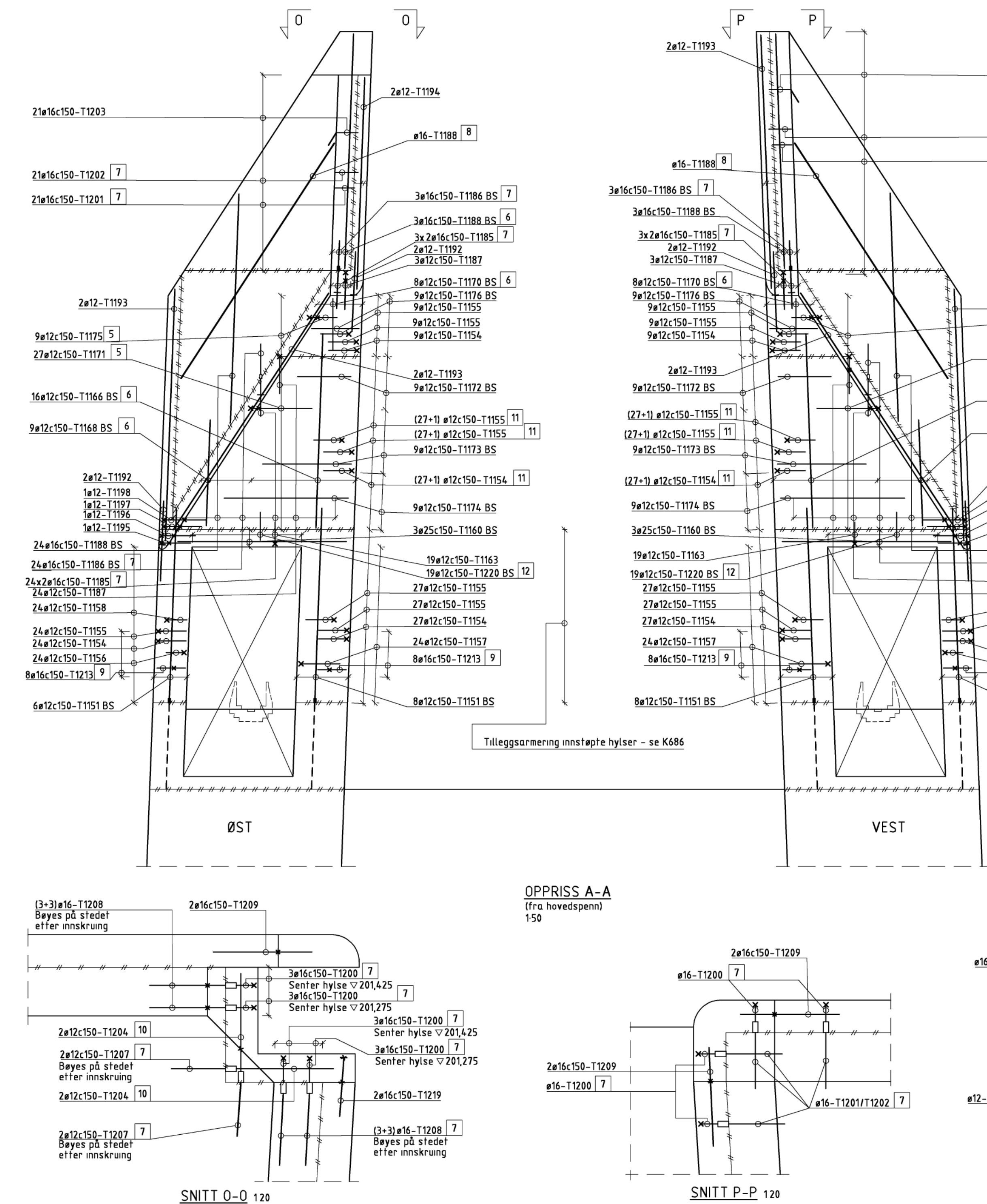

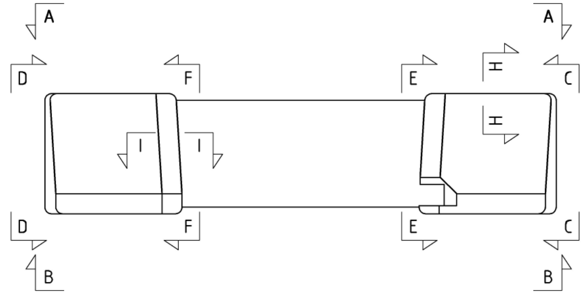

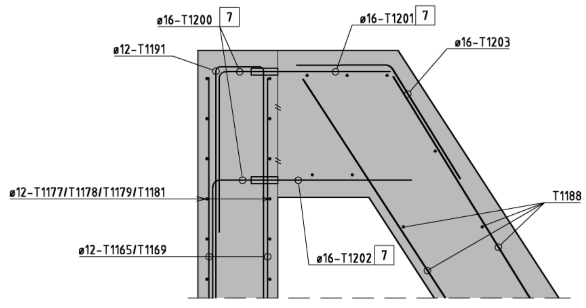

MERKNADER

1. Kontrollklasse. Utvidet kontroll iht. NS 3465
2. Armering: Kamstenger teknisk klasse B500NC iht. NS 3576-3
3. Armeringsoverdekning:
   55±15 mm til konstruktiv armering
   40±5 mm til ø12 monteringsstenger
   Flater som utføres med overforskaling
   65±15 mm til konstruktiv armering
   50±5 mm til ø12 monteringsstenger
4. Minimum omfaringslengde
   Φ12 = 400 mm, Φ16 = 500 mm, Φ20 = 600 mm, Φ25 = 800 mm, Φ32 = 1000 mm
5. Armeringen følger skrå skjæringslinje mellom tak og vegg. For horisontale jern gjelder oppgitt senteravstand i vertikalprojeksjonen. For vertikale jern gjelder oppgitt senteravstand i horisontalprojeksjonen
6. Armeringen settes i formen og tillpasses deretter skrå skjæringslinje ved kapping.
7. Armering utføres med skjøthylser. For plassering gjelder samme prinsipp som under merknad 5.
8. Pos T1188 i skrå takflate legges parallelt med skråflatens sidekanter. Dette betyr at de to armeringsretningene ikke er vinkelrette på hverandre
9. Pos T1213 legges mellom kote +187,6 og +188,65
10. T1204 produseres som rett stang og med muffeskjøt. T1204 bøyes til på stedet for tilpasning mot skrå takflate. Muffeskjøt plasseres slik at den passer med skrå takflaters overkantarmering. Det er ikke nødvendig med muffeskjøt i underkant der hvor T1204 legges i overkant
11. Gjelder T1154 og T1155. Det skal legges én ekstra ved kote +191,14. Dette kan gjøres ved å legge bunt ved den enheten som kommer nærmest kote +191,14
12. T1220 avsluttes på kote +191,4

HENVISNINGER
Tegning K401, Tårn Bu, Form
Tegning K440, Tårn Bu, Tårntopp, Plan og oppriss, Form
Tegning K441, Tårn Bu, Tårntopp detaljer og 3D-perspektiv, Form
Tegning K444, Tårntopp Bu, Vegger kt. 185 -187, Armering
Tegning K681, Tårntopp Bu, Oppriss B-B, Armering
Tegning K682, Tårntopp Bu, Oppriss C-C og D-D, Armering
Tegning K683, Tårntopp Bu, Oppriss E-E og F-F, Armering
Tegning K684, Tårntopp Bu, Snitt G-G, Armering
Tegning K685, Tårntopp Bu, Snitt K-K og L-L, Armering
Tegning K686, Tårntopp Bu, Innstøpte hylser, Armering
Tegning K687, Tårntopp Bu, Tabelloversikt, Armering
Bøyeliste side T115 - T122

Tegn nr	K680	Rev	SB

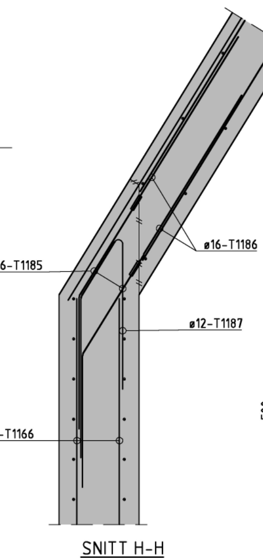

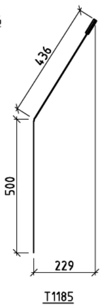

Rev	Revisjonen gjelder	Prosj	Kontr	Dato
SB	Som bygd	AGK	IMJ	20.06.2014
D	T1220, Støpeskjøt, Merknad 12, Henvisninger	AGK	MBR	17.03.2011
C	T1154/T1155, Merknad 11	AGK	MBR	14.03.2011
B	Snitt O-O og P-P, Snitt H-H, Merknad 3 og 10, Henvisninger	AGK	MBR	03.03.2011
A	Arbeidstegning	AGK	MBR	01.02.2011

Godkjent som arbeidstegning i notat fra Vegdirektoratet — Saksnr 2010/011531-041

Statens vegvesen

Rv. 7 / Rv. 13
12-2950 HARDANGERBRUA
Tårntopp Bu
Oppriss A-A
Armering

Prosj	AGK	Dato
Tegner	IMJ	18.01.2011
Prosj.leder	Bjørn Isaksen	
PROFnr	12r0013b_015	
Målestokk	1:50,1:20,1:10 (A1)	
Byggv nr	12-2950	
Tegn nr	K680	Rev SB

Prosjektert av: Statens vegvesen Vegdirektoratet, Bruseksjonen

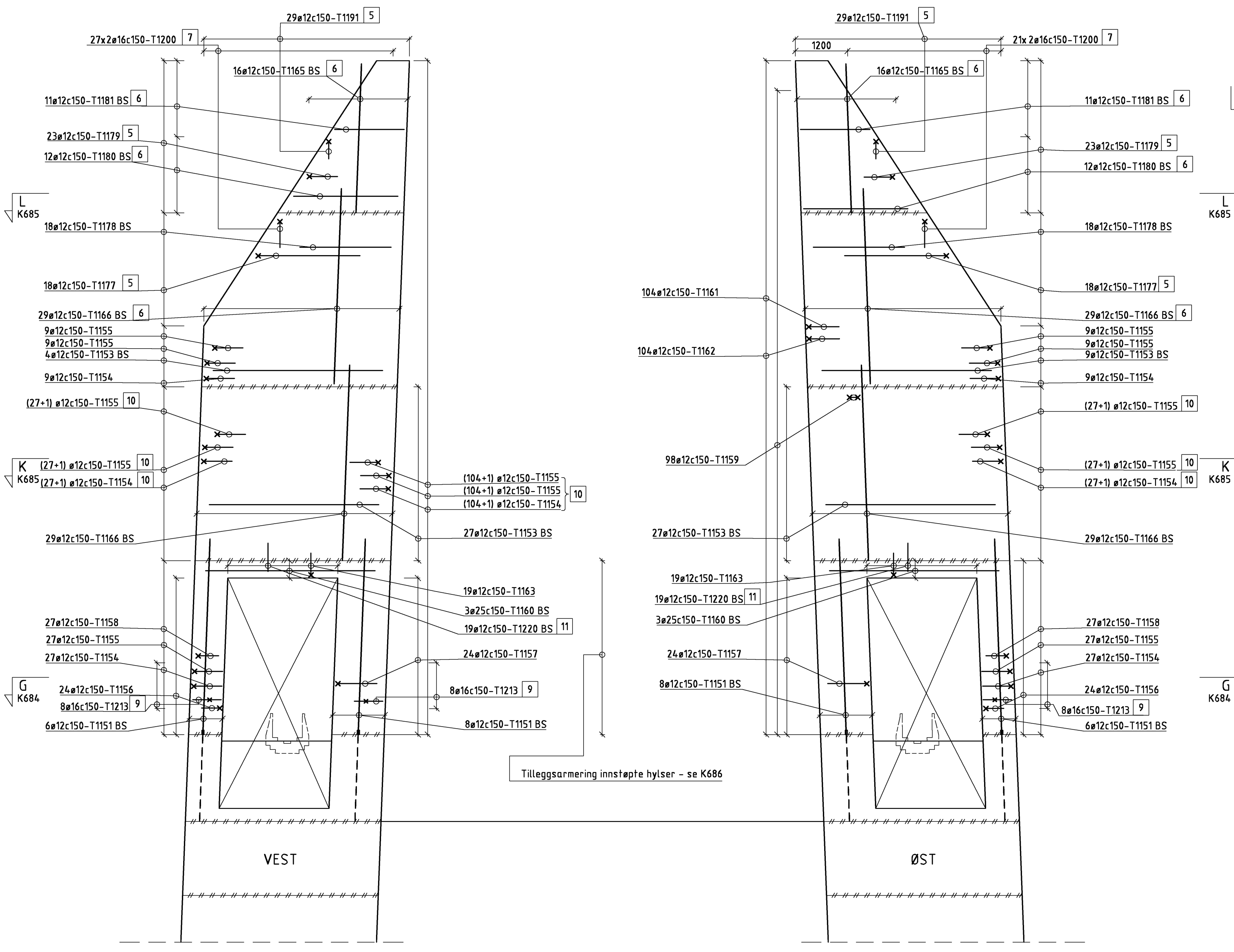

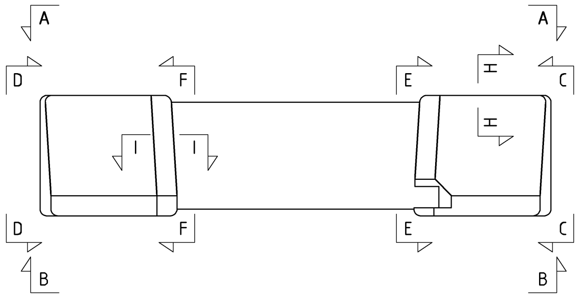

OVERSIKT SNITTANVISNING
1:100

OPPRISS B-B
(fra sidespenn)
1:50

MERKNADER

1. Kontrollklasse Utvidet kontroll iht NS 3465
2. Armering. Kamstenger teknisk klasse B500NC iht. NS 3576-3
3. Armeringsoverdekning:
   55±15 mm til konstruktiv armering
   40±5 mm til ø12 monteringsstenger
   Flater som utføres med overforskaling
   65±15 mm til konstruktiv armering
   50±5 mm til ø12 monteringsstenger
4. Minimum omfaringslengde:
   Φ12 = 400 mm
   Φ16 = 500 mm
   Φ20 = 600 mm
   Φ25 = 800 mm
   Φ32 = 1000 mm

5 Armeringen følger skrå skjæringslinje mellom tak og vegg. For horisontale jern gjelder oppgitt senteravstand i vertikalprojeksjonen. For vertikale jern gjelder oppgitt senteravstand i horisontalprojeksjonen

6 Armeringen settes i formen og tillpasses deretter skrå skjæringslinje ved kapping

7 Armering utføres med skjøthylser. For plassering gjelder samme prinsipp som under merknad 5.

8 Pos T1188 i skrå takflate legges parallelt med skråflatens sidekanter. Dette betyr at de to armeringsretningene ikke er vinkelrette på hverandre

9 Pos T1213 legges mellom kote +187,6 og +188,65.

10 Gjelder T1154 og T1155. Det skal legges én ekstra ved kote +191,14. Dette kan gjøres ved å legge bunt ved den enheten som kommer nærmest kote +191,14

11 T1220 avsluttes på kote +191,4.

HENVISNINGER

Tegning K401, Tårn Bu, Form
Tegning K440, Tårn Bu, Tårntopp, Plan og oppriss, Form
Tegning K441, Tårn Bu, Tårntopp detaljer og 3D-perspektiv, Form
Tegning K444, Tårntopp Bu, Vegger kt 185 -187, Armering
Tegning K680, Tårntopp Bu, Oppriss A-A, Armering
Tegning K682, Tårntopp Bu, Oppriss C-C og D-D, Armering
Tegning K683, Tårntopp Bu, Oppriss E-E og F-F, Armering
Tegning K684, Tårntopp Bu, Snitt G-G, Armering
Tegning K685, Tårntopp Bu, Snitt K-K og L-L, Armering
Tegning K686, Tårntopp Bu, Innstøpte hylser, Armering
Tegning K687, Tårntopp Bu, Tabelloversikt, Armering
Bøyeliste side T115 - T122

Tegn nr	K681	Rev	SB

Rev	Revisjonen gjelder	Prosj	Kontr	Dato
SB	Som bygd	AGK	IMJ	20.06.2014
D	T1220, Merknader 11, Henvisninger	AGK	MBR	17.03.2011
C	T1154/T1155, Merknad 10	AGK	MBR	14.03.2011
B	Antall T1200, Merknad 3, Henvisninger	AGK	MBR	03.03.2011
A	Arbeidstegning	AGK	MBR	01.02.2011

Godkjent som arbeidstegning i notat fra Vegdirektoratet — Saksnr 2010/011531-041

Statens vegvesen

Prosj	AGK	Dato
Tegner	IMJ	18.01.2011
Prosjleder	Bjørn Isaksen	
PROFnr	12r0013b_015	
Målestokk	1:50, 1:100 (A1)	
Byggv nr	12-2950	
Tegn nr	K681	Rev SB

Rv. 7 / Rv. 13
12-2950 HARDANGERBRUA
Tårntopp Bu
Oppriss B-B
Armering

Prosjektert av Statens vegvesen Vegdirektoratet, Bruseksjonen

NTNU
Norwegian University of
Science and Technology